

OPEN JOURNAL OF

NANAN



ISSN:2147-0081

Volume:8, Issue: 1, Year: 2023

A JOURNAL ABOUT
NANOSCIENCE

Open Journal of Nano

Editor in Chief

Dr. Mustafa CAN, Sakarya University of Applied Sciences, Turkey
mustafacan@subu.edu.tr

Editorial Board

Dr. Emrah ÖZAKAR, Ataturk University,
Erzurum, Turkey.
emrahozakar@atauni.edu.tr

Dr. Hamza ŞİMŞİR, Karabuk University,
Turkey.
hamzasimsir@karabuk.edu.tr

Dr. Harun GÜL, Sakarya University of
Applied Sciences, Turkey.
harungul@subu.edu.tr

Dr. Mustafa Zahid YILDIZ, Sakarya
University of Applied Sciences, Turkey.
mustafayildiz@sakarya.edu.tr

Dr. Numan GÖZÜBENLİ, Harran
University, Turkey.
gnuman@harran.edu.tr

Dr. Oğuz SARIBIYIK, Gümüşhane
University, Gumushane, Turkey.
oysaribiyik@gumushane.edu.tr

Dr. Tuğrul ÇETİNKAYA, Sakarya
University, Turkey.
tcetinkaya@sakarya.edu.tr

Dr. Yasin AKGÜL, Karabuk University,
Turkey.
yasinakgul@karabuk.edu.tr

Field Editors

Dr. Hasan HACİFAZLIOĞLU, İstanbul
University-Cerrahpaşa, İstanbul, Turkey.
hasanh@istanbul.edu.tr

Dr. Mithat ÇELEBİ, Yalova University,
Turkey.
mithat.celebi@yalova.edu.tr

Dr. Zafer Ömer ÖZDEMİR, University of
Health Sciences, Turkey.
zaferomer.ozdemir@sbu.edu.tr

Dr. Erol ALVER, Hitit University, Turkey.
erolalver@hitit.edu.tr

Dr. Kamal YUSOH, University Malaysia
Pahang, Malaysia.
kamal@ump.edu.my

Dr. Tetiana TEPLA, Lviv Polytechnic
National University, Ukraine.
tetiana.l.tepla@lpnu.ua

Dr. Birgül BENLİ, İstanbul Technical
University, Turkey.
benli@itu.edu.tr

Dr. Deniz ŞAHİN, Gazi University, Turkey.
dennoka1k@hotmail.com

Statistics Editor

Dr. Özer UYGUN, Sakarya University,
Sakarya, Turkey.
ouygun@sakarya.edu.tr

Editorial Assistants

Mücahid SARI, Sakarya University of Applied Sciences, Sakarya, Turkey.
<https://dergipark.org.tr/en/pub/@mucahidsari>

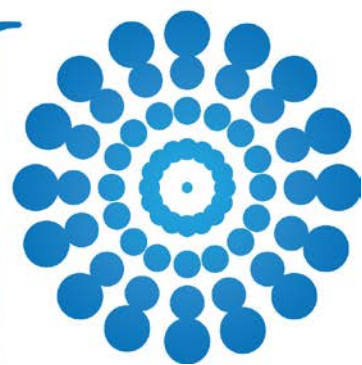
Dr. Hamza ŞİMŞİR, Karabuk University, Turkey.
hamzasimsir@karabuk.edu.tr

Engin Deniz PARLAR, Sakarya University of Applied Sciences, Sakarya, Turkey. denizparlar-97@hotmail.com

Nadir ATMACA, The Istanbul Metropolitan Municipality, Istanbul, Turkey.
nadiratmaca@gmail.com

Halid ÖZGÜR, FreshForty Media, Turkey
halid@freshforty.media

Enis AKSOY, Areya illüstrasyon, Sakarya, Turkey
enisaksoy@gmail.com

**Contents****Volume: 8, Issue: 1, Year: 2023****About DOI Service Activation**

(Editorial News)

01-01

Mustafa CAN**Molecular Docking Study of Midostaurin, an Effective Drug in the Treatment of Myeloid Leukemia**

(Research Article)

02-10

Sefa ÇELİK, Gözde YILMAZ, Ayşen ÖZEL, Sevim AKYÜZ**Computational Investigation of the Interaction Mechanism of Some anti-Alzheimer Drugs with the Acetylcholinesterase Enzyme**

(Research Article)

11-21

Sefa ÇELİK A. Demet DEMİRAG, Ali Osman COŞGUN, Ayşen ÖZEL, Sevim AKYÜZ**Toxicological Aspects and Bioanalysis of Nanoparticles: Zebrafish Model**

(Review Article)

22-35

Burcu YEŞİLBUDAK**Sonochemical Removal of Highly Toxic Aqueous Cd²⁺ and Cr⁶⁺ Ions Using Dandelion-like Co₃O₄ Nanoflowers**

(Research Article)

36-49

Elif Aybike BERBEROĞLU, Mümin Mehmet KOÇ, Nurdan KURNAZ YETİM, Cemile ÖZCAN**The study on determination interactions between liquid crystals and nanoparticle: Fluorescence spectra of nanoparticle-doped liquid crystals**

(Research Article)

50-64

Yunus Emre KARA, Yadigar GÜLSEVEN SIDIR, Sabit HOROZ

About DOI Service Activation

*¹ Mustafa CAN 

¹ Department of Metallurgical and Materials Engineering, Sakarya University of Applied Sciences, Sakarya, Turkey.

* Corresponding author, e-mail: mustafacan@subu.edu.tr

Abstract - Our Journal OPJ (*The Open Journal of Nano*) has started to assign DOI numbers with the prefix 10.56171/ to all its scientific articles as of the 1st issue of 2022.

DOI Hizmeti Hakkında

Öz - Dergimiz *The Open Journal of Nano* (OPJ) 2022 1. Sayısından itibaren tüm bilimsel makalelerine 10.56171/ öneki ile doi numarası atamaya başlamıştır.

English

As of the 1st issue of Open Journal of Nano 2022, our journal has started to assign doi numbers with the prefix 10.56171/ to all its scientific articles.

DOI number, which is short for "Digital Object Identifiers", can be translated into Turkish as Digital Object Identifier. The DOI number, which provides the representation of all digital content with a unique identifier without writing details such as title, author names, published date, etc., also ensures that scientific digital content such as articles, thesis, homework, scientific research in the academic literature is fixed on a web location. Even if the website where the content was originally published is closed, the content with a DOI address continues to be located on a fixed https link on the internet.

We would like to thank the **Dergipark Platform** for providing this service, which will ensure that the articles of all our authors are more accessible and in international scientific standards.

Türkçe

Dergimiz *Open Journal of Nano* 2022 1. Sayısından itibaren tüm bilimsel makalelerine 10.56171/ öneki ile doi numarası atamaya başlamıştır.

"Digital Object Identifiers" kelimesinin kısaltılmışı olan DOI numarası, Dijital Nesne Tanımlayıcı olarak Türkçeye çevrilebilir. Tüm dijital içeriklerin başlık, yazar adları, yayınlanan tarih vb gibi detayları uzunca yazmadan özgün bir tanımlayıcı ile temsilini sağlayan DOI numarası akademik literatürde makale, tez, ödev, bilimsel araştırma gibi bilimsel nitelik taşıyan dijital içeriklerin bir web konumuna sabitlenmesini de sağlamış olmaktadır. İçeriğin ilk olarak yayınlandığı web sitesi kapanmış olsa dahi DOI adresi tanımlanmış içerik internette sabit bir https linkinde yer almaya devam eder.

Tüm yazarlarımızın makalelerinin daha ulaşılabilir ve uluslararası bilimsel standartlarda olmasını sağlayacak bu hizmeti sağladığı için bulundurma hizmetini sağlayan **Dergipark Platformuna** teşekkürlerimizi sunarız.

¹ Corresponding author: E-mail: mustafacan@subu.edu.tr

Molecular Docking Study of Midostaurin, an Effective Drug in the Treatment of Myeloid Leukemia

*¹ Sefa Çelik , ² Gözde Yılmaz , ¹ Aysen E. Özel , ³ Sevim Akyüz 

¹ Istanbul University, Science Faculty, Physics Department, 34134, Istanbul, Turkey.

² Istanbul Kültür University, Vocational School, Opticianry Program, 34158, Istanbul, Turkey.

³ Istanbul Kültür University, Science and Letters Faculty, Physics Department, 34156, Istanbul, Turkey

* Corresponding author, e-mail: scelik@istanbul.edu.tr

Tel: +90 212 455 5700 Faks: +90 212 455 5766

Submission Date: 12.04.2022

Acceptation Date: 14.07.2022

Abstract - Midostaurin (C₃₅H₃₀N₄O₄) is a multi-target kinase inhibitor used to treat some types of acute myeloid leukemia in combination with other chemotherapy agents. Firstly, the structural preferences of the Midostaurin were evaluated due to the importance to determine the most stable conformer of a bioactive molecule to elucidate its bioactivity. The conformational analysis of the Midostaurin molecule was performed using the PM3, a semi-experimental method. The three most stable conformers and their relative energies were determined. The Epidermal Growth Factor receptor (EGFR) is an integral membrane protein, and its over-expression is associated with the development of a wide variety of tumors. For this reason, EGFR inhibitors can act as anticancer drugs as preventing the growth of EGFR-expressing tumors and increasing the survival rates of patients. On the other hand, DNA is an important target for anticancer drugs. To elucidate the anticancer properties of Midostaurin, the molecular docking simulations were performed against EGFR and DNA targets. The binding modes and binding affinities of the ligand-target receptor complexes were determined. Midostaurin showed strong binding affinity to DNA ($\Delta G = -8.6$ kcal/mol) and EGFR ($\Delta G = -9.6$ kcal/mol). The results revealed the significant anti-tumor effect of Midostaurin.

Keywords: Conformational analysis, DNA, EGFR, Midostaurin, Molecular docking

1. Introduction

Acute myeloid leukemia (AML) causes healthy hematopoietic cells to become mutated [1]. AML is defined as a malignant clonal disease that occurs as a result of incomplete maturation of blast cells and accumulation of abnormal immature cells first in the bone marrow and then rapidly in the blood [1-2]. It is known that AML disease has a genetic origin due to the transfer of mutated genes [1]. Whole genome sequencing, RNA sequencing and whole exome sequencing studies of AML disease have been important for a better understanding of its molecular structure. Genetic mutations, signaling, transcriptional regulation, nucleocytoplasmic shuttle, and chromatin modification have all been shown to produce genetic abnormalities in patients with AML [3].

Since AML is a heterogeneous disease, the response to treatment may vary depending on the risk factors of the patient. Treatment of AML disease is applied as chemotherapy and/or hematopoietic stem cell transplantation [4]. Nucleoside analogs and topoisomerase II inhibitors are two therapeutic chemotherapeutic agents used in the treatment of AML [5].

¹ Corresponding author: +90 212 455 5700 Fax: +90 212 455 5766

E-mail: scelik@istanbul.edu.tr

Fms-like tyrosine kinase 3 (FLT3) is a receptor tyrosine kinase and is expressed almost exclusively in the hematopoietic compartment. Mutations of the Fms-like tyrosine kinase 3 gene (FLT3) are seen in 30% of adults with newly diagnosed AML. Midostaurin is a versatile small molecule kinase inhibitor that is used to treat adult patients with AML who have AML FLT3 mutations [6-7]. In investigations employing animal models, midostaurin has been identified as an FLT3 inhibitor [8].

GI (gastrointestinal) toxicities such as vomiting, nausea, and diarrhea are the Midostaurin side effects [9]. Patients in the Phase I study of midostaurin reported nausea and vomiting as adverse effects. In another study, it was stated that no hematological toxicity and cardiac conduction abnormality were encountered if Midostaurin was not used together with a different agent [10]. In some studies, skin rash, gastrointestinal and hepatic toxicity were observed in midostaurin treatment [11].

Anticancer drugs are divided into several classes as antitumor antibiotics, which reduce DNA/RNA synthesis and hence slow cancer cell growth and division [12], mitotic inhibitors, which interfere with the mitosis phase of cells [13], and topoisomerase inhibitors, which impede DNA transcription [14].

The ErbB family of receptor tyrosine kinases has four members. EGFR is one of them. Many malignancies have overexpressed or mutated the receptor, underlining its potential as a therapeutic cancer diagnostic. EGFR has a role in a variety of biological activities, including proliferation, angiogenesis, and cell death suppression. It is a transmembrane protein that transmits important signals from the epithelial cell surface to the intracellular domain for cell proliferation, motility, and adhesion regulation. Overexpressed EGFR sends various signals to cells, causing them to grow faster and live longer [15-18]. It also plays a role in cancer carcinogenesis. A better understanding of molecular signal transduction has led to the development of new cancer therapy tactics and approaches. As a result, turning off EGFR's signal transduction is expected to stop cancer cells from growing and surviving. Because EGFR plays such a significant role in cancer, it is being investigated as a possible therapeutic target for cancer treatment [15-19].

To enlighten the anticancer activity of Midostaurin, conformational preferences of the molecule were searched in this work the energetically favorable conformer was determined. Afterwards, by using the most stable conformer of Midostaurin, molecular docking analysis into B-DNA and EGFR tyrosine kinase domains were performed. The binding modes, and binding affinities were determined.

2. Materials and Methods

The conformational analysis of the Midostaurin was performed with Spartan06, a molecular modelling and computational chemistry program [20]. The semiempirical PM3 method [21-24], which provides a reasonably accurate, rapid estimation of the probable conformations of a molecule, was used. The obtained most stable conformation of the Midostaurin was used as the initial conformation of the ligand molecule for docking studies. For docking studies, the crystal structure of DNA (PDB ID: 1BNA) and EGFR tyrosine kinase domain (PDB ID: 2GS2) were obtained from the protein data bank (<http://www.rcsb.org/pdb>). The CAVER program [25] was used to determine the possible binding sites on the receptor surface. On the obtained active sites, molecular docking was performed using AutoDock-Vina software [26]. For docking simulations, a semi-flexible docking protocol was applied, where the target receptors (DNA or EGFR) were kept rigid while the ligand was kept flexible for being docked upon.

3. Results and Discussions

3.1. Structure

Midostaurin has the five lowest energy conformers, as revealed by a conformational study. Table 1 lists the relative energies of the most stable three conformers, and Figure 1 depicts their molecular geometries.

Table 1. The energies of the most stable three conformations of Midostaurin.

Conformers	Total energy (kJ/mol)	Relative energy (kJ/mol)
Conformer I	-62.46	0
Conformer II	-62.45	0.01
Conformer III	-61.64	0.82

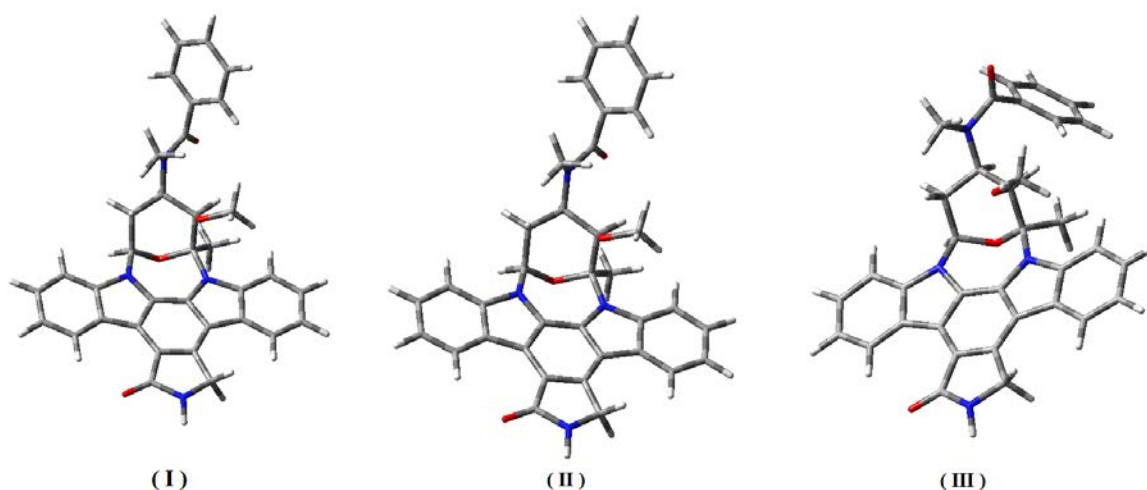


Figure 1. The obtained three lowest energy conformers of Midostaurin by conformational analysis.

3.2. Molecular Docking

As Midostaurin is known to have anticancer properties [27-28] we performed molecular docking studies with DNA and EGFR. Since DNA is the genetic information carrier, and the ability of anticancer agents to interfere the transcription and DNA replication has importance. On the other hand, EGFR is the target for anticancer agents, due to its role of signaling in proliferation, angiogenesis and suppression of cell death causing cancer.

AutoDockVina [26] was used to perform docking analyses. From the protein database [29], the crystal structure of DNA (PDB ID: 1BNA) was obtained and prepared for docking analysis. Water molecules were deleted, polar hydrogens were added, and Kollman's DNA charges were determined. The partial charges of the Midostaurin were computed using the Geistenger approach, and the active region of DNA was identified using a grid size of 40x40x40. The Midostaurin was found to interact with the nucleic acids DT8, DC9, DG10, DC13, and DC15 of DNA, through pi-alkyl, pi-pi-T shaped and pi-donor hydrogen bond interactions (Figure 2). The molecular docking simulations revealed the binding affinity (ΔG) of Midostaurin to DNA as -8.6 kcal/mol. The interactions between Midostaurin and DNA's nucleic acids are: Pi-alkyl interaction between DT8 and Midostaurin with a length of 5.28 Å; pi-pi-T shaped interactions between DC9 and Midostaurin with 5.23 and 5.28 Å lengths; pi-pi-T shaped and pi-donor hydrogen bond interactions between DG10 and Midostaurin with a length of 5.22 and 3.04 Å, respectively; pi-donor hydrogen bond interaction between DC13 and Midostaurin with a length of 3.15 Å; pi-donor hydrogen bond interactions between DC15 and Midostaurin with 2.57 and 3.24 Å lengths.

In the molecular docking study of 5-chlorouracil (5-FU) into DNA, 5-FU was found to interact with DG10, DC15 and DG16 nucleic acids, through hydrogen bond interactions [30]. In the molecular

docking simulations, the docked cyclic dipeptide, cyclo(Ala-His), into DNA, it was found that the peptide interacted with nucleic acids DC9, DG10, DC11, DG16 and DA17 of DNA through hydrogen bonding interactions with 3.1, 2.39, 2.96, 2.53, 2.39 and 2.99 Å lengths, respectively [31]. In the molecular docking studies of Acalabrutinib, an anticancer drug, and DNA, Acalabrutinib was found to interact DG10 (2.11 and 2.14 Å) and DG16 (2.06 and 2.47 Å) by hydrogen bond interactions [32]. In another study, the N4-tetradentate thiosemicarbazone docked into DNA was found to interact with the DT8, DC9, DG12, DG16, DA17 and DA18 residues [33]. The results indicated that Midostaurin was docked in a similar active region of DNA as described in the literature [30-33].

For docking study of Midostaurin into EGFR, the crystal structure of EGFR tyrosine kinase domain (PDB ID: 2GS2) was obtained from the protein database [34] and prepared for docking analysis. Water molecules were deleted, polar hydrogens were added, and EGFR tyrosine kinase domain charges of Kollman were determined. The partial charges of the Midostaurin were computed using the Geistenger approach, and the active region of the EGFR tyrosine kinase domain was identified using a grid size of $40\text{Å}\times 40\text{Å}\times 40\text{Å}$.

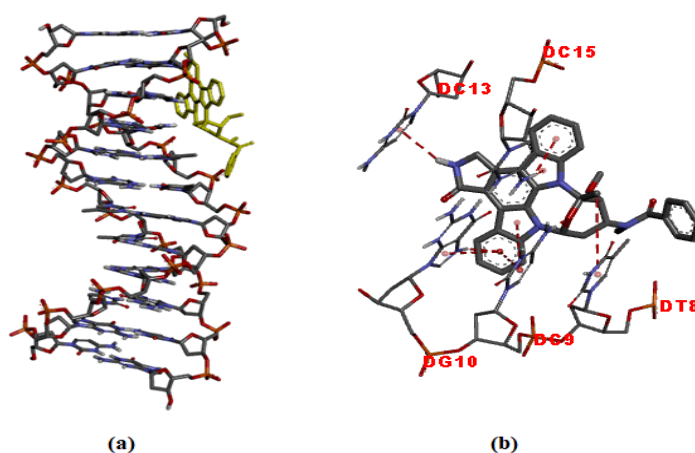


Figure 2. Molecular docked model of Midostaurin with DNA (a), The interactions between the Midostaurin and DNA are labeled using colored dashed lines (b) ($\Delta G = -8.6$ kcal/mol).

After preparing the EGFR tyrosine kinase domain and the ligand for molecular docking analysis, docking simulations were conducted on the active site of the target protein. The binding affinity of the investigated ligand was found to be -9.6 kcal/mol. Figure 3 shows a 3D view and interactions of docked Midostaurin in the active region of the EGFR tyrosine kinase domain.

The interactions between Midostaurin and the EGFR target receptor are as follows:

A 4.74 Å length pi-alkyl interaction with Leu694; 4.51 Å length pi-alkyl interaction with Ala698; 4.58 and 4.87 Å lengths pi-alkyl and 5.38 Å length alkyl interactions with Val702; 4.73 Å length pi-alkyl interaction with Ala719; 4.63 Å length alkyl interaction with Lys721; 5.49 Å length pi-sulfur interaction with Met742; 5.06 and 5.42 Å lengths pi-alkyl interactions with Leu820.

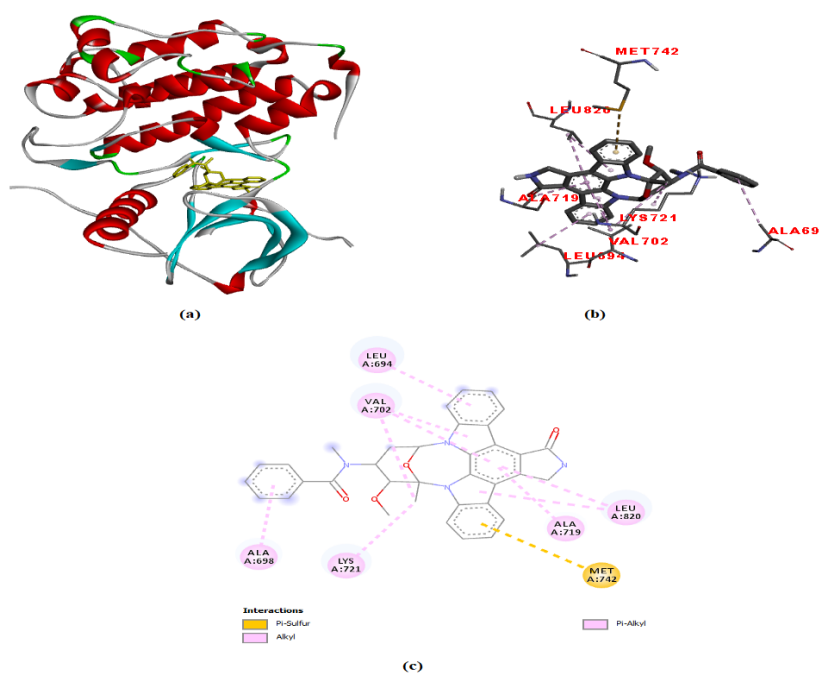


Figure 3. Molecular docked model of Midostaurin with EGFR tyrosine kinase domain (-9.6 kcal/mol) (a), 3D and 2D representations describing bindings of Midostaurin with the active site of EGFR tyrosine kinase domain (b-c).

Bahmani et al. investigated the pyrazolopyrimidine-based derivatives as EGFR inhibitors by molecular docking and multi-QSAR methods [35]. It was reported that the docked 1u compound of pyrazolopyrimidine-based derivative into EGFR, which showed the lowest binding energy to EGFR, was located in the locality of several hydrophobic amino acid residues including Phe699, Ala731, Ile735, Val762, phe832, and Leu834. The result concluded that hydrophobic interactions play the most important role in the formation of the 1u-EGFR complex. In addition, it was reported that 1u compound interacted with Lys721, Glu722, Glu734, Asp737, Glu738 and Lys836 residues by electrostatic interactions and formed a hydrogen bond with Gly833 [35]. In the molecular docking study of the cyclic octopeptide CVRACGAD into EGFR, cyclic octopeptide was found to interact with Lys721, Thr766 and Ala719, Asp831, Gly695, Gly772, Leu694, Leu768 residues of target receptor [36]. *In silico* docking studies of a series of 6, 7-dialkoxy-4-anilinoquinazolines against EGFR showed that compound 33 interacted with the Ser696, Gly700, Val702, Val704, Ala719, Lys721, Thr766, Met769, Glu738 and Asn818 residues of the target receptor, that were the same residues that the well-known anticancer drug Gefitinib interacted [37]. The comparison of the literature results with the molecular docking results of Midostaurin into EGFR revealed that investigated ligand was docked in a similar active region of EGFR as described in the literature [35-37].

To determine the binding free energy of small ligands to biological macromolecules, molecular mechanics Poisson-Boltzmann Surface Area (MM/PBSA) and molecular mechanics generalized born surface area (MM/GBSA) techniques are often used [38-43]. Since both the MM/PBSA and MM/GBSA techniques are important, Wang et al. (2019) [42] created a software that combines the two as the MM/PB(GB)SA approach.

The binding free energies of Midostaurin with DNA and the EGFR tyrosine kinase domain were computed in this investigation using Wang's program [42], which is based on the MM/PB(GB)SA approach. Using the MM/PB(GB)SA methods with the GAFF2 and ff14SB force field combinations and the GB6 process [42], the predicted binding free energies of Midostaurin with DNA and with the EGFR tyrosine kinase domain were -14.63 and -30.42 kcal/mol, respectively.

4. Conclusions

The conformational preferences of the Midostaurin were investigated using PM3 which is semi-experimental approach. The docking simulations were used to enlighten the biological activity of the title molecule in its most stable conformation. Because DNA and the EGFR tyrosine kinase domain are both prominent targets for anticancer medicines, docking simulations of Midostaurin with DNA and the EGFR protein were done to predict anticancer efficacy. Based on the binding affinity of -8.6 and -9.6 kcal/mol to DNA and EGFR, respectively, and their interactions with targets, molecular docking simulations suggest that Midostaurin ligand will have a significant anti-tumor effect.

Peer-review: Externally peer - reviewed.

Conflict of Interest: No conflict of interest was declared by the authors.

Financial Disclosure: This study was supported by the Research funds of Istanbul University (ÖNAP-2423).

References (Please use for reference management programs like Mendeley or Zetero)

- [1] Prada-Arismendy, J., Arroyave, J. C., Röthlisberger, S. 2017. Molecular biomarkers in acute myeloid leukemia, *Blood reviews* 31(1), 63-76.
- [2] Kumar, C. C. 2011. Genetic abnormalities and challenges in the treatment of acute myeloid leukemia, *Genes & cancer* 2(2), 95-107.
- [3] Rubnitz, J. E., Gibson, B., & Smith, F. O. 2008. Acute myeloid leukemia, *Pediatric clinics of North America* 55(1), 21-51.
- [4] Schiller, G. J. 2014. Evolving treatment strategies in patients with high-risk acute myeloid leukemia, *Leukemia & lymphoma* 55(11), 2438-2448.
- [5] Absalon, M. J., Smith, F. O. 2009. Treatment strategies for pediatric acute myeloid leukemia, *Expert opinion on pharmacotherapy* 10(1), 57-79.
- [6] Stone, R. M., Mandrekar, S. J., Sanford, B. L., Laumann, K., Geyer, S., Bloomfield, C. D., Thiede, C., Prior, T.W., Döhner, K., Marcucci, G., Lo-Coco, F., Klisovic, R.B., Wei, A., Sierra, J., Sanz, M.A., Brandwein, J.M., de Witte, T., Niederwieser, D., Appelbaum, F.R., Medeiros, B.C., Tallman, M.S., Krauter, J., Schlenk, R.F., Ganser, A., Serve, H., Ehninger, G., Amadori, S., Larson, R.A., Döhner, H. 2017. Midostaurin plus chemotherapy for acute myeloid leukemia with a FLT3 mutation, *New England Journal of Medicine* 377(5), 454-464.
- [7] Schlenk, R. F., Weber, D., Fiedler, W., Salih, H. R., Wulf, G., Salwender, H., Schroeder, T., Kindler, T., Lübbert, M., Wolf, D., Westermann, J., Kraemer, D., Götze, K.S., Horst, H.A., Krauter, J., Girschikofsky, M., Ringhoffer, M., Südhoff, T., Held, G., Derigs, H.G., Schroers, R., Greil, R., Griebhammer, M., Lange, E., Burchardt, A., Martens, U., Hertenstein, B., Marretta, L., Heuser, M., Thol, F., Gaidzik, V.I., Herr, W., Krzykalla, J., Benner, A., Döhner, K., Ganser, A., Paschka, P., Döhner, H. 2019. Midostaurin added to chemotherapy and continued single-agent maintenance therapy in acute myeloid leukemia with FLT3-ITD, *Blood* 133(8), 840-851.
- [8] Levis, M. 2017. Midostaurin approved for FLT3-mutated AML, *Blood* 129(26), 3403-3406.
- [9] Stemler, J., Koehler, P., Maurer, C., Müller, C., Cornely, O. A. 2020. Antifungal prophylaxis and novel drugs in acute myeloid leukemia: the midostaurin and posaconazole dilemma, *Annals of Hematology* 99(7), 1429-1440.
- [10] Gallogly, M. M., Lazarus, H. M. 2016. Midostaurin: an emerging treatment for acute myeloid leukemia patients, *Journal of Blood Medicine* 7, 73.
- [11] Berger, T., Rozovski, U., Moshe, Y., Yaari, S., Frisch, A., Hellmann, I., Apel, A., Aviram, A., Koren-Michowitz, M., Yeshurun, M., Ram, R., Raanani, P., Ofran, Y., Wolach, O. 2019. Midostaurin in

- combination with intensive chemotherapy is safe and associated with improved remission rates and higher transplantation rates in first remission-a multi-center historical control study, *Annals of hematology* 98(12), 2711-2717.
- [12] Patil, Y., Amitay, Y., Ohana, P., Shmeeda, H., Gabizon, A. 2016. Targeting of pegylated liposomal mitomycin-C prodrug to the folate receptor of cancer cells: Intracellular activation and enhanced cytotoxicity, *Journal of Controlled Release* 225, 87-95.
- [13] Michalska, M., Schultze-Seemann, S., Bogatyreva, L., Hauschke, D., Wetterauer, U., Wolf, P. 2016. In vitro and in vivo effects of a recombinant anti-PSMA immunotoxin in combination with docetaxel against prostate cancer, *Oncotarget* 7(16), 22531.
- [14] Olsen, I. H., Knigge, U., Federspiel, B., Hansen, C. P., Skov, A., Kjær, A., Langer, S. W. 2014. Topotecan monotherapy in heavily pretreated patients with progressive advanced stage neuroendocrine carcinomas, *Journal of Cancer* 5(8), 628.
- [15] Pomerantz, R. G., & Grandis, J. R. 2004. The epidermal growth factor receptor signaling network in head and neck carcinogenesis and implications for targeted therapy, *In Seminars in oncology* 31(6), 734-743.
- [16] Shiomitsu, K., Johnson, C. L., Malarkey, D. E., Pruitt, A. F., Thrall, D. E. 2009. Expression of epidermal growth factor receptor and vascular endothelial growth factor in malignant canine epithelial nasal tumours, *Veterinary and comparative oncology* 7(2), 106-114.
- [17] Higgins, R. J., Dickinson, P. J., LeCouteur, R. A., Bollen, A. W., Wang, H., Wang, H., Corely, L.J., Moore, L.M., Zang, W., Fuller, G. N. 2010. Spontaneous canine gliomas: overexpression of EGFR, PDGFR α and IGF2 demonstrated by tissue microarray immunophenotyping, *Journal of neuro-oncology* 98(1), 49-55.
- [18] Lee, H. J., Xu, X., Choe, G., Chung, D. H., Seo, J. W., Lee, J. H., Lee, C.T., Jheon, S., Sung, S.W., Chung, J. H. 2010. Protein overexpression and gene amplification of epidermal growth factor receptor in nonsmall cell lung carcinomas: Comparison of four commercially available antibodies by immunohistochemistry and fluorescence in situ hybridization study, *Lung Cancer* 68(3), 375-382.
- [19] Duan, L., Wu, R., Ye, L., Wang, H., Yang, X., Zhang, Y., Chen, X., Zuo, G., Zhang, Y., Weng, Y., Luo, J., Tang, M., Shi, Q., He, T., Zhou, L. 2013. S100A8 and S100A9 are associated with colorectal carcinoma progression and contribute to colorectal carcinoma cell survival and migration via Wnt/ β -catenin pathway, *PloS one* 8(4), e62092.
- [20] Shao, Y., Molnar, L. F., Jung, Y., Kussmann, J., Ochsenfeld, C., Brown, S. T., Gilbert, A.T.B., Slipchenko, L.V., Levchenko, S.V., O'Neill, D.P., DiStasio Jr, R.A., Lochan, R.C., Wang, T., Beran, G.J.O., Besley, N.A., Herbert, J.M., Lin, C.Y., Voorhis, T.V., Chien, S.H., Sodt, A., Steele, R.P., Rassolov, V.A., Maslen, P.E., Korambath, P.P., Adamson, R. D., Austin, B., Baker, J., Byrd, E.F.C., Dachselt, H., Doerksen, R.J., Dreuw, A., Dunietz, B.D., Dutoi, A. D., Furlani, T. R., Gwaltney, S. R., Heyden, A., Hirata, S., Hsu, C.P., Kedziora, G., Khalliulin, R. Z., Klunzinger, P., Lee, A. M., Lee, M.S., Liang, W. Z., Lotan, I., Nair, N., Peters, B., Proynov, E. I., Pieniazek, P. A., Rhee, Y. M., Ritchie, J., Rosta, E., Sherrill, C. D., Simonnet, A. C., Subotnik, J. E., Woodcock, H. L., Zhang, W., Bell, A. T., Chakraborty, A. K., Chipman, D. M., Keil, F.J., Warshel, A., Hehre, W.J., Schaefer, H.F., Kong, J., Krylov, A.I., Gill, P.M.W., Head-Gordon, M. 2006. Advances in methods and algorithms in a modern quantum chemistry program package, *Physical Chemistry Chemical Physics* 8(27), 3172-3191.
- [21] Stewart, J. J. 1989^a. Optimization of parameters for semiempirical methods I. Method, *Journal of computational chemistry* 10(2), 209-220.
- [22] Stewart, J. J. 1989^b. Optimization of parameters for semiempirical methods II. Applications, *Journal of computational chemistry* 10(2), 221-264.
- [23] Stewart, J. J. 1991. Optimization of parameters for semiempirical methods. III Extension of PM3 to Be, Mg, Zn, Ga, Ge, As, Se, Cd, In, Sn, Sb, Te, Hg, Tl, Pb, and Bi, *Journal of computational chemistry* 12(3), 320-341.

- [24] Stewart, J. J. 2004. Optimization of parameters for semiempirical methods IV: extension of MNDO, AM1, and PM3 to more main group elements, *Journal of Molecular Modeling* 10(2), 155-164.
- [25] Jurcik, A., Bednar, D., Byska, J., Marques, S. M., Furmanova, K., Daniel, L., Kokkonen, P., Brezovsky, J., Strnad, O., Stourac, J., Pavelka, A., Manak, M., Damborsky, J., Kozlikova, B. 2018. CAVER Analyst 2.0: analysis and visualization of channels and tunnels in protein structures and molecular dynamics trajectories, *Bioinformatics* 34(20), 3586-3588.
- [26] Trott, O., & Olson, A. J. 2010. AutoDock Vina: improving the speed and accuracy of docking with a new scoring function, efficient optimization, and multithreading, *Journal of computational chemistry* 31(2), 455-461.
- [27] El Fitori, J., Su, Y., Büchler, P., Ludwig, R., Giese, N. A., Büchler, M. W., Quentmeier, H., Hines, O.J., Herr, I., Friess, H. 2007. PKC 412 small-molecule tyrosine kinase inhibitor: Single-compound therapy for pancreatic cancer, *Cancer* 110(7), 1457-1468.
- [28] Stone, R. M., Fischer, T., Paquette, R., Schiller, G., Schiffer, C. A., Ehniger, G., Cortes, J., Kantarjian, H.M., DeAngelo, D.J., Huntsman-Labed, A., Dutreix, C., del Corral, A., Giles, F. 2012. Phase IB study of the FLT3 kinase inhibitor midostaurin with chemotherapy in younger newly diagnosed adult patients with acute myeloid leukemia, *Leukemia* 26(9), 2061-2068.
- [29] Drew, H. R., Wing, R. M., Takano, T., Broka, C., Tanaka, S., Itakura, K., Dickerson, R. E. 1981. Structure of a B-DNA dodecamer: Conformation and Dynamics, *Proceedings of the National Academy of Sciences* 78(4), 2179-2183.
- [30] Akalin, E., Celik, S., Akyuz, S. 2020. Molecular Modeling, Dimer Calculations, Vibrational Spectra, and Molecular Docking Studies of 5-Chlorouracil, *Journal of Applied Spectroscopy* 86(6), 975-985.
- [31] Celik, S., Yilmaz, G., Ozel, A. E., Akyuz, S. 2022. Structural and spectral analysis of anticancer active cyclo (Ala-His) dipeptide, *Journal of Biomolecular Structure and Dynamics* 40(2), 660-672.
- [32] Celik, S., Demirag, A.D., Arslan, S., Ozel, A.E., Akyuz, S. 2022. Conformational, Toxic, Physicochemical and Molecular Docking Analysis of the Anticancer Acalabrutinib Molecule, *Open Journal of Nano* 7(1), 1-9.
- [33] Eğlence-Bakır, S., Celik, S., Şahin, M., Ozel, A. E., Akyuz, S., & Ülküseven, B. 2021. Synthesis, molecular modelling, FT-IR, Raman and NMR characterization, molecular docking and ADMET study of new nickel (II) complex with an N4-tetradentate thiosemicarbazone, *Journal of Biomolecular Structure and Dynamics* 39(12), 4212-4224.
- [34] Zhang, X., Gureasko, J., Shen, K., Cole, P. A., Kuriyan, J. 2006. An allosteric mechanism for activation of the kinase domain of epidermal growth factor receptor, *Cell* 125(6), 1137-1149.
- [35] Bahmani, A., Tanzadehpanah, H., Hosseinpour Moghadam, N., & Saidijam, M. (2021). Introducing a pyrazolopyrimidine as a multi-tyrosine kinase inhibitor, using multi-QSAR and docking methods. *Molecular Diversity*, 25(2), 949-965.
- [36] Mishra, A., & Dey, S. (2019). Molecular docking studies of a cyclic octapeptide-cyclosaplin from sandalwood. *Biomolecules*, 9(11), 740.
- [37] Chandregowda, V., Kush, A. K., & Reddy, G. C. (2009). Synthesis and in vitro antitumor activities of novel 4-anilinoquinazoline derivatives. *European journal of medicinal chemistry*, 44(7), 3046-3055.
- [38] Hao, G. F., Wang, F., Li, H., Zhu, X. L., Yang, W. C., Huang, L. S., Wu, J.W., Berry, E.A., Yang, G. F. 2012. Computational discovery of picomolar Q_o site inhibitors of cytochrome bc₁ complex, *Journal of the American Chemical Society* 134(27), 11168-11176.
- [39] Cheron, N., Jasty, N., Shakhnovich, E. I. 2016. OpenGrowth: an automated and rational algorithm for finding new protein ligands, *Journal of medicinal chemistry* 59(9), 4171-4188.
- [40] Hao, G. F., Jiang, W., Ye, Y. N., Wu, F. X., Zhu, X. L., Guo, F. B., Yang, G. F. 2016. ACFIS: a web server for fragment-based drug discovery, *Nucleic acids research* 44(W1), W550-W556.
- [41] Yang, J. F., Wang, F., Jiang, W., Zhou, G. Y., Li, C. Z., Zhu, X. L., Hao, G.F., Yang, G. F. 2018.

- PADFrag: a database built for the exploration of bioactive fragment space for drug discovery, Journal of chemical information and modeling 58(9), 1725-1730.
- [42] Wang, Z., Wang, X., Li, Y., Lei, T., Wang, E., Li, D., Kang, Y., Zhu, F., Hou, T. 2019. farPPI: a webserver for accurate prediction of protein-ligand binding structures for small-molecule PPI inhibitors by MM/PB (GB) SA methods, Bioinformatics 35(10), 1777-1779.
- [43] Wang, E., Sun, H., Wang, J., Wang, Z., Liu, H., Zhang, J. Z., Hou, T. 2019. End-point binding free energy calculation with MM/PBSA and MM/GBSA: strategies and applications in drug design, Chemical reviews 119(16), 9478-9.

Computational Investigation of the Interaction Mechanism of Some anti-Alzheimer Drugs with the Acetylcholinesterase Enzyme

* ¹Sefa Celik , ²A. Demet Demirag , ³Ali Osman Cosgun , ¹Aysen E. Ozel ,
⁴Sevim Akyuz 

¹ Istanbul University, Faculty of Science, Department of Physics, Vezneciler, Istanbul, 34134 Turkiye.

² Yeditepe University, Vocational School, Internet and Network Technologies Department, Istanbul, 34755, Turkiye.

³ Mechatronic Department, Vocational School, Yeditepe University, Istanbul, Turkiye.

⁴ Istanbul Kultur University, Faculty of Science and Letters, Department of Physics, Istanbul, 34156 Turkiye.

* Corresponding author, e-mail: scelik@istanbul.edu.tr

Submission Date: 27.04.2022

Acceptation Date: 08.08.2022

Abstract - The molecular structures of the lowest-energy conformers of donepezil (C₂₄H₂₉NO₃), rivastigmine (C₁₄H₂₂N₂O₂), and galantamine (C₁₇H₂₁NO₃), which are extensively used in Alzheimer's disease and other memory disorders, were identified using the Spartan06 program and the MMFF method. The optimized geometries, obtained with the same method, were used as initial data in molecular docking investigations with the Acetylcholinesterase enzyme. The binding modes, binding affinities, and interactions were comparatively determined as consequence of the calculations.

Keywords: Acetylcholinesterase Enzyme, Alzheimer, Donepezil, Rivastigmine, Galantamine, Molecular docking.

1. Introduction

Alzheimer's disease is a common cause of cognitive impairment acquired in middle age and old age. However, age alone is not a major risk factor for this disease. Presence of one or more apolipoprotein gene E4 alleles (APOE4), severe traumatic brain injuries and cardiovascular factors are also important risk factors for Alzheimer's disease [1]. Apathy, anxiety and irritability are the most prominent neuropsychiatric symptoms in this disease. Symptoms that occur after dementia are appetite and sleep disturbances, disinhibition, hallucinations, or thought changes [2]. Brain tomography allows the detection of moderate and severe amyloid deposition in the brain [3].

Alzheimer's disease is also biologically characterized by the presence of plaques containing beta-amyloid and neurofibrillary tangles containing the tau gene or tau protein. Neurodegenerative diseases are characterized by the degeneration of some nerve cells by developing filamentous inclusions [4, 5]. The filamentous inclusions are found in diseases such as Alzheimer's disease, corticobasal degeneration, types of dementia head syndrome, Down syndrome, Parkinsonism, and Pick's disease. Normal aging contains hyperphosphorylated microtubule-associated tau protein, these diseases are known as taupathies [6, 7].

The name of a neurodegenerative disease, that occurs with abnormal tau protein accumulation in the brain, is taupathies [8,9]. The pathophysiologically important proteins in Alzheimer's disease are tau proteins [10]. Pick's disease, advanced paralysis, and corticobasal degeneration are tau pathologies [11]. Amyloid deposition in the brain is thought to begin 10-20 years before clinical symptoms appear [12]. In the dementia disease practice guide of the American Academy of Neurology, it is stated that it is possible to treat mild and moderate Alzheimer's patients with acetylcholinesterase inhibitors [13]. The entorhinal cortex is the primary source of information flow to the hippocampus. Granule cells are involved in this cortex [14]. There is an exchange of signals between the entorhinal cortex and the hippocampus [15]. The decrease in entorhinal cortex volume is

¹ Corresponding author: Tel: +90 212 455 5700 - Extension: 15266
E-mail: scelik@istanbul.edu.tr

associated with Alzheimer's disease. The entorhinal cortex is associated with the cognitive disorder schizophrenia [16]. Memory loss occurs due to memory and spatial learning function. The hippocampus is a region in the medial temporal lobe of the brain that plays an important role in memory and navigation and influences particularly short-term memory [17-18].

The most used cholinergic neuronal markers are choline acetyltransferase (ChAT) and acetylcholinesterase (AChE) and their loss is one of the most consistent neurotransmitter changes found in the brain of Alzheimer's patients [19-23]. Alzheimer's disease is expressed as the loss of learning and memory abilities in the elderly population [24]. The enzyme acetylcholinesterase (AChE) plays an important role in the hydrolysis of the neurotransmitter acetylcholine, and because of this feature, it is the therapeutic target of most drugs used in the treatment of Alzheimer's disease [25]. Since the exact mechanism of this disease is unknown, its treatment is still not possible. AChE is an enzyme that catalyzes the hydrolysis of a chemical bond. This enzyme enables the development of mechanism-based inhibitors [26, 27]. It inhibits β -amyloid-induced damage and cytokine release from cell free radical toxicity [28].

Increasing the level of acetylcholine in the brain using acetylcholinesterase inhibitors is an important approach to treat this disease [29]. Various AChE inhibitors are under investigation for the treatment of Alzheimer's disease. AChE inhibitors such as tacrine, donepezil, rivastigmine, and galantamine have been approved by the Food and Drug Administration in the United States [30]. Among other strategies not explored, monoamine oxidase inhibitors have also been proposed for the treatment of AD [29].

Acetylcholinesterase (AChE) is a carboxylesterase enzyme secreted from muscle and primarily found at postsynaptic neuromuscular junctions, especially in muscles and nerves. Its altered activity is caused to some congenital and acquired diseases [31]. Sudden blockade of AChE is lethal, and its gradual loss is associated with progressive deterioration of cognitive, autonomic, and neuromuscular functions, as in Alzheimer's disease, multiple system atrophy, and other conditions [32]. It immediately hydrolyzes a neurotransmitter acetylcholine (ACh) and breaks it down into acetic acid and choline [32]. The primary role of AChE is to prevent ACh dispersal and activation of nearby receptors, in order to terminate neuronal transmission and signaling between synapses. It also plays a role in neural development [32]. Organophosphorus compounds such as pesticides and nerve agents are AChE inhibitors. Since the 1990s, AChE inhibitors have been known to provide some benefits for Alzheimer's disease [33]. Inhibition of AChE reduces the breakdown of ACh and as a result ACh accumulates. This accumulated ACh leads to increased stimulation of muscarinic and nicotinic receptors, resulting in some therapeutic relief for memory deficits in Alzheimer's disease [34]. Thus Acetylcholinesterase (AChE) is an important target for symptomatic improvement in Alzheimer's disease (AD) [35].

The microtubule-associated protein tau is one of the major pathophysiologically relevant proteins in Alzheimer's disease [36]. Tau pathology is the underlying cause of a variety of sporadic and genetic illnesses. These are referred to as tauopathies. The spectrum of tau pathologies includes Pick's disease, progressive supranuclear palsy, and corticobasal degeneration [37, 38]. Emerging pathologies include primary age-related tauopathies, including globular glial tauopathies, chronic traumatic encephalopathy, and aging-related tau astroglial pathology [39]. Clinical symptoms include frontotemporal dementia, corticobasal syndrome, Richardson syndrome, parkinsonism, and rarely motor neuron symptoms [40, 41].

Today, some special molecules are used in treatment of this disease. These molecules are donepezil ($C_{24}H_{29}NO_3$), rivastigmine ($C_{14}H_{22}N_2O_2$) and galantamine ($C_{17}H_{21}NO_3$). Since Alzheimer's disease is not a reversible disease, treatment is provided only by using acetylcholinesterase inhibitor drugs such as donepezil, rivastigmine and galantamine to stop or reduce the progression of the disease [42, 43].

The development of donepezil began in 1983 at the Japanese pharmaceutical company Eisai [44]. The active ingredient was first approved in the USA in 1996. Generics with the active ingredient donepezil have been on the market since 2010 [45, 46]. In the treatment of Alzheimer's disease in which cholinergic neurons are deficient, it works with the principle of operating the decreased acetylcholine amount more effectively by inhibiting the acetylcholinesterase enzyme, which is the enzyme that breaks down acetylcholine [47]. At the same time Donepezil is a medicine that most commonly prescribed for the treatment of Alzheimer's disease. Functional studies have shown that donepezil conditions slow the progression of mild-to-moderate Alzheimer's disease [48, 49].

Rivastigmine is used to treat dementia in persons with Alzheimer's disease (a brain ailment that affects the ability to remember, think effectively, communicate, and perform daily activities, as well as mood and personality changes) [50]. Rivastigmine belongs to the cholinesterase inhibitors group of drugs and it improves mental function (such as memory and reasoning) in the brain by increasing the amount of a natural substance [51]. Furthermore, rivastigmine is utilized to treat Lewy body dementia on occasion [52].

Galantamine is a reversible and selective competitive AchE inhibitor obtained from several botanical sources. AchE inhibitors have historically been the first line of treatment for Alzheimer's Disease. Galantamine also has a lower rate of adverse drug responses than other AchE inhibitors [53,54]. In addition Galantamine is it is also used in the treatment of Alzheimer's, polio, narrow-angle glaucoma and as an antidote after poisoning [55]. It is currently under investigation for use in the treatment of alcohol and nicotine addiction, schizophrenia, and cognitive memory disorders [56].

In this study, due to close relation between structure and function of the bioactive molecules, firstly the conformation analyses were performed on donepezil, rivastigmine, and galantamine molecules, and their lowest energy conformations were determined. Afterwards, the interaction of the donepezil, rivastigmine, and galantamine with Acetylcholinesterase enzyme were investigated by in silico docking simulations, and binding affinities and binding modes were determined.

2. Methods and Calculations

The most stable molecular structures (Figure 1) of donepezil, rivastigmine, and galantamine molecules were determined using the MMFF method [57] and the Spartan06 [58] program, by conformational analysis, following by geometric optimization. The optimized molecular structures were then used as the starting data for docking with the acetylcholinesterase enzyme. The docking studies were performed by using AutoDock-Vina program [59].

3. Results and Discussions

3.1. Structure

The most stable conformers of donepezil ($C_{24}H_{29}NO_3$), rivastigmine ($C_{14}H_{22}N_2O_2$) and galantamine ($C_{17}H_{21}NO_3$) molecules are shown in **Figure 1**.

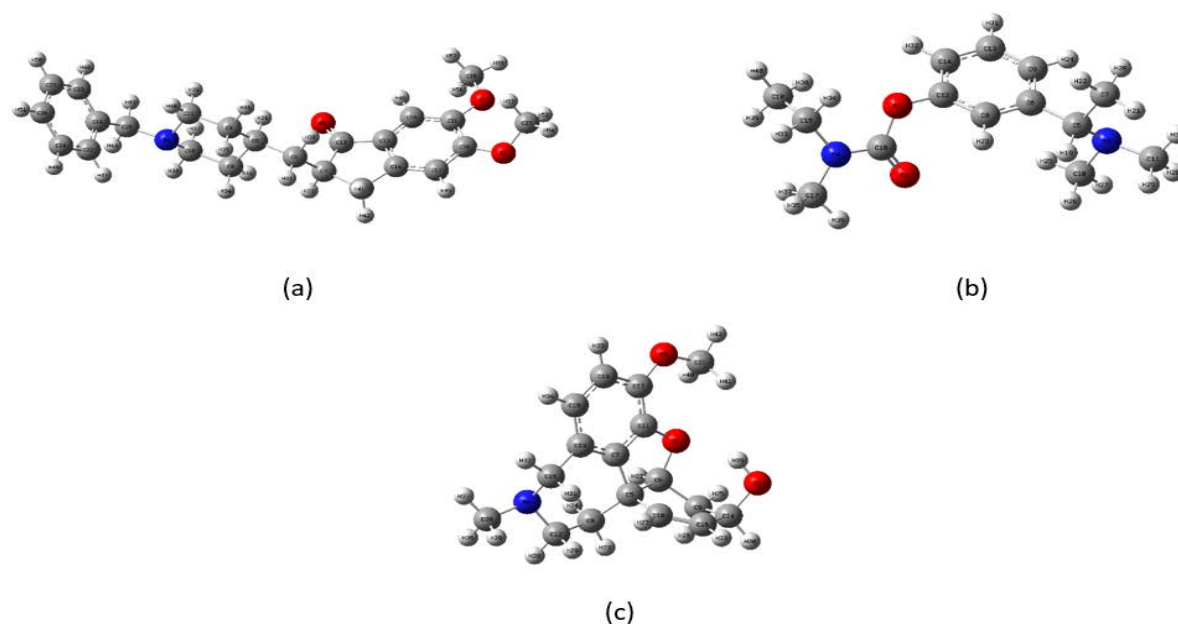


Figure 1. The most stable conformer of donepezil (a), rivastigmine (b) and galantamine (c).

3.2. Molecular Docking

The crystal structures of Acetylcholinesterase enzyme (PDB ID:1DX4, 4EY4, 4EY7) was obtained from the protein database [60, 61]. The acetylcholinesterase enzyme was prepared for docking by removing water molecules and replacing them with polar hydrogens. Its Kollman charges were computed before the docking study. The partial charges of the donepezil, rivastigmine and galantamine molecules were assigned by Geisterger method and the active region of Acetylcholinesterase enzyme was labeled as $40\text{\AA} \times 40\text{\AA} \times 40\text{\AA}$ grid.

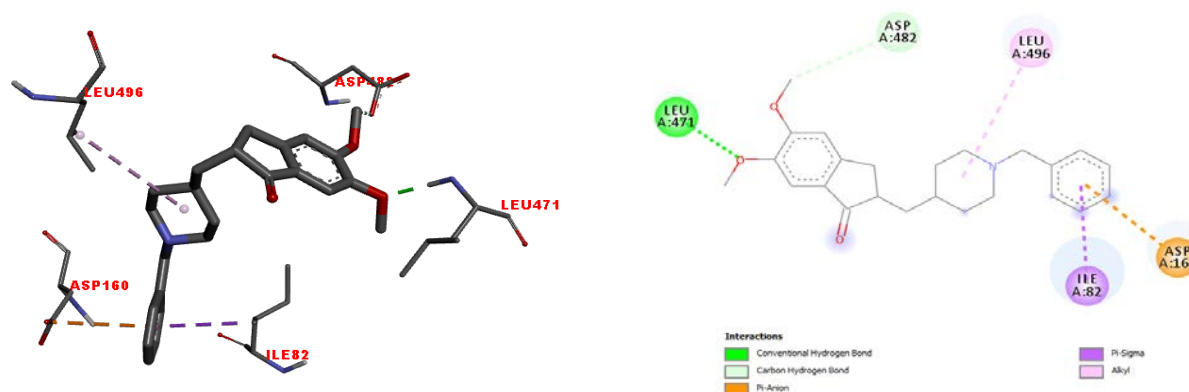


Figure 2. The 3D docked views of the most stable conformer of donepezil in active site of acetylcholinesterase (PDB ID:1DX4, -7.4 kcal/mol).

The 3D docked views of donepezil, rivastigmine and galantamine were shown in Figures 2-4.

As seen in **Figure 2**, the donepezil molecule interacted with:

Ile82 through pi-sigma interaction with 3.86\AA length;

Asp160 through pi-anion interaction with 4.14\AA length;

Leu471 through 1.83\AA long hydrogen bond interaction;

With Asp482 through 3.39\AA long carbon hydrogen bond interaction;

and with Leu496 through an alkyl pi-sigma interaction with a length of 5.47\AA

The binding affinity was determined to be -7.4 kcal/mol .

In the molecular docking studies of triterpenoid (azadirachtin A) into acetylcholinesterase enzyme (PDB ID:1DX4) performed by Rodrigues et al., it was found that triterpenoid (azadirachtin A)

interacted with Tyr71, Gly79, Glu80, Ile82, Trp83, Asn84, Tyr148, Gly149, Gly150, Gly151, Phe152, Met153, Thr154, Gly155, Leu159, Tyr162, Trp321, Tyr324, Phe330, Tyr370, Phe371, Leu479, His480, Asp482 and Glu485 amino acids of AChE receptor [62].

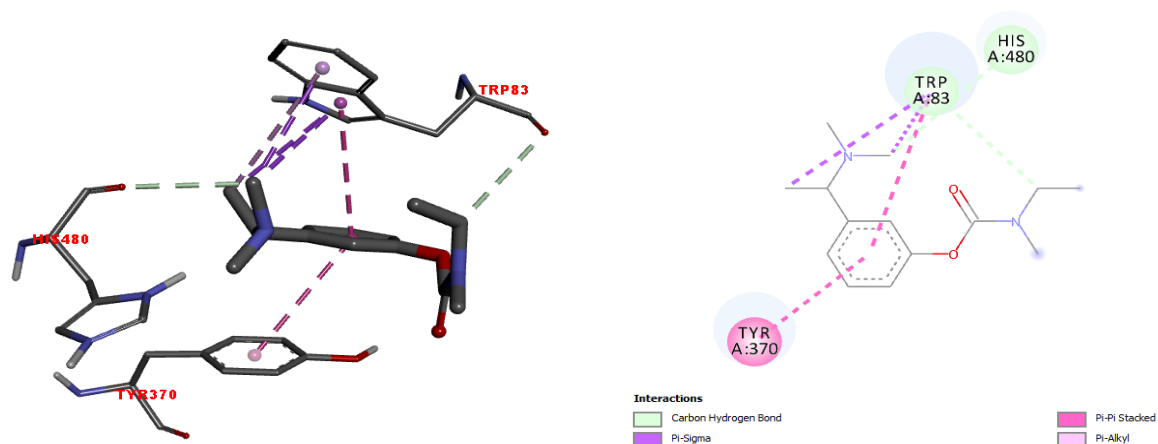


Figure 3. The 3D docked views of the most stable conformer of rivastigmine in active site of acetylcholinesterase (PDB ID:1DX4, -7.0 kcal/mol).

As seen in **Figure 3**, rivastigmine was interacted with;

Trp83 through carbon hydrogen bond interaction with 3.77 Å length, pi-pi stacked interaction with 4.28 Å length, pi-sigma interactions with 3.72, 3.97 and 4 Å length, pi-alkyl interaction with 4.81 Å length;

Tyr370 through pi-pi stacked interaction with 4.45 Å length;

and with His480 through a carbon hydrogen bond interaction with a length of 3.32 Å (Figure 3). The binding affinity was calculated as -7.0 kcal/mol.

In the molecular docking studies of Tacrine and Hesperetin molecules into AChE receptor (PDB ID:1DX4) performed by Kondapalli et al., it was found that Tacrine molecule interacted with Trp83, Tyr370, His480 amino acids and Hesperetin molecule interacted with Trp83, Thr154, His480 amino acids of AChE receptor. Our results are in accord with the previous findings [63].

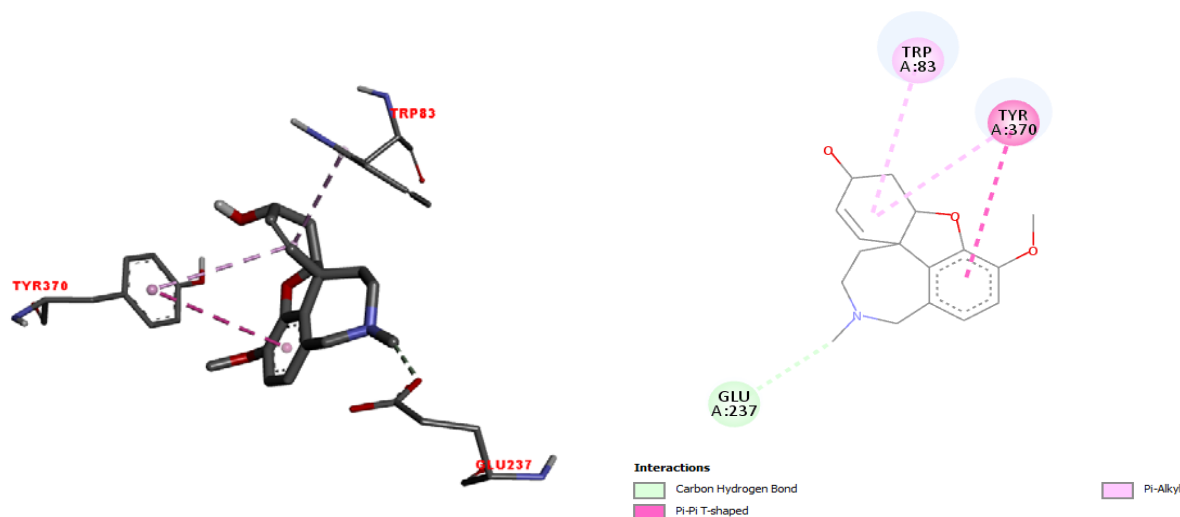


Figure 4. The 3D docked views of the most stable conformer of galantamine in active site of acetylcholinesterase (PDB ID:1DX4, -9.7 kcal/mol).

As seen in **Figure 4**, galantamine molecule was interacted with:
Trp83 through pi-alkyl interaction with 4.74Å length;

Glu237 through carbon hydrogen bond interaction with 3.53Å length; and with Tyr370 through a pi-alkyl interaction with a length of 5.09Å and a pi-pi t-shaped interaction with a length of 5.17Å. The binding affinity was determined to be -9.7 kcal/mol.

In the molecular docking study of Methomyl and 9-(3-phenylmethylamine)-1,2,3,4-tetrahydroacridine molecules into AChE receptor (PDB ID:1DX4), Methomyl molecule was found to interact with Trp83, Tyr370, Trp472, Leu479, His480 amino acids and 9-(3-phenylmethylamine)-1,2,3,4-tetrahydroacridine found to interact with Trp83, Gly150, Gly151 ve His480 residues of the AChE receptor [64]. Our findings are consistent with those of Rodrigues et al. [64].

The donepezil, rivastigmine and galantamine drugs, used in the study are known as AChE inhibitors, and their half maximal inhibitory concentrations (IC_{50}) which are measure of their potency in inhibiting AChE are available in the literature [65]. The results of the docking of these molecules to AChE were compared with the pIC_{50} results of the molecules and were given in **Table 1**.

Table 1. The calculated binding affinities of donepezil, rivastigmine and galantamine molecules to acetylcholinesterase enzyme, in comparison with their experimental half-maximal inhibitory concentration (pIC_{50}).

	PDB ID: 1DX4 Binding affinity (kcal/mol)	PDB ID: 4EY4 Binding affinity (kcal/mol)	PDB ID: 4EY7 Binding affinity (kcal/mol)	pIC_{50}^a
	This study			[65]
Donepezil	-7.4	-8.6	-11.4	8.699
Rivastigmine	-7.0	-6.0	-7.9	7.268
Galantamine	-9.7	-7.5	-10.1	6.523

^a: $pIC_{50} = -\log IC_{50}$ (IC_{50} values were taken from ref [65]).

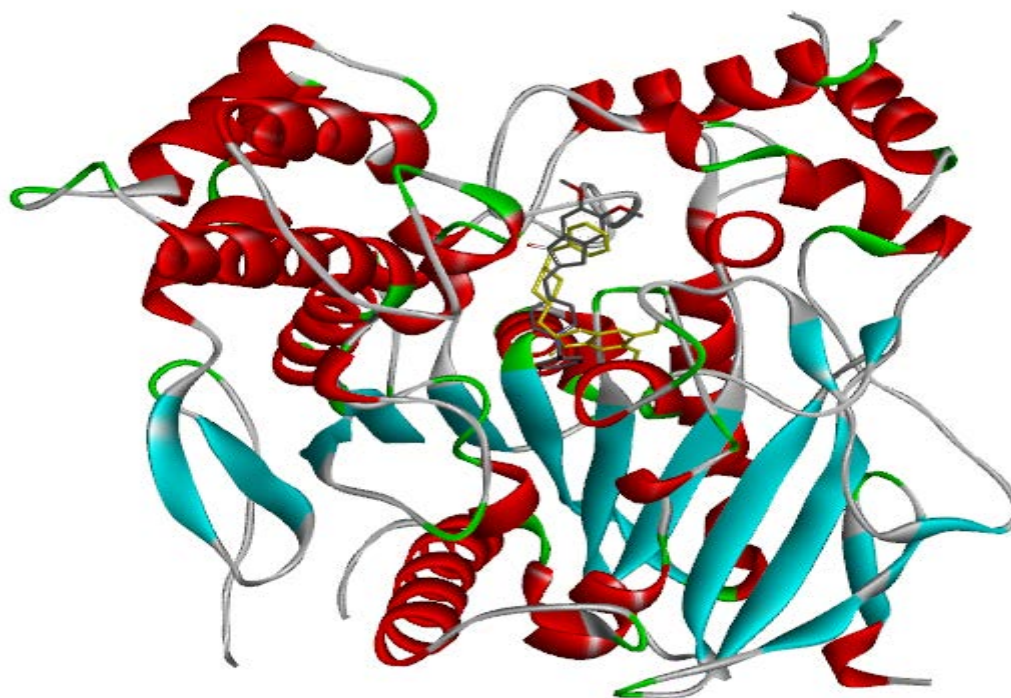


Figure 5. The orientations of donepezil docked into AChE, obtained in this study (yellow) and donepezil in the crystal structure of AChE-Donepezil complex taken from (PDB ID: 4EY7) (grey).

The 3D orientation of Donepezil in AChE target, obtained the study, was compared with the existing ligand orientation in the AChE-donepezil complex crystal structure (see **Figure 5**) and were found to be in agreement.

Recently, Baskaran et al [66] were performed molecular docking calculations of Donepezil and Rivastigmine molecules into 4EY7 target receptor, using AutodockVina program and found the binding affinities as -9.8 and 7.1 kcal/mol, respectively. In this study the binding affinities of

donepezil and risvatigmine molecules to the 4EY7 receptor (AChE) were found to be -11.4 and -7.9 kcal/mol, respectively. The results indicated that the active site found in this study was more stable. Moreover, as seen in Fig 5 that the location donepezil binding site in the AChE target is highly compatible with the location of the donepezil molecule in donepezil-AChE complex.

4. Conclusions

Because the function-activity relationship is so important for bioactive molecules, the most stable conformer of donepezil, rivastigmine, and galantamine molecules was determined. To shed light into their biological activities and to examine the inhibitory effects on Acetylcholinesterase enzyme, the binding mechanisms of donepezil, risvastigmine and galantamine with Acetylcholinesterase enzyme were elucidated by performing molecular docking studies with AChE targets (PDB IDs: 1DX4, 4EY4 and 4EY7). Donepezil, rivastigmine, and galantamine were found to bind to Acetylcholinesterase enzyme (PDB ID:1DX4) with -7.4, -7.0, and -9.7 kcal/mol binding affinities, respectively. In the molecular docking studies of triterpenoid (azadirachtin A) into acetylcholinesterase enzyme (PDB ID:1DX4) [62], It was found that triterpenoid was interacted also with Ile82, Trp83, Tyr370, His480, Asp482 residues of the target receptor. Our results are highly consistent with previous findings [62]. The docking studies revealed that donepezil, rivastigmine, and galantamine binds to 4EY4 with -8.6, -6.0 and -7.5 kcal/mol and to 4EY7 with -11.4, -7.9 and -10.1 kcal/mol binding affinities, respectively. The results indicated that the investigated molecules have good inhibitory impact on the Acetylcholinesterase enzyme.

Peer-review: Externally peer - reviewed.

Author contributions: Concept, Data Collection &/or Processing, Literature Search, Writing – S. C., A. D. D., A. O. C., A. E. O., S. A.

Conflict of Interest: No conflict of interest was declared by the authors.

Financial Disclosure: This study was supported by the Research funds of Istanbul University (ÖNAP-2423).

References

1. Soreq, H., Seidman, S. Acetylcholinesterase — new roles for an old actor. *Nature Reviews Neuroscience* 2, 294–302 (2001). <https://doi.org/10.1038/35067589>.
2. Villemagne, V. L., Burnham, S., Bourgeat, P., Brown, B., Ellis, K. A., Salvado, O., ... & Masters, C. L. (2013). Amyloid β deposition, neurodegeneration, and cognitive decline in sporadic Alzheimer's disease: a prospective cohort study. *The Lancet Neurology*, 12(4), 357-367.
3. Jack, C. R., Knopman, D. S., Jagust, W. J., Shaw, L. M., Aisen, P. S., & Weiner, M. W. & Trojanowski JQ (2010). *Hypothetical model of dynamic biomarkers of the Alzheimer's pathological cascade*. *The Lancet Neurology*, 9(1), 119-128.
4. Huang, H. C., & Jiang, Z. F. (2009). Accumulated amyloid- β peptide and hyperphosphorylated tau protein: relationship and links in Alzheimer's disease. *Journal of Alzheimer's disease*, 16(1), 15-27.
5. Iqbal, K., & Grundke-Iqbal, I. (2010). Alzheimer's disease, a multifactorial disorder seeking multitherapies. *Alzheimer's & Dementia*, 6(5), 420-424.
6. Shoghi-Jadid, K., Small, G. W., Agdeppa, E. D., Kepe, V., Ercoli, L. M., Siddarth, P., ... & Barrio, J. R. (2002). Localization of neurofibrillary tangles and beta-amyloid plaques in the brains of living patients with Alzheimer disease. *The American Journal of Geriatric Psychiatry*, 10(1), 24-35.

7. De Felice, F. G., Wu, D., Lambert, M. P., Fernandez, S. J., Velasco, P. T., Lacor, P. N., ... & Klein, W. L. (2008). Alzheimer's disease-type neuronal tau hyperphosphorylation induced by A β oligomers. *Neurobiology of aging*, 29(9), 1334-1347.
8. Norstrom, E. (2017). Metabolic processing of the amyloid precursor protein—new pieces of the Alzheimer's puzzle. *Discovery Medicine*, 23(127), 269-276.
9. Edwards III, G., Zhao, J., Dash, P. K., Soto, C., & Moreno-Gonzalez, I. (2020). Traumatic brain injury induces tau aggregation and spreading. *Journal of neurotrauma*, 37(1), 80-92.
10. Kovacs, G. G. (2018). Tauopathies. *Handbook of clinical neurology*, 145, 355-368.
11. Iqbal, K., Liu, F., Gong, C. X., & Grundke-Iqbal, I. (2010). Tau in Alzheimer disease and related tauopathies. *Current Alzheimer Research*, 7(8), 656-664.
12. Panza, F., Lozupone, M., Logroscino, G., & Imbimbo, B. P. (2019). A critical appraisal of amyloid- β -targeting therapies for Alzheimer disease. *Nature Reviews Neurology*, 15(2), 73-88.
13. Doody, R. S., Stevens, J. C., Beck, C., Dubinsky, R. M., Kaye, J. A., Gwyther, L. M. S. W., ... & Cummings, J. L. (2001). Practice parameter: Management of dementia (an evidence-based review): Report of the Quality Standards Subcommittee of the American Academy of Neurology. *Neurology*, 56(9), 1154-1166.
14. Frank, L. M., Brown, E. N., & Wilson, M. (2000). Trajectory encoding in the hippocampus and entorhinal cortex. *Neuron*, 27(1), 169-178.
15. Pennanen, C., Kivipelto, M., Tuomainen, S., Hartikainen, P., Hänninen, T., Laakso, M. P., ... & Soininen, H. (2004). Hippocampus and entorhinal cortex in mild cognitive impairment and early AD. *Neurobiology of aging*, 25(3), 303-310.
16. Gómez-Isla, T., Price, J. L., McKeel Jr, D. W., Morris, J. C., Growdon, J. H., & Hyman, B. T. (1996). Profound loss of layer II entorhinal cortex neurons occurs in very mild Alzheimer's disease. *Journal of Neuroscience*, 16(14), 4491-4500.
17. Eichenbaum, H., & Lipton, P. A. (2008). Towards a functional organization of the medial temporal lobe memory system: role of the parahippocampal and medial entorhinal cortical areas. *Hippocampus*, 18(12), 1314-1324.
18. Goldman-Rakic, P. S. (1996). The prefrontal landscape: implications of functional architecture for understanding human mentation and the central executive. *Philosophical Transactions of the Royal Society of London. Series B: Biological Sciences*, 351(1346), 1445-1453.
19. Perry, J. (1977). Frege on demonstratives. *The philosophical review*, 86(4), 474-497.
20. PERRY, E. K., Perry, R. H., Blessed, G., & Tomlinson, B. E. (1978). Changes in brain cholinesterases in senile dementia of Alzheimer type. *Neuropathology and applied neurobiology*, 4(4), 273-277.
21. Atack, J. R., Perry, E. K., Bonham, J. R., Perry, R. H., Tomlinson, B. E., Blessed, G., & Fairbairn, A. (1983). Molecular forms of acetylcholinesterase in senile dementia of Alzheimer type: selective loss of the intermediate (10S) form. *Neuroscience letters*, 40(2), 199-204.
22. Fishman, E. B., Siek, G. C., MacCallum, R. D., Bird, E. D., Volicer, L., & Marquis, J. K. (1986). Distribution of the molecular forms of acetylcholinesterase in human brain: alterations in dementia of the Alzheimer type. *Annals of neurology*, 19(3), 246-252.
23. Palmert, M. R., Podlisny, M. B., Witker, D. S., Oltersdorf, T., Younkin, L. H., Selkoe, D. J., & Younkin, S. G. (1989). The beta-amyloid protein precursor of Alzheimer disease has soluble derivatives found in human brain and cerebrospinal fluid. *Proceedings of the National Academy of Sciences*, 86(16), 6338-6342.

24. Zhang, L., Tang, W., Chao, F. L., Zhou, C. N., Jiang, L., Zhang, Y., ... & Tang, Y. (2020). Four-month treadmill exercise prevents the decline in spatial learning and memory abilities and the loss of spinophilin-immunoreactive puncta in the hippocampus of APP/PS1 transgenic mice. *Neurobiology of Disease*, 136, 104723.
25. Çokuğraş, A. N. (2003). Butyrylcholinesterase: structure and physiological importance. *Turk J Biochem*, 28(2), 54-61.
26. Dasarathy, S., & Merli, M. (2016). Sarcopenia from mechanism to diagnosis and treatment in liver disease. *Journal of hepatology*, 65(6), 1232-1244.
27. Walsh, C. T. (1984). Suicide substrates, mechanism-based enzyme inactivators: recent developments. *Annual review of biochemistry*, 53(1), 493-535.
28. Chao, C. C., Hu, S. X., Ehrlich, L., & Peterson, P. K. (1995). Interleukin-1 and tumor necrosis factor- α synergistically mediate neurotoxicity: involvement of nitric oxide and of N-methyl-D-aspartate receptors. *Brain, behavior, and immunity*, 9(4), 355-365.
29. Enz, A., Amstutz, R., Boddeke, H., Gmelin, G., & Malanowski, J. (1993). Brain selective inhibition of acetylcholinesterase: a novel approach to therapy for Alzheimer's disease. *Progress in brain research*, 98, 431-438.
30. Zarotsky, V., Sramek, J. J., & Cutler, N. R. (2003). Galantamine hydrobromide: an agent for Alzheimer's disease. *American journal of health-system pharmacy*, 60(5), 446-452.
31. McHardy, S. F., Wang, H. Y. L., McCowen, S. V., & Valdez, M. C. (2017). Recent advances in acetylcholinesterase inhibitors and reactivators: an update on the patent literature (2012-2015). *Expert opinion on therapeutic patents*, 27(4), 455-476.
32. Trang, A., & Khandhar, P. B. (2021). Physiology, acetylcholinesterase. In *StatPearls [Internet]*. StatPearls Publishing.
33. McGleenon, B. M., Dynan, K. B., & Passmore, A. P. (1999). Acetylcholinesterase inhibitors in Alzheimer's disease. *British journal of clinical pharmacology*, 48(4), 471.
34. Lazarevic-Pasti, T., Leskovac, A., Momic, T., Petrovic, S., & Vasic, V. (2017). Modulators of acetylcholinesterase activity: From Alzheimer's disease to anti-cancer drugs. *Current medicinal chemistry*, 24(30), 3283-3309.
35. Mehta, M., Adem, A., & Sabbagh, M. (2012). New acetylcholinesterase inhibitors for Alzheimer's disease. *International Journal of Alzheimer's disease*, 2012.
36. Gong, C. X., Liu, F., Grundke-Iqbal, I., & Iqbal, K. (2005). Post-translational modifications of tau protein in Alzheimer's disease. *Journal of neural transmission*, 112(6), 813-838.
37. Komori, T. (1999). Tau-positive dial Inclusions in Progressive Supranuclear Palsy, Corticobasal Degeneration and Pick's Disease. *Brain pathology*, 9(4), 663-679.
38. Kovacs, G. G. (2019). Molecular pathology of neurodegenerative diseases: principles and practice. *Journal of clinical pathology*, 72(11), 725-735.
39. Iida, M. A., Farrell, K., Walker, J. M., Richardson, T. E., Marx, G. A., Bryce, C. H., ... & Crary, J. F. (2021). Predictors of cognitive impairment in primary age-related tauopathy: an autopsy study. *Acta Neuropathologica Communications*, 9(1), 1-12.
40. Respondek, G., & Höglinger, G. U. (2016). The phenotypic spectrum of progressive supranuclear palsy. *Parkinsonism & related disorders*, 22, S34-S36.
41. Levin, J., Kurz, A., Arzberger, T., Giese, A., & Höglinger, G. U. (2016). The differential diagnosis and treatment of atypical parkinsonism. *Deutsches Ärzteblatt International*, 113(5), 61.
42. Faujan, N. H., Zakaria, N., & Mohammad, N. N. (2019). Molecular docking studies on the interaction of anti-Alzheimer compounds with amyloid beta peptides. *J. Multidiscip. Eeng. Sci. Technol.*, 6, 132-136.

43. Zarini-Gakiye, E., Amini, J., Sanadgol, N., Vaezi, G., & Parivar, K. (2020). Recent updates in the Alzheimer's disease etiopathology and possible treatment approaches: a narrative review of current clinical trials. *Current Molecular Pharmacology*, 13(4), 273-294.
44. Sugimoto, H., Ogura, H., Arai, Y., Imura, Y., & Yamanishi, Y. (2002). Research and development of donepezil hydrochloride, a new type of acetylcholinesterase inhibitor. *The Japanese journal of pharmacology*, 89(1), 7-20.
45. Heravi, M. M., & Zadsirjan, V. (2020). Prescribed drugs containing nitrogen heterocycles: An overview. *RSC Advances*, 10(72), 44247-44311.
46. Fowler, A. C. (2020). Pharmaceutical line extensions in the United States.
47. Yan, Z., & Feng, J. (2004). Alzheimer's disease: interactions between cholinergic functions and β -amyloid. *Current Alzheimer Research*, 1(4), 241-248.
48. Howard, R. J., Juszczak, E., Ballard, C. G., Bentham, P., Brown, R. G., Bullock, R., ... & Rodger, M. (2007). Donepezil for the treatment of agitation in Alzheimer's disease. *New England Journal of Medicine*, 357(14), 1382-1392.
49. Hashimoto, M., Kazui, H., Matsumoto, K., Nakano, Y., Yasuda, M., & Mori, E. (2005). Does donepezil treatment slow the progression of hippocampal atrophy in patients with Alzheimer's disease?. *American Journal of Psychiatry*, 162(4), 676-682.
50. Emre, M., Aarsland, D., Albanese, A., Byrne, E. J., Deuschl, G., De Deyn, P. P., ... & Lane, R. (2004). Rivastigmine for dementia associated with Parkinson's disease. *New England Journal of Medicine*, 351(24), 2509-2518.
51. Ravisankar, P., Parvathi, Y. S., Sri, K. C., Ameen, S. A., Kiranmai, D., Ram, R. S., ... & Babu, P. S. (2017). A Comprehensive Analysis on Different Types of Hypothesis, Diagnosis and Treatment of Alzheimer's Disease. *IOSR-JDMS*, 16(4), 97-108.
52. Hampel, H., Mesulam, M. M., Cuello, A. C., Farlow, M. R., Giacobini, E., Grossberg, G. T., ... & Khachaturian, Z. S. (2018). The cholinergic system in the pathophysiology and treatment of Alzheimer's disease. *Brain*, 141(7), 1917-1933.
53. Scott, L. J., & Goa, K. L. (2000). Galantamine. *Drugs*, 60(5), 1095-1122.
54. Rodda, J., Morgan, S., & Walker, Z. (2009). Are cholinesterase inhibitors effective in the management of the behavioral and psychological symptoms of dementia in Alzheimer's disease? A systematic review of randomized, placebo-controlled trials of donepezil, rivastigmine and galantamine. *International psychogeriatrics*, 21(5), 813-824.
55. Shanbhag, T., & Shenoy, S. (2015). *Pharmacology: Prep Manual for Undergraduates E-book*. Elsevier Health Sciences.
56. Sugarman, D. E., De Aquino, J. P., Poling, J., & Sofuoglu, M. (2019). Feasibility and effects of galantamine on cognition in humans with cannabis use disorder. *Pharmacology Biochemistry and Behavior*, 181, 86-92.
57. Halgren, T. A. (1996). Merck molecular force field. I. Basis, form, scope, parameterization, and performance of MMFF94. *Journal of computational chemistry*, 17(5-6), 490-519.
58. Shao, Y., Molnar, L. F., Jung, Y., Kussmann, J., Ochsenfeld, C., Brown, S. T., ... & DiStasio Jr, R. A. (2006). Advances in methods and algorithms in a modern quantum chemistry program package. *Physical Chemistry Chemical Physics*, 8(27), 3172-3191.
59. Trott, O.; Olson, A.J. AutoDock Vina: Improving the speed and accuracy of docking with a new scoring function, efficient optimization, and multithreading. *J. Comput. Chem.* 2010,31, 455-461.
60. Harel, M., Kryger, G., Rosenberry, T. L., Mallender, W. D., Lewis, T., Fletcher, R. J., ... & Sussman, J. L. (2000). Three-dimensional structures of *Drosophila melanogaster*

- acetylcholinesterase and of its complexes with two potent inhibitors. *Protein Science*, 9(6), 1063-1072.
61. Cheung, J., Rudolph, M. J., Burshteyn, F., Cassidy, M. S., Gary, E. N., Love, J., ... & Height, J. J. (2012). Structures of human acetylcholinesterase in complex with pharmacologically important ligands. *Journal of medicinal chemistry*, 55(22), 10282-10286.
 62. Rodrigues, G. C., Scotti, L., & Scotti, M. (2017). Molecular docking study of triterpenoid azadirachtin A on acetylcholinesterase of *Drosophila melanogaster* (Diptera: Drosophilidae), *MOL2NET*, 3, 10.3390/mol2net-03-05054.
 63. Kondapalli, N., Sruthi, K. (2020). Novel Tacrine and Hesperetin analogues: Design, Molecular docking and in silico ADME studies to identify potential Acetyl choline esterase inhibitors for Alzheimer's disease. *Journal of Faculty of Pharmacy of Ankara University*, 44(1), 18-32.
 64. Rodrigues, G. C. S., dos Santos Maia, M., Silva Cavalcanti, A. B., de Sousa, N. F., Scotti, M. T., & Scotti, L. (2021). In silico studies of lamiaceae diterpenes with bioinsecticide potential against *Aphis gossypii* and *Drosophila melanogaster*. *Molecules*, 26(3), 766.
 65. NIH, National Library of Medicine, <https://pubchem.ncbi.nlm.nih.gov>.
 66. Baskaran, K. P., Arumugam, A., Kandasamy, R., & Alagarsamy, S. (2020). Insilico method for prediction of maximum binding affinity and ligand-protein interaction studies on Alzheimer's disease. *Int J Res Granthaalayah*, 8(11), 362-370.

Toxicological Aspects and Bioanalysis of Nanoparticles: Zebrafish Model

*¹Burcu Yeşilbudak 

¹Çukurova University, Biology Department, Adana, Turkey.
* Corresponding author, e-mail: yesilbudak@gmail.com

Submission Date: 15.10.2022

Acceptation Date: 29.11.2022

Abstract - Nanoparticles increase their availability and diversity in the environment day by day with the natural formation processes of the world geography and the development of advanced technological industry. Due to their intelligent and kaleidoscopic physico-chemical structural forms, they can cause toxic effects in various metabolic steps (in structural proteins, genetic structure, organelles, cells, tissues, organs, metabolic systems) in the organism. Despite these harmful situations some magnetite nanoparticles such as gold nanoparticles, silver nanoparticles, nanodiamonds, dendrimers, polymeric and liposomic smart nanoparticles can be used in medical studies, pharmaceutical industry, nanotheranostic studies and molecular methods. Zebrafish (*Danio rerio*), which is used a model species in many study disciplines, has been used in many studies to reveal the potential toxic effects and positive effects of the tested nanoparticles. Both *in vivo* and *in vitro* test systems and interdisciplinary studies conducted in recent years were analyzed and evaluated via the traditional review method in the current study. Besides, many studies were grouped in order to obtain fast and efficient results on the characterization of nanoparticles and understanding their mechanism of action. A systematic search was conducted based on the keywords of this study in databases such as PubMed, Google Scholar, Web of Science and Carrot², in May 2022. In addition to recognizing the toxic effects of nanoparticles, several studies were emphasized, in which the utilitarian status of nanoparticles in medical, pharmaceutical, molecular and genetic applied studies was understood more clearly day by day.

Keywords: Model species, Nanoparticle, Toxic, Zebrafish

Nanopartiküllerin Toksikolojik Yönleri ve Biyo-Analizleri: Zebra Balığı Modeli

Öz - Nanopartiküller, dünya coğrafyasının doğal oluşum süreçleri ve ileri teknolojik sanayinin gelişimi ile çevredeki bulunurluklarını ve çeşitliliğini her geçen gün arttırmaktadır. Akıllı ve sürekli değişen fiziko-kimyasal yapısal formları nedeniyle organizmada çeşitli metabolik basamaklarda (yapı proteinlerinde, genetik yapıda, organellerde, hücrede, dokuda, organlarda, metabolik sistemlerde) toksik etkilere neden olabilmektedirler. Bu zararlı durumlara karşın altın nanopartiküller, gümüş nanopartiküller, nanoelmaslar, dendrimerler, polimerik ve lipozomik akıllı nanopartiküller gibi bazı manyetit nanopartiküller medikal çalışmalarda, eczacılık endüstrisinde, nanoteranostik çalışmalarda ve moleküler yöntemlerde kullanılabilirlerdir. Birçok çalışma disiplinde model tür olarak kullanılan zebra balığı (*Danio rerio*) test edilen nanopartiküllerin potansiyel toksik etkileri ile pozitif etkilerini ortaya çıkarmak için bir çok çalışmada kullanılmıştır. Halihazırdaki bu çalışmayla son yıllardaki hem *in vivo* hem de *in vitro* test sistemleri ile interdisipliner boyutlu çalışmalar geleneksel derleme yöntemiyle araştırılmış ve değerlendirilmiştir. Ayrıca nanopartiküllerin karakterizasyonları ile etki mekanizmalarını anlamak konusunda hızlı ve verimli sonuçlar almak için birçok çalışma gruplandırılmıştır. Mayıs 2022'de PubMed, Google Scholar, Web of Science ve Carrot² gibi veri tabanlarında bu çalışmanın anahtar kelimeleri baz alınarak sistematik bir tarama yapıldı. Nanopartiküllerin toksik etkilerinin anlaşılmasının yanı sıra medikal, eczacılık, moleküler ve genetik uygulamalı çalışmalarda nanopartiküllerin faydacı durumlarının her geçen gün daha da anlaşıldığı çeşitli çalışmalar vurgulanmıştır.

Anahtar kelimeler: Model tür, Nanopartikül, Toksik, Zebra balığı

¹ Corresponding author: ORCID ID: 0000-0002-3627-0024

E-mail: yesilbudak@gmail.com

1. Introduction

While science has focused on optical and electronic devices with nanoparticle structure for the past half-century, it has now begun to include a large amount of research including nanoparticle-based biological studies and biological measurements made by nanoparticle methods. As the perspective of use of nanoscale materials in advanced technological studies expands, examining their possible toxic effects has become vital in terms of environmental welfare and public health [1]. Nanotechnology has modulated the chemical, physical and optical properties of metals at nanoscale and thus, gained great momentum in the 21st century. The term nano means one billionth of a meter, and these tiny dust particles formed the basis of two- or three-dimensional technological materials [2,3]. Nanoparticles can take many forms such as nanofibers, nanotubes, nanocomposites and nanostructured material [4]. In the use of nanomaterials, it has been shown in many studies that nanomaterials are classified according to their shape and morphology, as well as their composition, agglomeration, size, surface reactivity and uniformity [5,6]. Nanoparticles reach the environment through corrosion processes that occur naturally in the earth's structure, anthropogenic ways and advanced technological studies. Therefore, in recent years, we have had to encounter nanoparticles more and more in our daily lives. Two or three-dimensional particles smaller than 100 nanometers are called nanoparticles and are simply classified into three main groups including carbon-based nanoparticles, metal-based and metal-oxide nanoparticles, and semiconductor-based nanoparticles [3]. Toxic effects of nanoparticles in aquatic ecosystems are increasing in parallel with the increase in advanced technologies [7]. It is stated in many reports that industrial facilities and domestic wastes emitted to wetlands, and nano-sized materials in these wastes also mix with aquatic environments [8]. Many animal models have been used to determine the effect of nanoparticles. Zebrafish (*Danio rerio*), as an important animal model in recent years, has been found suitable for both *in vivo* and *in vitro* studies [9,10,11]. In this systematic review, the studies covering the effects of different types of nanoparticles, which are widely used in many industrial areas, on zebrafish, a member of aquatic ecosystems, in the years between 2007-2022 were discussed. In addition, the application areas, toxicological aspects and bio-measurements of nanoparticles in recent years have been examined. This review was to aim the forming basis for the logistics and problem-based selection of suitable nanoparticles for future studies.

2. Classification of Nanoparticles

2.1. Carbon-based nanoparticles

Carbon-based particles are mostly composed of carbon nanotubes, fullerenes and their derivatives, carbon black, nano diamonds, graphite nanoparticles, graphene nanoparticles and graphene oxide [12]. Fullerenes and multi-walled carbon nanotubes are in these nanoparticles and extremely insoluble in water. In a drug development study, the *in vivo* and *in vitro* effects of various nanoparticles were compared. Accordingly, it was observed that carbon nanoparticles (other than C60 fullerene) such as multi-walled carbon, single-walled carbon and mixed carbon nanotubes caused more stimulation of thrombocyte aggregation than conventional particle (SRM1648, size: 1.4 μ) and accelerated vascular thrombosis in the carotid arteries [13]. Nanodiamonds with their functional convenience and high biocompatibility [14], which have been used in drug design and gene transfer studies in recent years, and carbon C60 nanotubes [15,16] with their antioxidant capacity utilized in environmental, cosmetic and drug design have become very important. Unprocessed forms of nanoparticles, which are increasing in the environment day by day due to their usage areas in the electronics, informatics and aeronatics industries, remain in the air because they are very light. Hence, it has been determined that nanoparticles have the potential to affect living creatures toxicologically by respiration [17].

2.2. Metal-based and metal-oxide nanoparticles

Gold nanoparticles are widely used in biomedical fields due to their various advantages and properties such as adjustable size, easy synthesis, easy modification and strong optical properties [18]. It has been shown that nanoparticles in the cobalt-chromium mixture cause more free radicals, DNA damage, aneuploidy and cytotoxicity in soft tissue cultures than other nanoparticles [19]. The antibacterial, antifungal, antiviral and antiflora properties of silver nanoparticles lead to the use of these particles for biomedical purposes such as antimicrobial agents, drug delivery, molecular imaging, biomedical sensing and even cancer photodynamic therapy [20,21,22,23]. Zinc oxide is generally recognized as safe by the U.S. Food and Drug Administration (FDA) and is called GRAS for short [3]. Some researchers have stated that aluminum oxide (AlO) is less toxic than other metal-based nanomaterials [24,25]. However, crude aluminum has long been known to be a potential neurotoxin [26]. Aluminum oxide (AlO) nanoparticles have been shown to induce cell death by disrupting cellular components both *in vivo* and *in vitro* [27,28]. Testicular damage and changes in gene expression profiles of organisms induced by intragastric administration of titanium dioxide (TiO₂) nanoparticles were investigated. Accordingly, it was observed that TiO₂ nanoparticles crossed the blood-testicular barrier to reach the testis and caused testicular lesions, sperm malformations and changes in serum sex hormone levels. Therefore, the production and application of TiO₂ nanoparticles should be done carefully, especially by people of reproductive age [29]. It is believed that platinum (Pt) nanoparticles can release platinum ions through surface oxidation, which may contribute to their anti-cancerous properties [30]. Superparamagnetic iron oxide nanoparticles (SPION) have great utilitarian potential in a variety of biomedical applications, including magnetic resonance imaging (for example, as contrast agents), drug delivery, hyperthermia, transfections, *in vivo* cell tracking, and tissue repair [31,32,33,34].

2.3. Semiconductor-based and metal-oxide nanoparticles

Quantum dots are processed smart materials that are very important in medical imaging, biomedicine, nanobiotechnology, and microelectronics [35]. Quantum dots are nanometer-scale semiconductor crystals composed of group elements II-VI or III-V. They are defined as particles whose physical dimensions are smaller than the Bohr radius of the exciton [36].

Dendrimers are being used in drug delivery systems due to their flexible dimensions and sizes ranging from 1-100 nm [37]. Silica nanoparticles, also known as silicon dioxide, have received great attention due to their large surface area-volume ratios, adjustable pore size, and unique properties such as connectivity, biocompatibility, and ease of surface modification [38,39]. These features have made them attractive tools for biomedical and biotechnological fields such as medical diagnosis, drug delivery, gene therapy, biomolecule detection, photodynamic therapy, and bioimaging [40]. However, it has been shown that exposure to silica nanoparticles can induce the formation of ROS and cause oxidative stress [41]. Polymeric nanoparticles have been recognized as excellent drug carriers in cancer therapy due to their distinguished pharmacokinetic properties such as drug loading, drug release, structure stability and nanoparticle degradation [42].

3. Utilization and Importance of *Danio rerio* in Toxicity Studies

Nanotechnological elements are preferred in proteomic and genomic analyses using various biomarkers, in various imaging techniques such as ultrasonography (USG), in radiological fields such as magnetic resonance (MR), fluorescent imaging, nuclear and computed tomography, in molecular imaging techniques, in pharmacological studies including targeted cancer treatments and drug development studies, and in many other fields of research based on many other reasons [20,21,22,18,23]. In addition to such useful technological contributions to environmental welfare and human health, various studies have been carried out to determine the toxic effects of nanotechnological elements on respiratory, hematological, neurophysiological, gastrointestinal and dermatological systems due to their advantages in molecular structures [43].

Animal models are useful in investigating the possible physiological, molecular and biochemical effects of such advanced technological products [44]. Not only do zebrafish have many physiological and genetic similarities to human beings including the brain, digestive system, musculature, vasculature, and innate immune system, but also 70% of human disease genes are functionally similar to those of zebrafish [10,11]. In these studies, it was stated that fish was an extremely important vertebrate model in various fields of developmental biology, genetics and toxicology [9].

Many topics have been studied on the effects of a wide variety of nanoparticles on the activities of tissues and organs of *Danio rerio*. These are basically the effects of nanoparticles on fish mortality, fertility, embryo development, oxidative damage, gene expression, hemostasis, body growth, exposure status, swimming performance, histological and biochemical changes followed by cancer diagnosis, drug development, fluorescence emission studies [45,46,47,48,49,50,51,52,53] (Figure 1-2).

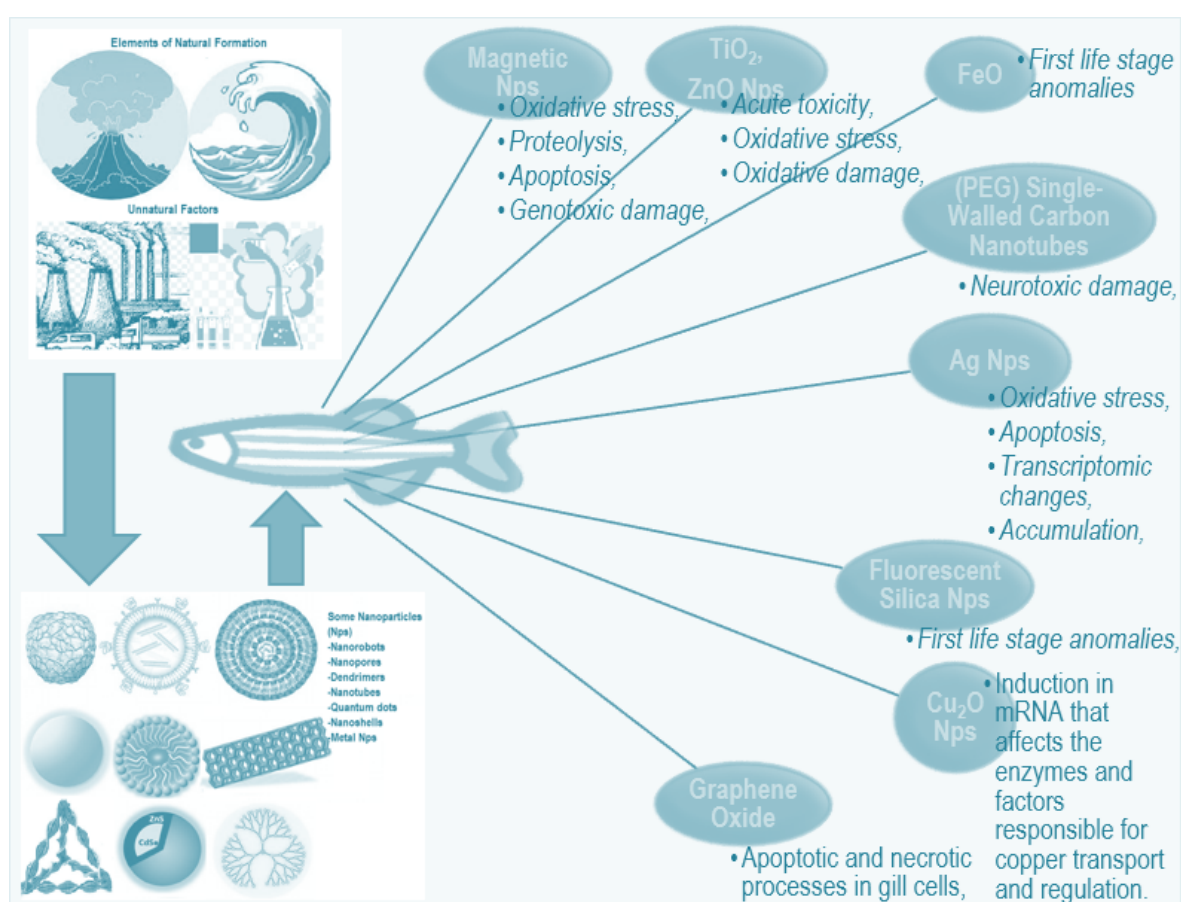


Figure 1. Intoxications of various nanoparticles on *Danio rerio*.

Zebrafish have become popular in the last quarter-century and have been used for a wide variety of purposes. To summarize some of them; it has played an important role in the diagnosis of diseases, parallel studies in genetics and experimental embryology, studies of embryonic axis formation, examination of organogenesis and neural networks, as it allows the development of transparent embryos to be observed in the embryonic development of such vertebrate organisms [54]. The timing of spawning of fish is provided under control with a molecular circadian timer in experimental studies, providing experimental convenience and control [55]. In adult zebrafish, both the fin and heart can quickly repair themselves after an experimental lesion. Zebrafish have optimized cost in all aspects

(time, labor, financial support) due to their ease of maintenance, small size and practicality of the experimental design, the ability to obtain hundreds of embryos per day, and the accessibility of early developmental stages and experimental speed, thus providing various advantages over other model species [54].

4. Bioanalysis Applications of Nanoparticles

A total of 454 articles with a nanoparticles content, which were published between 2007 and 2022 in different disciplines, were searched in web search engines such as PubMed (biomedical database), Google Scholar (full text or metadata of scientific literature), WOS (Web of Science) and Carrot² (cluster database), and the effects of nanoparticles on zebrafish were investigated in May 2022. Accordingly, a total of 155 articles on the effects of different nanoparticles on zebrafish and their distribution over the years were examined. In this study, the theme-based distribution of studies on zebrafish (*Danio rerio*) with a nanoparticles content was visualized by the cluster engine and Office software. Nanoparticulate studies on zebrafish were carried out at most in 2021 (18.72%) and at least in 2012 (0.88%) (Figure 3). Although one may assume that as it is a fish species, the literature review about zebrafish should largely include zoological studies, the review of studies from different disciplines in this study revealed that the most studies were indeed conducted in the field of toxicology (40.53%) and the least in the field of zoology (6.17%) (Figure 4). This shows that zebrafish is an important experimental animal in research and development studies such as toxicity studies [56], drug development [57], nanotheranostic studies [58], and medical-molecular methods [59].

In studies on zebrafish in the fields of toxicology, environmental science, biochemistry and molecular biology, aquatic biology and zoology between 2007 and 2022, the most examined nanoparticles were silver-containing nanoparticles (29.03%), followed by titanium (14.84%), copper (12.90%) and metal-based particles such as zinc oxide (7.10%). The nanoparticles that were studied the least or whose effects aroused the least curiosity were identified to be polymethylmethacrylate (1.29%), fluorescent silica (1.29%), zero-valent iron (0.65%), chromium oxide (1.29%), lead sulfide (1.29%), cobalt coride (1.29%), ponatinib loaded PLGA-PEG-PLGA (1.29%), BSA/ASN/POL (407) (1.29%), cerium oxide (1.29%), palladium (1.29%), ferrous magnetites (1.29%), chitosan and those containing chitosan (1.29%) (Figure 5). Moreover, despite the low use of zero-valent iron nanoparticles in zebrafish, it was stated that zero-valent iron nanoparticles caused developmental toxic disorders in early life stages at a higher rate than oxidation products in another fish species, *Oryzias latipes* [60].

Various analyse methods were performed to determine the effects of different nanoparticles on zebrafish. The most common types of bioanalysis tests conducted were zebrafish's liver glutathione activity (GSH) (14.19%), apoptosis mechanism (10.97%), fish larval development anomalies (10.32%), polymerase chain reaction (qRT-PCR) (7.1%), and neurotoxicity (5.81%). Food chain (1.94%), environmental risk assessment (1.29%), fish skeletal development (1.94%), and mRNA-enabled studies of the first life stage (1.94%) were among the least studied subjects (Figure 6). Despite the limited number of studies conducted on the trophic transmission of TiO₂ [61] and ZnO [62] nanoparticles to zebrafish, trophic-level environmental monitoring studies were based only on certain nanoparticles. In fact, there was very little information about these substances due to many reasons such as the lack of methods in distinguishing the size and form of nanoparticles, and the uncertainty of their long-term toxicological effects. As a result, it becomes difficult to follow the studies on this subject in environmental welfare and public health studies [63].

In a study, in which an inulin-based fructan obtained from chicory plant extract was structured and characterized with selenium nanoparticles (CIP-SeNPs) to improve antitumor effects, CIP-SeNPs were found to significantly suppress the proliferation and spread of tumors as well as angiogenesis in transgenic zebrafish in the concentration range of 1-4 µg/mL [57]. It was shown that PLGA-PEG-PLGA nanoparticles loaded with ponatinib at a concentration of 001 mg/ml were not cardiotoxic in

the conventional zebrafish xenograft model [64]. It was also revealed that many nanoparticle therapies used in the diagnosis and treatment of various types of cancer could be usefully utilized as an initial step (Figure 7). In addition, gold nanocluster-based ratiometric fluorescent probes were used as a sensitive biosensor for rapid biological detection and imaging of mercury ions in zebrafish [65]. Titanium dioxide nanoparticles (TiO₂) were reported to alleviate cardiotoxicity by reducing the bioconcentration of azoxystrobin and changes in cardiac-related gene expression in zebrafish larvae.

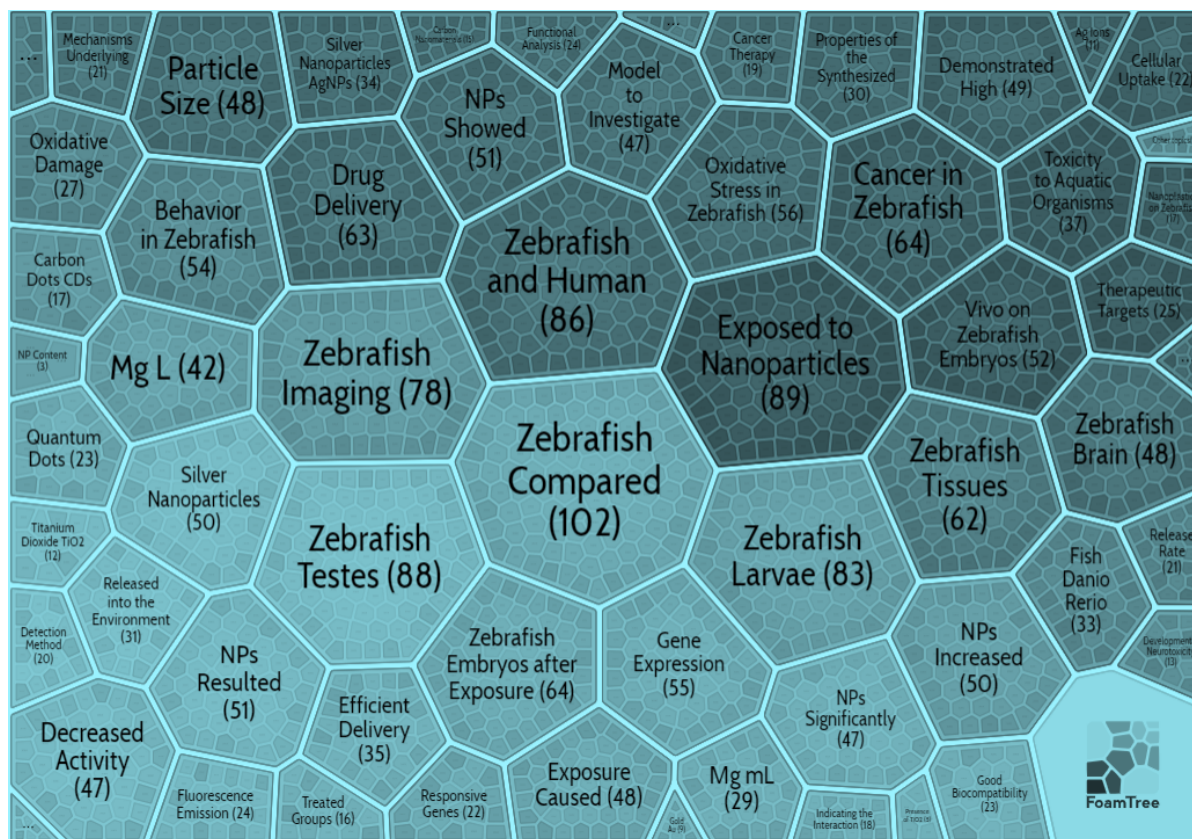


Figure 2. Thematic distribution of nanoparticle studies applied on *Danio rerio*.

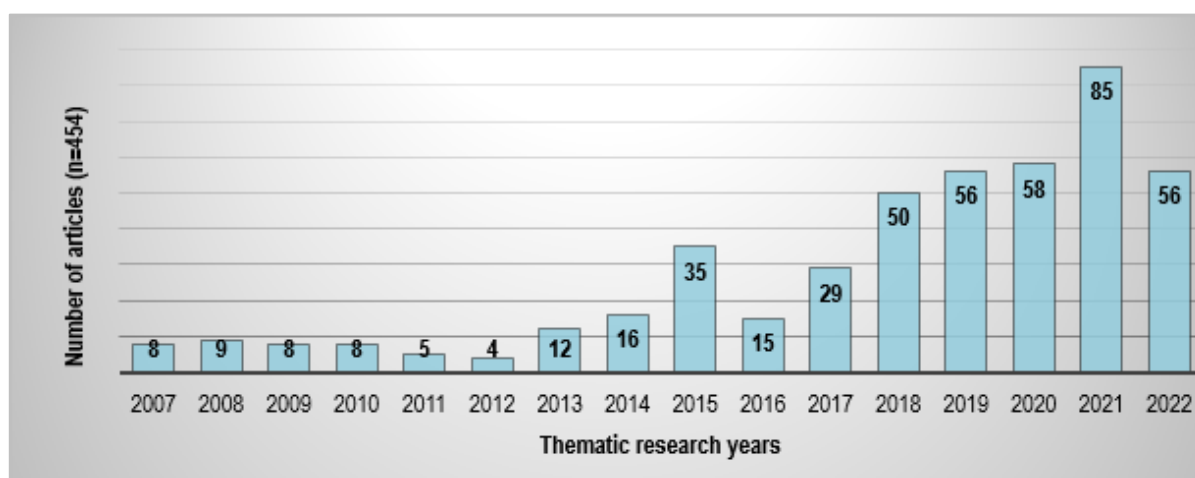


Figure 3. Distribution of nanoparticle-containing studies *Danio rerio* by years between 2007-2022.

In further studies, it was determined that azoxystrobin and TiO₂ nanoparticles together reduced total-ATPase and Ca²⁺ ATPase, Na⁺/K⁺-ATPase activities [66]. As a new approach to

ecological risk management, this and similar studies are important in creating a biosensor in the organism as a protection method against the toxicity caused by the common relationships of pollutants in the environment and examining the changes in gene expression and enzyme activities as a response to the various effects of pollutants (Figure 7).

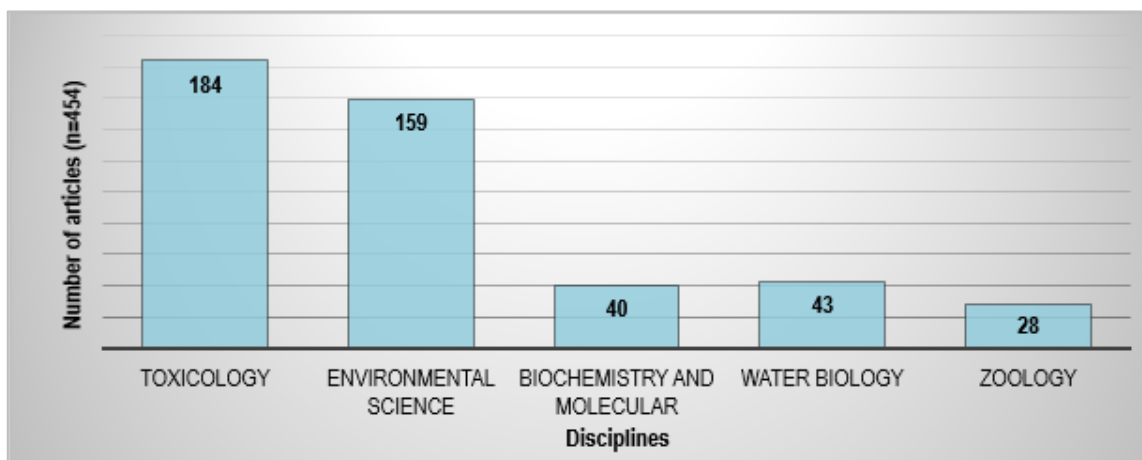


Figure 4. Distribution of nanoparticles studied on *Danio rerio* between 2007-2022 according to scientific disciplines.

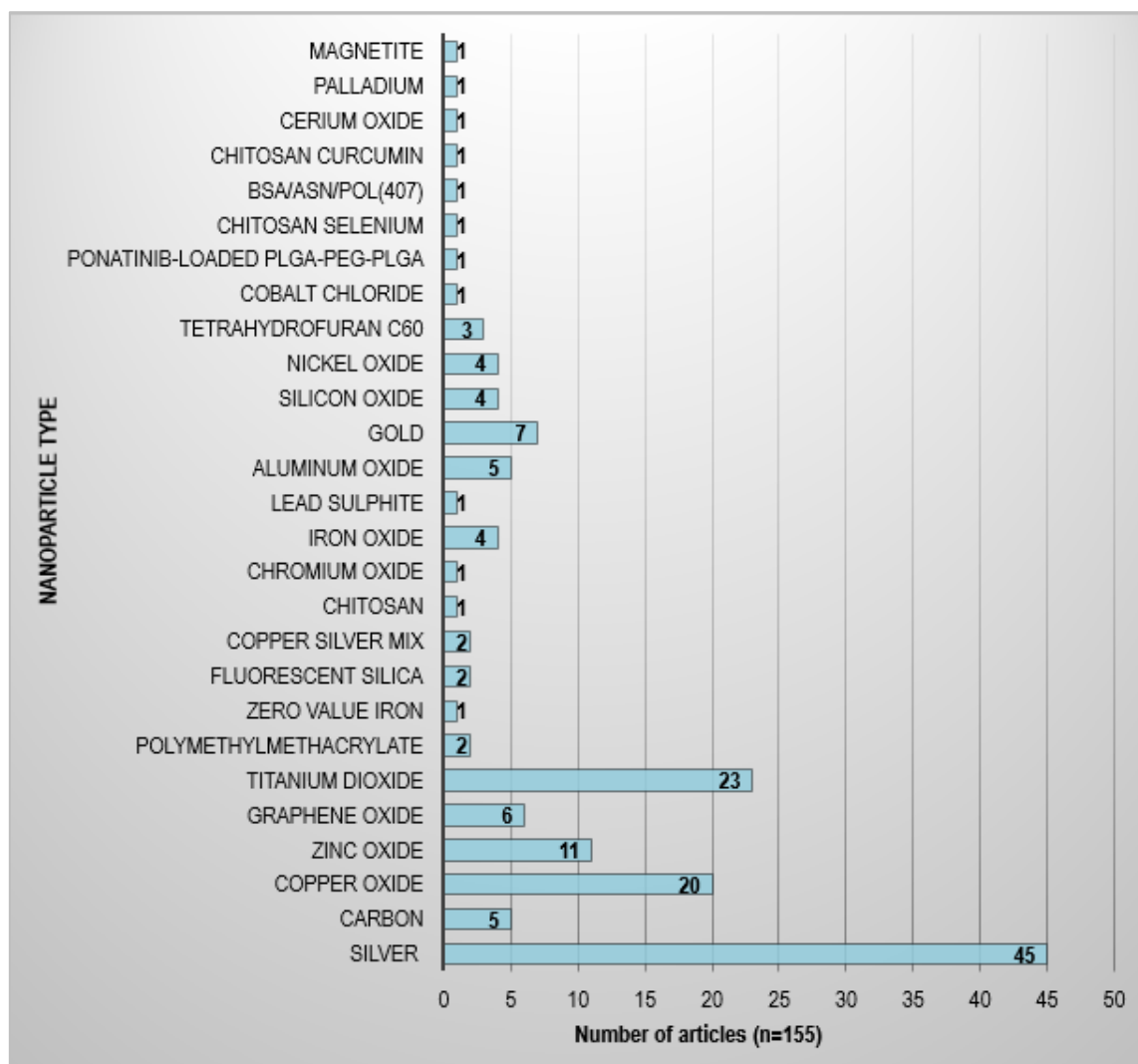


Figure 5. Number and types of nanoparticles studied on *Danio rerio* by years between 2007-2022.

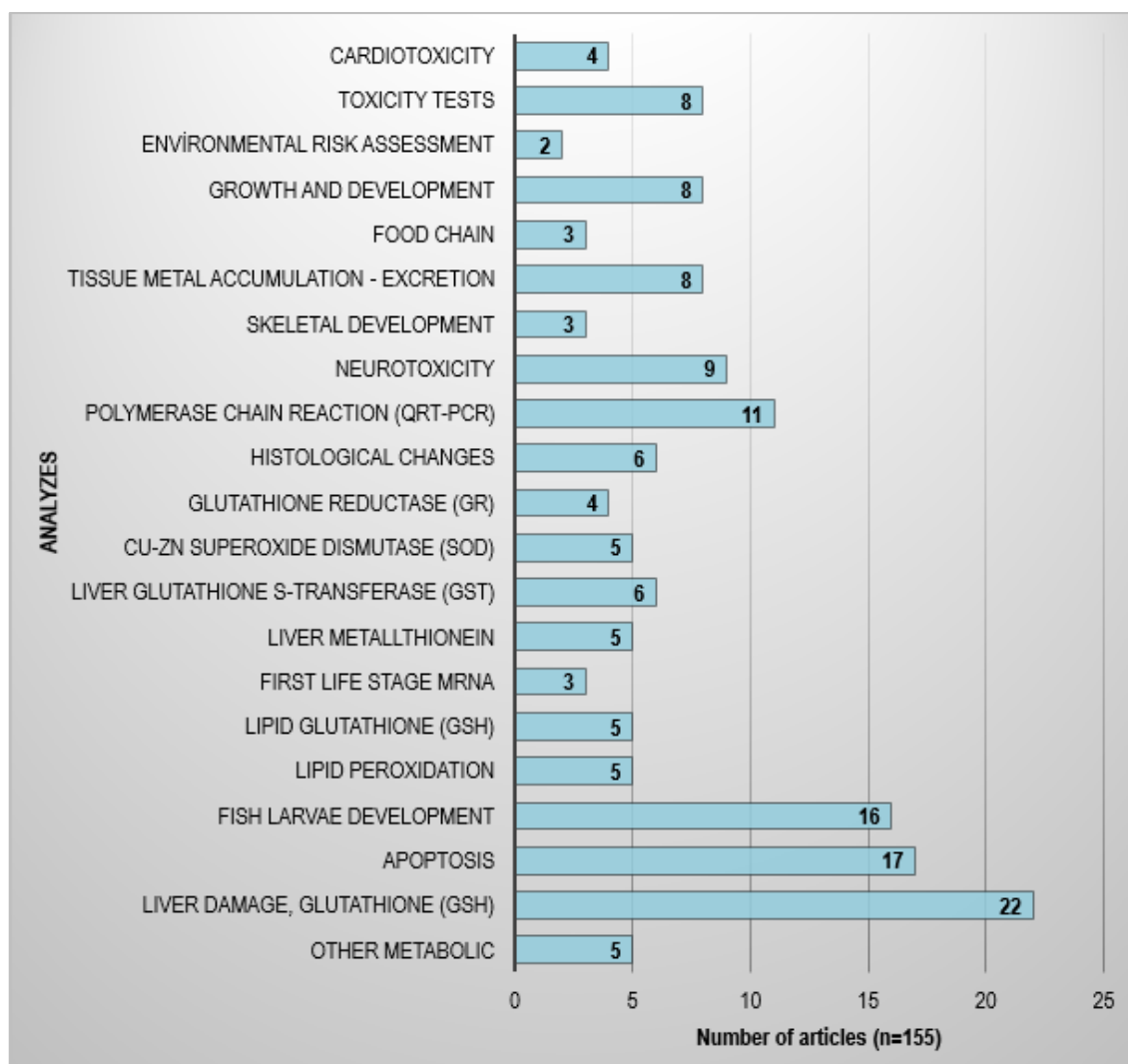


Figure 6. Analysis of the nanoparticle effects on *Danio rerio* in recent years.

5. Conclusions

The studies on the subject in pure zoology, biochemistry and molecular-based fields, which form the basis of applied sciences, are less than the others (Figure 4). It is thought that especially the small number of nanoparticles indicated in Figure 5 will provide advantages and innovations in medicine-based molecular studies and health technology (Figure 7). There is no homogeneous distribution between the environmental risk analyzes, metabolic function of the organism and mRNA studies of the analyzes of nanoparticles and the oxidative stress parameters that have been studied much (Figure 6). It should be ensured that bioanalyses are functionalized in application areas with a holistic perspective.

References

- [1] Kroll, A., Pillukat, M. H., Hahn, D., and Schnekenburger, J. (2009). Current in vitro methods in nanoparticle risk assessment: limitations and challenges. *Euro. J. Pharmaceut. Biopharmac.*, 72(2), 370-377. DOI:10.1016/j.ejpb.2008.08.009
- [2] Gong P, Li H, He X, Wang K, Hu J, and Tan W. (2007). Preparation and antibacterial activity of Fe₃O₄@ Ag nanoparticles. *Nanotech.*, 18(28), 285604.
- [3] Jiang, J., Pi, J., and Cai, J. (2018). The advancing of zinc oxide nanoparticles for biomedical applications. *Bioinorganic Chemistry and Applications*, 1-18. DOI:10.1155/2018/1062562.
- [4] Asmatulu, R., Nguyen, P., and Asmatulu, E. (2013). Nanotechnology safety in the automotive industry. In *Nanotech*. Elsevier, Amsterdam, pp 57-72. DOI:10.1016/B978-0-444-59438-9.00005-9.
- [5] Buzea, C., Pacheco, I., and Robbie, K. (2007). Nanomaterials and nanoparticles: sources and toxicity. *Biointerphases*, 2(4), Mr17-Mr71. DOI:10.1116/1.2815690
- [6] Rizwan, M., Shoukat, A., Ayub, A., Razzaq, B., and Tahir, M.B. (2021). Types and classification of nanomaterials. In *Nanomaterials: Synthesis, Characterization, Hazards and Safety*. Elsevier, Amsterdam, pp. 31-54.
- [7] Domingos, R.F., Tufenkji, N., and Wilkinson, K.J. (2009). Aggregation of titanium dioxide nanoparticles: role of a fulvic acid. *Environ. Sci. Tech.*, 43(5),1282-1286. DOI: 10.1021/es8023594.
- [8] Daughton, C.G. (2004). Non-regulated water contaminants: Emerging research. *Environment. Impact. Assess. Rev.*, 24, 711-732. DOI: 10.1016/j.eiar.2004.06.003.
- [9] Asztemborska, M., Jakubiak, M., Książyk, M., Stęborowski, R., Polkowska-Motrenko, H., and Bystrzejska-Piotrowska, G. (2014). Silver nanoparticle accumulation by aquatic organisms-neutron activation as a tool for the environmental fate of nanoparticles tracing. *Nukleonika*, 59(4), 169-173. DOI: 10.2478/nuka-2014-0023.
- [10] Santoriello, C. and Zon, L.I. (2012). Hooked! Modeling human disease in zebrafish. *The J. Clin. Invest.*, 122(7), 2337-2343. DOI:10.1172/JCI60434
- [11] Zhao, S., Huang, J., and Ye, J. (2015). A fresh look at zebrafish from the perspective of cancer research. *J. Experiment. Clin. Cancer. Res.*, 34(1), 1-9. DOI: 10.1186/s13046-015-0196-8.
- [12] Patel, K.D., Singh, R.K., and Kim, H.W. (2019). Carbon-based nanomaterials as an emerging platform for theranostics. *Mater. Horiz.*, 6(3), 434-469. DOI:10.1039/c8mh00966j.
- [13] Radomski, A., Jurasz, P., Alonso-Escolano, D., Drews, M., Morandi, M., Malinski, T., and Radomski, M.W. (2005). Nanoparticle-induced platelet aggregation and vascular thrombosis. *Br. J. Pharmacol.*, 146, 882-893. DOI:10.1038/sj.bjp.0706386.
- [14] Mengesha, A.E. and Youan, B.B.C. (2013). Nanodiamonds for drug delivery systems. In *Diamond-based materials for biomedical applications*. Woodhead Publishing, Cambridge, pp. 186-205. DOI:10.1533/9780857093516.2.186.
- [15] Aschberger, K., Johnston, H., Stone, V., Aitken, R., Tran, C., Hankin, S., Peters, S., and Christensen, F. (2010). Review of fullerene toxicity and exposure-appraisal of a human health risk assessment, based on open literature. *Regul. Toxicol. Pharmacol.*, 58(3), 455-473. DOI:10.1016/j.yrtph.2010.08.017.
- [16] Ming, Z., Feng, S., Yilihamu, A., Ma, Q., Yang, S., and Yang, S. T. (2018). Toxicity of pristine and chemically functionalized fullerenes to white rot fungus *Phanerochaete chrysosporium*. *Nanomater.*, 8(2), 120. DOI:doi.org/10.3390/nano8020120.

- [17] Asmatulu, E., Andalib, M.N., Subeshan, B., and Abedin, F. (2022). Impact of nanomaterials on human health: a review. *Environ. Chem. Lett.*, 1-21.
- [18] Jia, Y.P, Ma, B.Y., Wei, X.W., and Qian, Z.Y., (2017). The *in vitro* and *in vivo* toxicity of gold nanoparticles. *Chin. Chem. Lett.*, 28(4), 691-702. DOI:10.1016/j.ccllet.2017.01.021.
- [19] Papageorgiou, I., Brown, C., Schins, R., Singh, S., Newson, R., and Davis, S. (2007). The effect of nano- and micron-sized particles of cobalt-chromium alloy on human fibroblasts *in vitro*. *Biomater.*, 28(19), 2946-2958. DOI:10.1016/j.biomaterials.2007.02.034.
- [20] Cameron, S.J., Hosseini, F., Willmore, W.G. (2018). A current overview of the biological and cellular effects of nanosilver. *Int. J. Mol. Sci.*, 19(7), 2030. DOI:10.3390/ijms19072030.
- [21] Chen, L.Q., Fang, L., Ling, J., Ding, C.Z., Kang, B., and Huang, C.Z. (2015). Nanotoxicity of silver nanoparticles to red blood cells: size dependent adsorption, uptake, and hemolytic activity. *Chem. Res. Toxicol.*, 28(3), 501-509. DOI:10.1021/tx500479m.
- [22] Guo, Z., Zeng, G., Cui, K., Chen, A. (2019). Toxicity of environmental nanosilver: mechanism and assessment. *Environ. Chem Lett.* 17(1), 319-333. DOI:10.1007/s10311-018-0800-1.
- [23] Pulit-Prociak, J., Stokłosa, K., and Banach, M. (2014). Nanosilver products and toxicity. *Environ. Chem. Lett.*, 13(1), 59-68. DOI:10.1007/s10311-014-0490-2.
- [24] Radzium, E., Wilczyńska, J.D., Książek, I., Nowak, K., Anuszevska, E.L., Kunicki, A., Olszyna, A., and Ząbkowski, T. (2011). Assessment of the cytotoxicity of aluminum oxide nanoparticles on selected mammalian cells. *Toxicol. In Vitro*, 25, 1694-1700. DOI:10.1016/j.tiv.2011.07.010.
- [25] Sun, J., Wang, S., Zhao, D., Hun, F.H., Weng, L., and Liu, H. (2011). Cytotoxicity, permeability, and inflammation of metal oxide nanoparticles in human cardiac microvascular endothelial cells: cytotoxicity, permeability, and inflammation of metal oxide nanoparticles. *Cell. Biol. Toxicol.*, 27, 333-342. DOI:10.1007/s10565-011-9191-9.
- [26] Kumar, V. and Gill, K.D. (2009). Aluminium neurotoxicity: neurobehavioural and oxidative aspects. *Archives of toxicology*, 83(11), 965-978. DOI:10.1007/s00204-009-0455-6.
- [27] Alshatwi, A.A., Vaiyapuri Subbarayan, P., Ramesh, E., Al-Hazzani, A.A., Alsaif, M.A., and Alwarthan, A.A. (2012). Al₂O₃ nanoparticles induce mitochondriamediated cell death and upregulate the expression of signaling genes in human mesenchymal stem cells. *J. Biochem. Mol. Toxicol.*, 26, 469-476. DOI:10.1002/jbt.21448.
- [28] Zhang, Q.L., Li, M.Q., Ji, J.W., Gao, F.P., Bai, R., Chen, C.Y., Wang, Z.W., Zhang, C., and Niu, Q. (2011). In vivo toxicity of nano-alumina on mice neurobehavioral profiles and the potential mechanisms. *Int. J. Immunopathol. Pharmacol.* 24(1), 23S-29S. PMID: 21329562.
- [29] Gao, G., Ze, Y., Zhao, X., Sang, X., Zheng, L., Ze, X., Gui, S., Sheng, L., Sun, Q., Hong, J., Yu, X., Wang, L., and Zhang, F.H. (2013) Titanium dioxide nanoparticle-induced testicular damage, spermatogenesis suppression, and gene expression alterations in male mice. *J. Hazard. Mater.*, 258, 133-143. DOI:10.1016/j.jhazmat.2013.04.046
- [30] Gao, J., Liang, G., Zhang, B., Kuang, Y., Zhang, X., and Xu, B. (2007). FePt@CoS(2) yolk-shell nanocrystals as a potent agent to kill HeLa cells. *J. Am. Chem. Soc.*, 129, 1428-1433. DOI:10.1021/ja067785e.
- [31] Laurent, S., Duts, S., Hafeli, U., and Mahmoudi, M. (2011). Magnetic fluid hyperthermia: Focus on superparamagnetic iron oxide nanoparticles. *Adv. Colloid Interface Sci.*, 166, 8-23. DOI:10.1016/j.cis.2011.04.003.
- [32] Mahmoudi, M., Hosseinkhani, H., Hosseinkhani, M., Boutry, S., Simchi, A., Journeay, W.

S., Subramani, K., and Laurent, S. (2011). Magnetic resonance imaging tracking of stem cells in vivo using iron oxide nanoparticles as a tool for the advancement of clinical regenerative medicine. *Chem. Rev.*, 111, 253-280. DOI:10.1021/cr1001832.

[33] Mailander, V., Lorenz, M. R., Holzapfel, V., Musyanovych, A., Fuchs, K., Wiesneth, M., Walther, P., Landfester, K., and Schrezenmeier, H. (2008). Carboxylated superparamagnetic iron oxide particles label cells intracellularly without transfection agents. *Mol. Imaging Biol.*, 10, 138-146. DOI:10.1007/s11307-007-0130-3.

[34] Gupta, A. K., Naregalkar, R.R., Vaidya, V.D., and Gupta, M. (2007). Recent advances on surface engineering of magnetic iron oxide nanoparticles and their biomedical applications. *Nanomed.* 2, 23-39. DOI:10.2217/17435889.2.1.23.

[35] Anonymous. (2022). Nanotechnology Now. Retrieved from <http://www.nanotechnology.com/2003-Awards>. (21.08.2022)

[36] Chan, W.C.W., Maxwell, D.J., Gao, X.H., Bailey, R.E., Han, M.Y., and Nie, S.M. (2002). Luminescent quantum dots for multiplexed biological detection and imaging. *Curr. Opin. Biotech.*, 13, 40-6. DOI:10.1016/S0958-1669(02)00282-3.

[37] Babu, V.R., Nikhat, M.S.R., and Srikanth, G. (2010). Dendrimers: a new carrier system for drug delivery. *Int. J. Pharmaceutic. App.Sci.*, 1(1), 1-10.

[38] Geranio, L., Hommes, G., Shahgaldian, P., Wirth-Heller, A., Pielas, U., and Corvini, P.F.X. (2010). Radio (¹⁴C)-and fluorescent-doubly labeled silica nanoparticles for biological and environmental toxicity assessment. *Environ. Chem. Lett.*, 8(3), 247-251. DOI:10.1007/s10311-009-0213-2.

[39] Kim, I.S., Baek, M., and Choi, S-J. (2010). Comparative cytotoxicity of Al₂O₃, CeO₂, TiO₂ and ZnO nanoparticles to human lung cells. *J. Nanosci. Nanotechnol.*, 10(5), 3453-3458. DOI:10.1166/jnn.2010.2340.

[40] Duan, J., Yu, Y., Li, Y., Yu, Y., Li, Y., Zhou, X., Huang, P., and Sun, Z. (2013). Toxic effect of silica nanoparticles on endothelial cells through DNA damage response via Chk1-dependent G2/M checkpoint. *PLOS ONE* 8(4), e62087. DOI:10.1371/journal.pone.0062087.

[41] Zhou, F., Liao, F., Chen, L., Liu, Y, Wang, W., and Feng, S. (2019). The sizedependent genotoxicity and oxidative stress of silica nanoparticles on endothelial cells. *Environ. Sci. Pollut. Res. Int.*, 26(2), 1911-1920. DOI:10.1007/s11356-018-3695-2.

[42] Li, A., Zhang, C., and Zhang, Y.F. (2017). Thermal conductivity of graphene-polymer composites: Mechanisms, properties, and applications. *Polyme*, 9(9), 437. DOI:10.3390/polym9090437.

[43] Medina, C., Santos-Martinez, M.J., Radomski, A., Corrigan, O.I., and Radomski, M.W. (2007). Nanoparticles: pharmacological and toxicological significance. *Br. J. Pharmacol.*, 150(5), 552-558. DOI:10.1038/sj.bjp.0707130.

[44] Kumari, M., Singla, M., Sobti, R.C. (2022). Animal models and their substitutes in biomedical research. In *Advances in Animal Experimentation and Modeling*. Academic Press, Cambridge, 87-101. DOI:10.1016/B978-0-323-90583-1.00014-3.

[45] Chen, D., Zhang, D., Jimmy, C. Y., and Chan, K.M. (2011). Effects of Cu₂O nanoparticle and CuCl₂ on zebrafish larvae and a liver cell-line. *Aquat. Toxicol.*, 105(3-4), 344-354. DOI:10.1016/j.aquatox.2011.07.005.

[46] Choi, J. E., Kim, S., Ahn, J. H., Youn, P., Kang, J. S., Park, K., and Ryu, D.Y. (2010). Induction of oxidative stress and apoptosis by silver nanoparticles in the liver of adult

zebrafish. *Aquat. Toxicol.*, 100(2), 151-159. DOI: 10.1016/j.aquatox.2009.12.012.

[47] Fent, K., Weisbrod, C. J., Wirth-Heller, A., and Pieves, U. (2010). Assessment of uptake and toxicity of fluorescent silica nanoparticles in zebrafish (*Danio rerio*) early life stages. *Aquat. Toxicol.*, 100(2), 218-228. DOI: 10.1016/j.aquatox.2010.02.019.

[48] Griffitt, R.J., Lavelle, C.M., Kane, A.S., Denslow, N.D., and Barber, D.S. (2013). Chronic nanoparticulate silver exposure results in tissue accumulation and transcriptomic changes in zebrafish. *Aquat. Toxicol.*, 130, 192-200. DOI: 10.1016/j.aquatox.2013.01.010.

[49] Kaloyianni, M., Dimitriadi, A., Ovezik, M., Stamkopoulou, D., Feidantsis, K., Kastrinaki, G., Gallios, G., Tsiaoussis, I., Koumoundouros, G., and Bobori, D. (2020). Magnetite nanoparticles effects on adverse responses of aquatic and terrestrial animal models. *J. Hazard. Material.*, 383, 121204. DOI:10.1016/j.jhazmat.2019.121204.

[50] Souza, J.P., Baretta, J.F., Santos, F., Paino, I.M., and Zucolotto, V. (2017). Toxicological effects of graphene oxide on adult zebrafish (*Danio rerio*). *Aquat. Toxicol.*, 186, 11-18. DOI: 10.1016/j.aquatox.2017.02.017.

[51] Weber, G.E., Dal Bosco, L., Gonçalves, C.O., Santos, A.P., Fantini, C., Furtado, C.A. and Barros, D.M. (2014). Biodistribution and toxicological study of PEGylated single-wall carbon nanotubes in the zebrafish (*Danio rerio*) nervous system. *Toxicol. App. Pharmacol.*, 280(3), 484-492. DOI: 10.1016/j.taap.2014.08.018.

[52] Xiong, D., Fang, T., Yu, L., Sima, X., and Zhu, W. (2011). Effects of nano-scale TiO₂, ZnO and their bulk counterparts on zebrafish: acute toxicity, oxidative stress and oxidative damage. *Sci. Total Environ.*, 409, 1444-1452. DOI:10.1016/j.scitotenv. 2011.01.015.

[53] Zhu, X., Tian, S., and Cai, Z. (2012). Toxicity assessment of iron oxide nanoparticles in zebrafish (*Danio rerio*) early life stages. *PLoS One* 7(9), e46286. DOI:10.1371/journal.pone.0046286.

[54] Holtzman, N. G., Iovine, M. K., Liang, J. O., and Morris, J. (2016). Learning to fish with genetics: a primer on the vertebrate model *Danio rerio*. *Genetics*, 203(3), 1069-1089. DOI: 10.1534/genetics.116.190843 .

[55] Blanco-Vives, B., and Sanchez-Vazquez, F. J. (2009). Synchronisation to light and feeding time of circadian rhythms of spawning and locomotor activity in zebrafish. *Physiol. Behav.*, 98, 268-275. DOI: 10.1016/j.physbeh.2009.05.015 .

[56] Wang, X. and Wang, W.X. (2022). Cu-based nanoparticle toxicity to zebrafish cells regulated by cellular discharges. *Environ. Pollut.*, 292, 118296. DOI:10.1016/j.envpol.2021.118296

[57] Shi, L., Li, Y., Zhang, S., Gong, X., Xu, J., and Guo, Y. (2022). Construction of inulin-based selenium nanoparticles to improve the antitumor activity of an inulin-type fructan from chicory. *Int. J. Biol. Macromolecul.*, 210, 261-270. DOI:10.1016/j.ijbiomac.2022.04.125.

[58] Igartúa, D.E., Azcona, P. L., Martinez, C.S., del Valle Alonso, S., Lassalle, V. L., and Prieto, M.J. (2018). Folic acid magnetic nanotheranostics for delivering doxorubicin: toxicological and biocompatibility studies on Zebrafish embryo and larvae. *Toxicol. App. Pharmacol.*, 358, 23-34. DOI:10.1016/j.taap.2018.09.009.

[59] Nellore, J., Pauline, C., and Amarnath, K. (2013). Bacopa monnieri phytochemicals mediated synthesis of platinum nanoparticles and its neurorescue effect on 1-methyl 4-phenyl 1, 2, 3, 6 tetrahydropyridine-induced experimental parkinsonism in zebrafish. *J. Neurodegener. Dis.*, 2013, 1-8. DOI:10.1155/2013/972391.

[60] Chen, P.J., Wu, W.L., and Wu, K.C.W. (2013). The zerovalent iron nanoparticle causes higher

developmental toxicity than its oxidation products in early life stages of medaka fish. *Wat. Res.*, 47(12), 3899-3909. DOI:10.1016/j.watres.2012.12.043.

[61] Zhu, X., Wang, J., Zhang, X., Chang, Y., and Chen, Y. (2010). Trophic transfer of TiO₂ nanoparticles from daphnia to zebrafish in a simplified freshwater food chain. *Chemosph.*, 79(9), 928-933. DOI: 10.1016/j.chemosphere.2010.03.022.

[62] Skjolding, L.M., Winther-Nielsen, M., and Baun, A. (2014). Trophic transfer of differently functionalized zinc oxide nanoparticles from crustaceans (*Daphnia magna*) to zebrafish (*Danio rerio*). *Aquat. Toxicol.*, 157, 101-108. DOI:10.1016/j.aquatox.2014.10.005.

[63] Boxall, A.B.A., Chaundhry, Q., Sinclair, C., Jones, A., Aitken, R., Jefferson, B., and Watts, C. (2007). Current and future predicted environmental exposure to engineered nanoparticles. Report by the Central Science Laboratory (CSL) York for the Department of the Environment and Rural Affairs (DEFRA), UK, pp. 89.

[64] Al-Thani, H. F., Shurbaji, S., Zakaria, Z. Z., Hasan, M. H., Goracinova, K., Korashy, H. M., and Yalcin, H.C. (2022). Reduced Cardiotoxicity of Ponatinib-Loaded PLGA-PEG-PLGA Nanoparticles in Zebrafish Xenograft Model. *Material.*, 15(11), 3960. DOI:10.3390/ma15113960.

[65] Yu, F., Xiang, H., He, S., Zhao, G., Cao, Z., Yang, L., and Liu, H. (2022). Gold nanocluster-based ratiometric fluorescent probe for biosensing of Hg²⁺ ions in living organisms. *Analyst.* 147, 2773-2778. DOI:10.1039/D2AN00369D.

[66] Nie, H., Pan, M., Chen, J., Yang, Q., Hung, T.C., Xing, D., Peng, M., Peng, X., Li, G., and Yan, W. (2022). Titanium dioxide nanoparticles decreases bioconcentration of azoxystrobin in zebrafish larvae leading to the alleviation of cardiotoxicity. *Chemosph.*, 307, 135977. DOI:10.1016/j.chemosphere.2022.135977.

Sonochemical Removal of Highly Toxic Aqueous Cd²⁺ and Cr⁶⁺ Ions Using Dandelion-like Co₃O₄ Nanoflowers

¹Elif Aybike Berberoğlu , ^{2,3}Mümin Mehmet Koç , ¹Nurdan Kurnaz Yetim , *¹Cemile Özcan 

¹ Kırklareli University, Department of Chemistry, Faculty of Literature and Sciences, Kırklareli, Türkiye.

² Kırklareli University, Department of Medical Service and Techniques, School of Medical Service, Kırklareli, Türkiye.

³ Kırklareli University, Department of Physics, Faculty of Literature and Sciences, Kırklareli, Türkiye.

* Corresponding author, e-mail: cemilebal.ozcan@klu.edu.tr

Submission Date: 20.10.2022

Acceptation Date: 05.01.2023

Abstract –In this work, cobalt(II/III) oxide (Co₃O₄) nano/microflowers were practically synthesized in laboratory conditions. Adsorbance properties of the nanoflowers were investigated for the removal of cadmium and chromium heavy metal ions. To assess the chemical and morphological characteristics of Co₃O₄ nanoflowers, Fourier transform infrared spectroscopy (FTIR), X-ray diffractometry (XRD), field emission electron microscopy (FESEM), Energy dispersive spectroscopy (EDS), and was used. To determine the adsorbance mechanism in detail, eluent concentration, eluent type, solution pH, adsorbent amount, solution volume, and adsorption duration were studied. In these assessments, flame atomic absorption spectroscopy (FAAS) was used. For Cr⁶⁺, adsorption optimum parameters were determined as 3M HNO₃, pH 6.5, 150mg, 30mL, 60min. For Cd²⁺, optimum parameters were determined as 3M HNO₃, pH 6.0, 100mg, 10mL, 30min. Co₃O₄, nanoflowers are eco-friendly adsorbent materials for the adsorption of Cd⁶⁺ and Cd²⁺ heavy metal ions since the production method is affordable and practical.

Keywords: Co₃O₄ Nanoflowers; Solid phase extraction; FAAS; Cr⁶⁺; Cd²⁺

Yüksek Toksikiteye Sahip Cd²⁺ and Cr⁶⁺ İyonlarının Karahindiba Şeklindeki Co₃O₄ Nanoçiçek Yapılar Kullanılarak Sonokimyasal Yöntemle Sudan Ayrıştırılması

Öz - Bu çalışmada, hidrotermal yöntem ile kobalt(II/III) oksit (Co₃O₄) nano/mikroçiçek yapılar laboratuvar şartlarında pratik bir şekilde sentezlendi. Krom ve kadmiyum gibi ağır metal iyonlarının uzaklaştırılması için bu nanoflowerların adsorban olarak uygulanması araştırıldı. Co₃O₄ nanoçiçeklerinin, morfolojik analizi ve kimyasal bileşimini karakterize etmek için X ışını kırınım analizi (XRD), alan emisyonlu taramalı elektron mikroskopisi (FESEM), enerji dağılım X-ışınları spektroskopisi (EDS) ve FTIR teknikleri kullanılarak gerçekleştirildi. Adsorpsiyon sisteminin optimum koşullarını belirlemek amacı ile elüent derişimi ve türü, çözeltinin pH'ı, adsorban miktarı, çözelti hacmi ve adsorpsiyon süresi gibi parametrelerin etkisi incelendi. Elde edilen çözeltide metal iyonlarının alevli atomik adsorpsiyon spektrometrisi (FAAS) analiz sonuçları doğrultusunda optimumum parametreler belirlendi. Bu parametre sonuçları sırasıyla Co₃O₄ nanofloweri ile Cr⁶⁺ için 3 M HNO₃, pH 6.5, 150 mg, 30 mL, 60 dk; Cd²⁺ için 3 M HNO₃, pH 6.0, 100 mg, 10 mL, 30 dk olarak bulundu. Co₃O₄ nanoçiçekleri; adsorpsiyon kapasitelerinin yüksek olması, kolayca sentezlenebilir ve imalat maliyetlerinin nispeten düşük olmasından dolayı krom, kadmiyum ve diğer ağır metal iyonlarının sulu sistemlerden uzaklaştırılmasında verimli ve çevre dostu adsorbanlar olabileceklerini göstermektedirler.

Anahtar kelimeler: Co₃O₄ Nanoçiçekler; Katı faz ekstrasyonu; FAAS; Cr⁶⁺; Cd²⁺

¹ Corresponding author: Tel: +90 028 824 6173 - Extension: 1150
E-mail: cemilebal.ozcan@klu.edu.tr

1. Introduction

Heavy metals were detected different water sources around the world, and they can be used in different industrial products including dyes, pharmaceuticals, personal hygiene products, etc [1, 2]. Contamination of fresh waters and aquatic systems by heavy metals is becoming an emerging problem for the world. Such contaminated waters could include different heavy metal ions such as Hg(II), Pb(II), Cr(VI), Cd(II), and Ni [2]. Such heavy metal ions were found to be toxic and can be dangerous to marine life and aquatic animals [3–5]. Different research illustrates that, several unit operations such as adsorption, membrane filtration, chemical precipitation, coagulation - flocculation and floatation, ion exchange, or liquid-liquid extraction can be utilized to separate heavy metals from the samples [5–8]. Among those, adsorption is a common method where a low cost, selective, reusable and simple application was promised [5–8].

Recently, various materials like activated carbon, activated alumina, clay, zeolite, etc. were used for the removal of heavy metal ions [5–8]. However, such materials have limited adsorption capacity and some of them are not reusable. On contrary, metal oxide nanostructures have outstanding adsorption capacity due to their high surface/volume ratio and well-defined surface morphology [9]. Therefore, they found to be promising materials as next generation adsorbent materials.

Nanostructures are becoming attractive materials for the people from different areas since they can be applied to semiconductors and different technological applications due to their interesting chemical and physical properties with outstanding morphology [10]. Recently, three dimensional (3D) nanostructures with well-defined morphologies increases their popularity [11, 12]. Among those, nanoflowers in fiber, tube and flake forms are becoming popular due to their unique structural characteristics [11]. Co₃O₄ nanoflowers are a special kind of nanoflowers with magnetic characteristics which can be used in magnetic applications, gas sensor applications, catalysis applications, etc. [13] Different groups around the world tries to produce Co₃O₄ nanostructures in 3D; some of them managed to produce nanospheres, nanocubes, nanorodes using physical and chemical methods [10]. For this purpose, different production methods like solvothermal synthesis, chemical spray pyrolysis, chemical vapor deposition, sol-gel hydrothermal synthesis, simple precipitation, etc. were reported [14–18]. Hydrothermal synthesis could be used in the production of inorganic or organic/inorganic (hybrid) nanomaterials and/or nanocomposites. While other methods are having different drawbacks like high calcination temperature, toxic reactants, long reaction durations, multiple reaction steps and low production efficiency, hydrothermal synthesis provide affordable and reliable experimental media. Hydrothermal method is a highly efficient production process with minimum production cost which enables researchers to control nanostructure morphology. The method also provide good nanostructure size and shape control [19].

In this work, heavy metal adsorption potential of Co₃O₄ nanoflowers, which were previously reported by our group [20], were investigated for the recovery of chromium and cadmium in sea water (SRM) sample. Co₃O₄ nanoflowers used in the investigation were produced using hydrothermal synthesis method. Structural characterization of the nanoparticles was performed using various characterization techniques such as FESEM, XRD, FTIR and EDS. Then, Cr⁶⁺ and Cd²⁺ heavy metal ion recovery potential of the nanoflowers were assessed. Adsorption processes were optimized where influence of different parameters like eluent type, eluent concentration, pH, adsorbent amount, solution volume adsorption duration, etc. on adsorption characteristics were studied. Analytical recovery activity was also assessed regarding the analysis result of metal ions obtained from flame atomic absorption spectroscopy (FAAS) (See Figure 1).

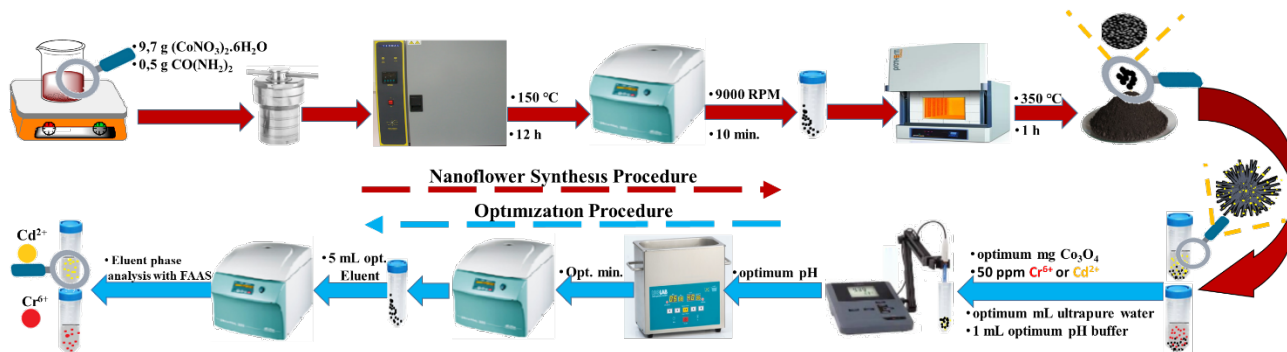


Figure 1. Schematics illustrate the production and investigation process followed in this work.

2. Materials & Methods

2.1. Spectroscopic and crystallographic investigation.

X-ray diffraction investigations were employed using RIKAGU diffractometer. Scanning was conducted between 10 and 90 degrees. Scanning electron microscope used in the structural investigation is FEI Quanta 400F supported with EDS (energy dispersive X-ray spectroscopy). Brunauer–Emmett–Teller (BET) investigation was performed using Quantachrome Nova 4000E. The infrared spectrum was recorded by a JASCO FTIR-6700 spectrometer between wavelengths of 400 and 4000 cm^{-1} . The FAAS investigation was performed using Agilent 240 AA Duo AAS. Cr^{6+} and Cd^{2+} heavy metal ions were assessed using Agilent hollow cathode lamps. Parameters used for the determination of metals are presented in Table 1.

Table 1. Parameters used in the FAAS analysis for the determination of metals

	Cr^{6+}	Cd^{2+}
Air Flow; mL/min	-	13.5
Slit Width (nm)	0.2	0.5
Lamp Current (mA)	7.0	4.0
Acetylene Flow	6.80	2.00
Used Flame	$\text{N}_2\text{O}/\text{Acetylene}$	$\text{Air}/\text{Acetylene}$
Wavelength (nm)	357.9	326.1
N_2O flow; mL/min	10.00	-

All chemicals utilized during the experimental process were analytical level (Merck quality). Ultra-pure water (ELGA, 18.2 $\text{M}\Omega\text{ cm}$) is used in the whole experimental process.

For standard metal solution, 1000 mg/L stock solutions (NIST standard) were used. 3; 2; 1; 0.5; 0.25; 0.1; and 0.05 mg/L solutions were prepared from standards of Cr^{6+} and Cd^{2+} which were prepared by dissolving 0.2 M HNO_3 . They were scanned by FAAS.

2.2. Production of Co_3O_4 nanoflowers

Co_3O_4 nanoflowers were synthesized using hydrothermal method in the lab regarding our previous recipe which was reported in our previous papers [20]. In the synthesis process 9.7 gr of cobalt nitride hexahydrate ($\text{Co}(\text{NO}_3)_2 \cdot 6\text{H}_2\text{O}$) and 0.5 gr of urea $\text{CO}(\text{NH}_2)_2$ were stirred in 35 mL of deionized pure water for 1h. Solution was placed into the Teflon autoclave. The autoclave was placed in oven for 12 h at 150 °C. 12 h later autoclave was taken and left for cool. The solution was then centrifuged and several times to collect the precipitate in the solution. Precipitate was washed a couple of times using ethanol and deionized water. The precipitate was transferred to the oven set at 80°C and kept there for 24 hours. Precipitate was then transferred to the ash furnace at 150°C; the temperature of the furnace was increased step by step where 2°C/1 min step increase rate was employed. When the

temperature reach 300 °C, precipitate was kept there for 1 h whereas the calcinated Co₃O₄ nanoflower powder was obtained [20, 21].

2.3. Solid phase extraction methodology

50 mL of falcon tubes were used for the optimization of eluent type, eluent concentration, pH, sample amount, eluent volume and application time where optimum conditions for the removal of Cr⁶⁺ and Cd²⁺ metal ions were determined.

Standard experimental procedure is as follows:

50 mg of nanoflower was placed in 50 mL falcon tube where 10 mL deionized water containing 0.25 mL (50 ppm) heavy metal ion and 1 mL of buffer solution (pH: 6.0) was added. Solution pH was set to pH: 6.0 by adding 0.01M NaOH and 0.01 M HCl. The solution was topped up with ultra-pure water and set to 25 mL. After 10 mins of sonication, the solution was centrifuged at 9000 rpm for 10 mins. Liquid phase was kept for analysis; 5 mL of acid solution was added to the solid phase. Samples were sonicated for 10 mins and centrifuged at 9000 rpm for 10 mins. The second liquid phase was also kept. Each step was repeated for Cr⁶⁺ and Cd²⁺ heavy metal ion concentration.

For the eluent optimization steps of 0.1-1-2-3 M HNO₃ and 1M of HCl were studied. For pH optimization, pH values of 5, 5.5, 6, 6.5, 7, 7.5 and 8 were studied. For adsorbent amount, 50 mg, 100 mg, 150 mg and 200 mg of Co₃O₄ nanoflower amounts were studied. For the fluent volume study, activity in 5 mL, 10 mL, 20 mL and 30 mL pure water was assessed. For the optimization of sonication duration, 5 mins, 10 mins, 30 mins and 60 mins were studied.

2.3.1 Analysis of real samples: NRC-CNRC certified sea water was assessed for the validation of SRM (standard reference material) where standard addition method was used in the assessment. Before the analysis, 0.5 g of solid sample was taken and 5 mL of HNO₃:H₂O₂ (2:1, h/h) were added on them. Wet samples were placed in shaker water bath and kept at 50°C until the samples get dry. For liquid phase samples, samples were centrifuged at 9000 rpm for 20 mins liquid phase was evaporated until samples totally dry. 4.5 mL standard sea water and 0.5 mL HNO₃ solutions were dried at shaker water bath at 50°C.

Table 2. The chemical properties of synthetic natural water.

Concentration	
pH	8.0
Zn	0.200 ± 0.003
Na	9.00 ± 0.01
Ca	40.9 ± 0.3
Mn	0.200 ± 0.001
K	7.50 ± 0.02
Fe	0.200 ± 0.001
Cu	0.050 ± 0.002

2.3.2 Validation of Method-Analytical Performance: RSD (relative standard deviation), LOD (limit of detection), calibration equation, LOQ (the limit of quantification) and linear regression were defined. Determined values were illustrated in Table 3. The LOD and LOQ were calculated as three times the standard deviation (S.D.) (3σ) and (10σ) of the blank signal. The applied method had been confirmed by NRC-CNRC SRM (NASS-6) (Table 5). The method was also employed to the real seawater (see the Table 6). Moreover, the EF (enrichment factor) was assessed by the formula below [22–25] :

$$EF = \frac{Q_T}{Q_M} \cdot \frac{Q_T^0}{Q_M^0} \quad (1)$$

Table 3. Optimum conditions for Cr⁶⁺ and Cd²⁺

	Cr ⁶⁺	Cd ²⁺
Eluent type,	3 M HNO ₃	3 M HNO ₃
Correlation coefficients (R ²)	0.9985	0.9991
Linear regression (y=ax+b)	0.0229x – 0.0006	0.0187x – 0.002
LOD, µg/L	0.6	1.8
LOQ, µg/L	2	6
RSD%	0.2-9.7	0.7-9.2
Amount of nanoflower, mg	150	100
Sonication time, min	60	30
Enrichment factor, fold	6	2
Sample volume, mL	30	10
pH	6.5	6.0

3. Results and Discussions

3.1. Characterization of Co₃O₄ nanoflowers

Co₃O₄ nanoflowers were produced using hydrothermal synthesis, nanoparticles were then analyzed using FTIR, XRD, FESEM, and EDS methods. Figure 2 illustrates FTIR spectrum of Co₃O₄ nanoflowers between 400 and 4000 cm⁻¹. Straight line illustrating the band between 665 and 575 cm⁻¹ illustrate ν(Co-O) tension graph occurs due to Co₃O₄ structure. The large band observed 3400 cm⁻¹ belongs to O-H tension vibration of hydroxyl groups originated from adsorbed water molecules [20].

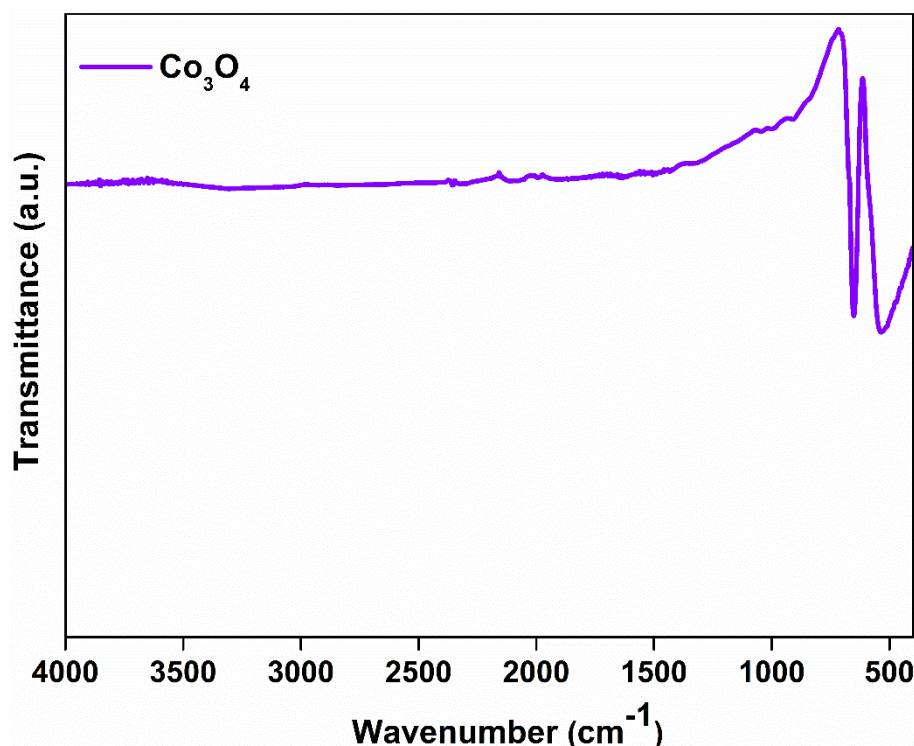


Figure 2. FTIR spectrum of Co₃O₄ nanoflowers.

XRD patterns of Co₃O₄ nanoflowers were presented in Figure 3 where diffraction pattern was plotted in purple color. It was seen that there are various peaks which indicate different types of crystal formations. Peaks at 19,0°, 31,3°, 36,8°, 38,5°, 44,8°, 55,6°, 59,4°, 65,2°, 77,3° degrees were observed; such peaks are corresponding to face centered cubic crystal structures in (111), (220), (311), (222), (400), (422), (511), (440) orientation. Sharp peaks observed in crystal diffraction pattern correspond to face centered cubic crystal formation [20]. It illustrates that the production method can

produce pure crystals in stable crystal type. Therefore, no different types of crystal formation were observed.

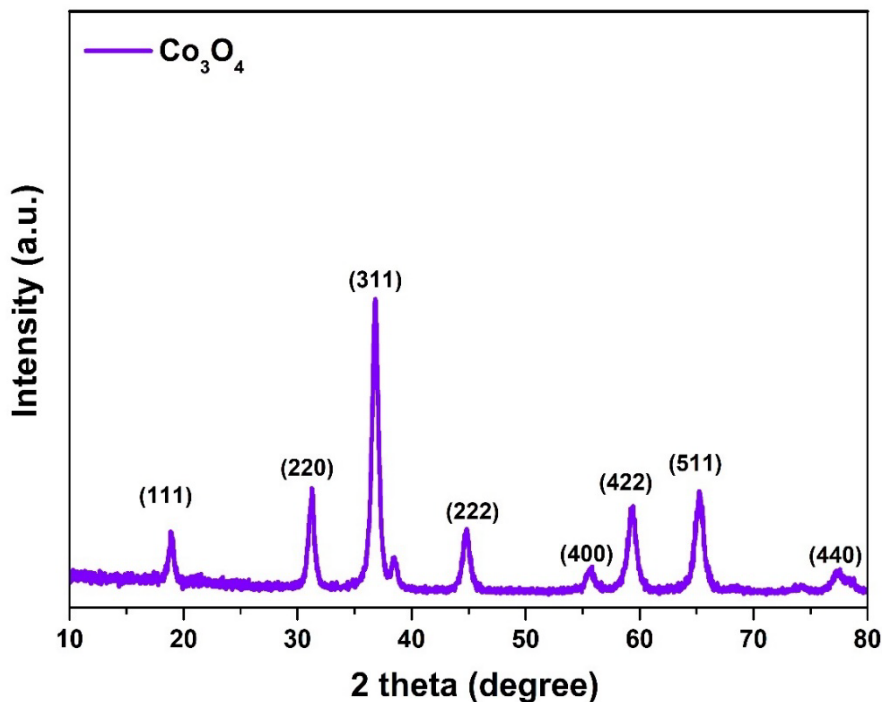


Figure 3. XRD diffraction pattern of Co_3O_4 nanoflowers

FESEM images of nanoflowers were illustrated in Figure 4. In Figure 4, different images were presented. The image on the left illustrates a larger scaled version where different nanoflowers can be seen all of which are in flower form. In the image in the right zoomed version was presented. Co_3O_4 nanoflowers contain fiber like structures that come together and form a dandelion like structure. Nanofibers in the nanoflowers are pointing out such a case enhances the surface area/surface volume rate and porosity. Such a case enables us to obtain enhanced adsorption capacity with outstanding electronic and catalytic activity.

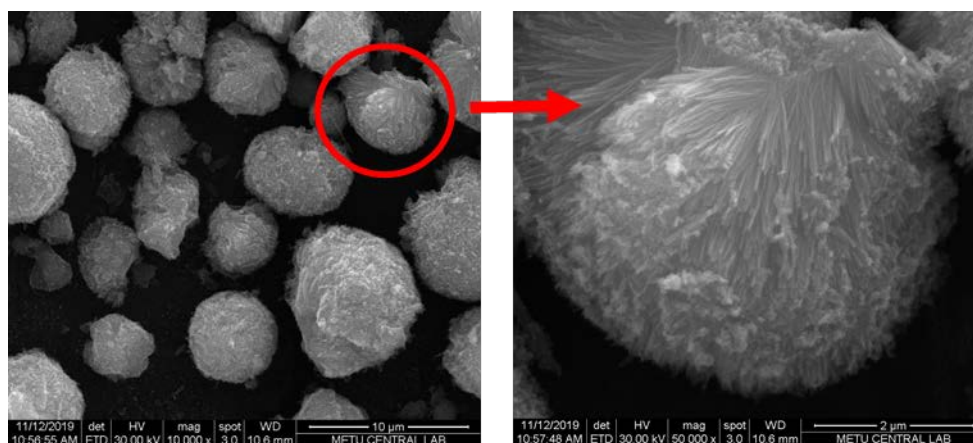


Figure 4. FESEM images of Co_3O_4 nanoflowers.

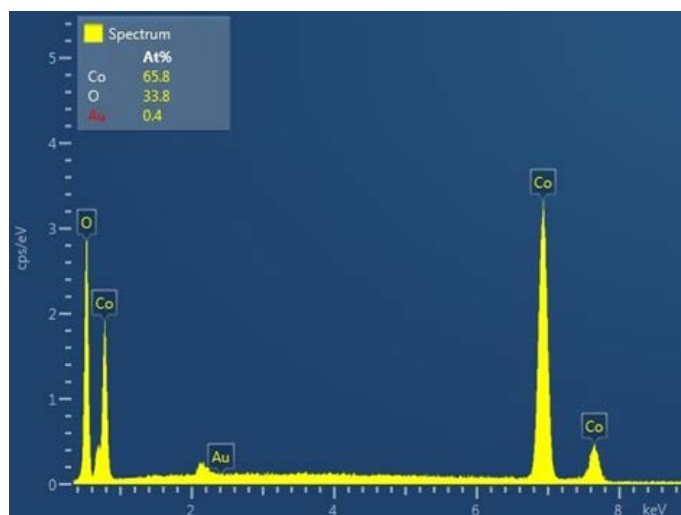


Figure 5. EDS spectra of Co_3O_4 nanoflowers [20].

EDS spectra were presented in Figure 5. Elemental analysis was performed using EDS apparatus of FESEM. Apparent Co and O related peaks could be addressed in the spectra. EDS spectrum confirmed that nanoflowers consisted of Co and O atoms where no residual distortion peaks were seen in the spectra.

Surface area of the nanoflowers were investigated using BET analysis. The surface area of the nanoflowers was measured as $50.73 \text{ m}^2\text{g}^{-1}$. The average pore volume was found to be 168.9913 \AA and the average pore width was determined as 165.819 \AA . Measured surface area was found to be consistent with the results reported for Co_3O_4 nanoflowers in the literature [26, 27]. N_2 adsorption – desorption BET isotherms were presented in Figure 6.

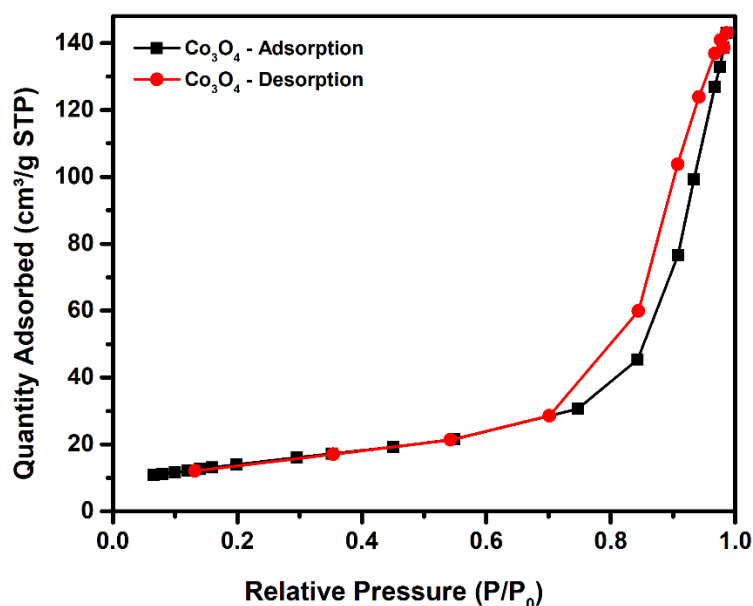


Figure 6. N_2 adsorption – desorption BET isotherm plots of Co_3O_4 nanoflowers.

3.2. Removal of heavy metal ions (Cr^{6+} , Cd^{2+})

3.2.1 Effect of eluent type: To promote the influence between Co_3O_4 nanoflowers and Cr^{6+} , Cd^{2+} heavy metal ions in aqueous media, sonication was employed to the solution. Samples were sonicated at room temperature for 10 mins. After the sonication, centrifugation process was held at 9000 rpm for 10 mins. To assess the Cr^{6+} , Cd^{2+} content, AAS investigation was employed to the filtered supernatants. Eluent type influence for the Co_3O_4 nanoflowers based recovery of Cr^{6+} , Cd^{2+} metal ions were investigated for 1 M HCl and 0.1 M HNO_3 , 1 M HNO_3 , 2 M HNO_3 , and 3 M HNO_3 . Results

were illustrated in Figure 7. Co_3O_4 nanoflowers successfully recovered the 99.7% and 92.8% for 3 M HNO_3 for Cr^{6+} and Cd^{2+} respectively.

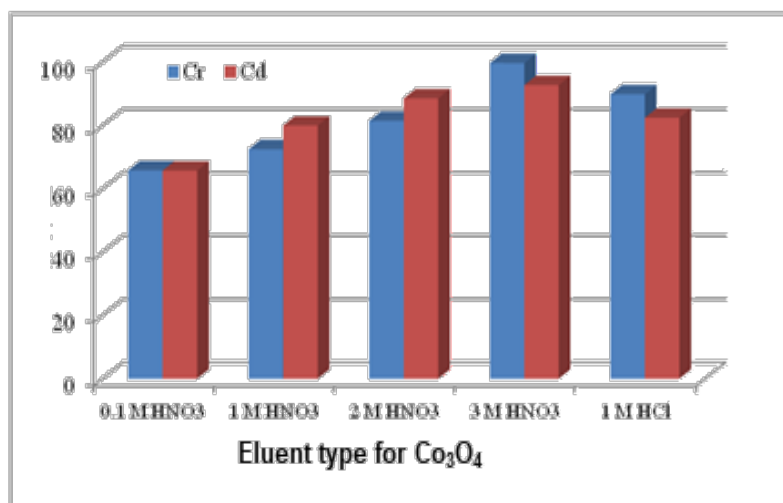


Figure 7. The effect of eluent on Cr^{6+} , Cd^{2+} ion removal.

3.2.2. Effect of pH: pH value has a significant effect on metal ion solubility. Therefore, pH is an important parameter affecting the recovery rate of heavy metals. Thus, pH is an essential parameter that addressed in the recovery studies. Hence, effect of pH on Cr^{6+} , Cd^{2+} heavy metal ion removal in the existence of Co_3O_4 nanoflowers was investigated. pH related Cr^{6+} , Cd^{2+} metal removal rate was illustrated in Figure 8. By scanning between pH 5.5 and 8.0, the pH value with maximum recovery was determined as 6.5 and 6.0 optimum for Cr^{6+} and Cd^{2+} , respectively. Removal percentage starts to decrease by pH 6.0 and 6.5 for Cr^{6+} and Cd^{2+} , respectively. Maximum removal rate for Cr^{6+} and Cd^{2+} were obtained as 97.8% and 93.6%, respectively. We concluded that Cr^{6+} and Cd^{2+} metal ions prefer a soft acidic condition for optimum recovery process.

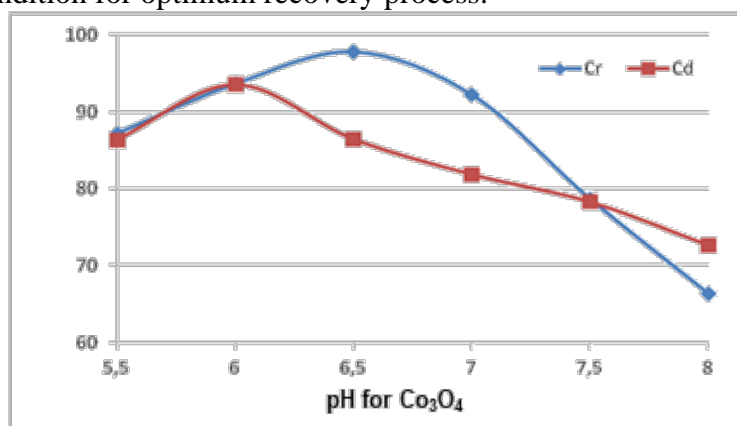


Figure 8. The effect pH for the removal of Cr^{6+} , Cd^{2+} ions

3.2.3. Effect of adsorbent amount: Optimization of Co_3O_4 nanoflower adsorbent amount is a critical parameter for not to overuse the adsorbents. The graph presented below shows recovery percentage of Cr^{6+} and Cd^{2+} ions. Heavy metal ions removal rate depending on nanoflower concentration was illustrated in Figure 9. The best recovery rates for Cr^{6+} and Cd^{2+} were achieved as 99.0% and 96.3% with 150 mg Co_3O_4 and 100 mg Co_3O_4 , respectively.

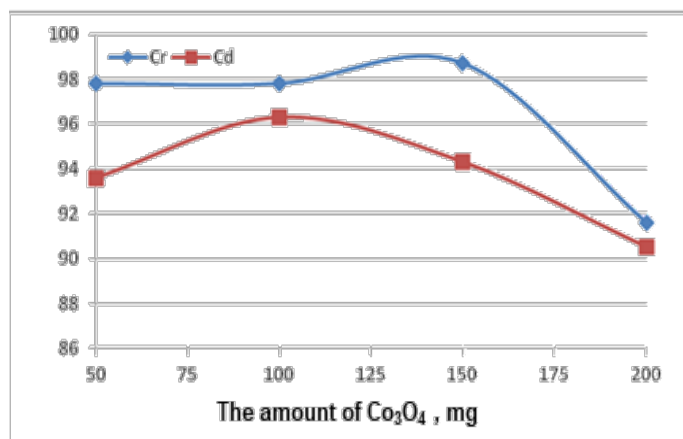


Figure 9. The effect of nanoflower dosage on Cr^{6+} , Cd^{2+} heavy metal ion recovery.

3.2.4. Effect of solvent volume: The plot in Figure 10 illustrates the solvent volume effect on removal rate of Cr^{6+} and Cd^{2+} in the presence of Co_3O_4 . To investigate the influence of solvent volume on removal rates, different volumes 5 mL, 10 mL, 25 mL, 20 mL and 30 mL were studied. The max removal rate for Cr^{6+} and Cd^{2+} were found to be 99.0% and 97.8% with 30 mL and 10 mL, respectively.

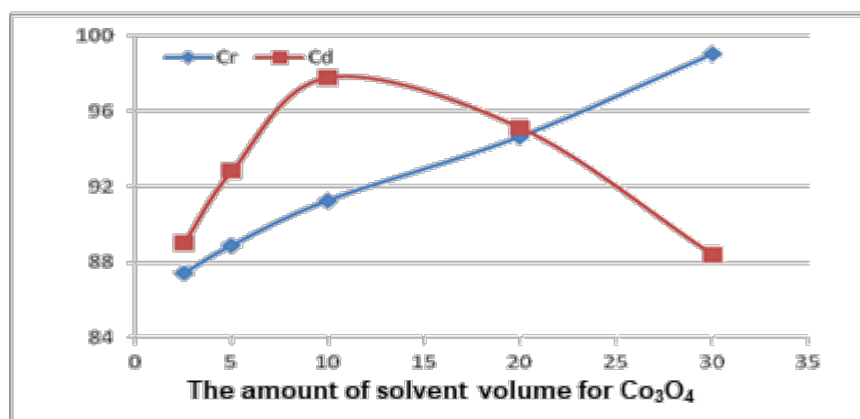


Figure 10. The effect of solvent amount for the removal of Cr^{6+} , Cd^{2+} ions

3.2.5. Influence of sonication duration: To speed up the nanoflower adsorption of metal ions, sonic vibration was applied to samples. To assess the sonication effect on the removal rate of Cr^{6+} and Cd^{2+} , various sonication time periods were studied like 5 mins 10 mins, 15 mins, 20 mins, 30 mins, and 60 mins. Plots showing the effect of sonication duration on removal rate of Cr^{6+} and Cd^{2+} were illustrated in Figure 11. The graph shows that the optimum removal duration was obtained at 30 mins. The recovery percentage increased gradually till 30 mins of sonication, after that recovery percentage starts to diminish. Removal percentages at 30 mins of sonication is 98.6% and 98.7% for Cr^{6+} and Cd^{2+} , respectively.

3.2.6 Repeatability: In the extraction time optimization, the last remaining solid phase was washed several times using pure water. The optimum conditions were repeated 6 times and the residue was analyzed using FAAS. Results were presented in Table 4. The table clearly illustrates that matrix ions affect the recovery of heavy metal ions. All in all, recovery rates were found to be quite high. Therefore, the presented procedure is able to recover heavy metal ions from the aqueous media and could be used in enrichment applications.

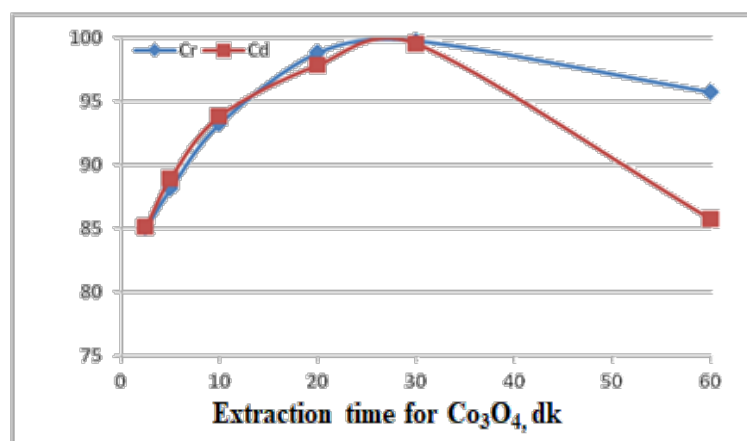


Figure 11. The effect of sonication time for the removal of Cr⁶⁺, Cd²⁺ ions.

Table 4. Influences of matrix ions on the recoveries of Cr⁶⁺ and Cd²⁺ (N = 3)

Ions	Added as	Concentration (mg/L)	Cr ⁶⁺	Cd ²⁺
Na ⁺	NaCl	500	97 ± 2	97 ± 3
K ⁺	KCl	150	95 ± 3	95 ± 3
Ca ²⁺	CaCl ₂	150	96 ± 2	96 ± 2
Mg ²⁺	MgCl ₂	100	97 ± 3	99 ± 1
Na ⁺	NaCl	500	97 ± 2	97 ± 3
Cu ²⁺	Cu(NO ₃) ₂	5	97 ± 3	97 ± 3
Fe ³⁺	Fe(NO ₃) ₂	0.5	98 ± 3	97 ± 3
Mn ²⁺	Mn(NO ₃) ₂	0.5	99 ± 1	98 ± 3
Zn ²⁺	Zn(NO ₃) ₂	1	95 ± 2	96 ± 2
Ni ²⁺	Ni(NO ₃) ₂	0.2	97 ± 2	98 ± 2
Pb ²⁺	Pb (NO ₃) ₂	0.2	97 ± 1	97 ± 2

3.2.7 Reliability of the method and nanoflowers enrichment application on real samples: To check the reliability of the method, results obtained using certified reference material (CRM) were presented in Table 5. These values were quantitative, and it shows that the presented procedure could be applied for the preconcentration of heavy metal ions in real samples. Our results were compared with similar works in literature. Results comparing our work with similar works was presented in Table 7.

Table 5. Analysis result of certified reference materials (N=3).

		Cr ⁶⁺	Cd ²⁺
Sea Water (SRM)	Certified Value (µg/L)	0.118 ± 0.008	0.0311 ± 0.0019
	Result, µg/mL	0,116 ± 0,008	0.0301 ± 0.0019
	Recovery, %	98.3 ± 0.9	96.8 ± 0.5

Results obtained after the application of nanoflowers for real samples in optimum conditions were presented in Table 6.

Table 6. Cr⁶⁺ and Cd²⁺ levels before and after from enrichment in various samples (N=3)

Ions	Before		After	
	Cr ⁶⁺ , µg/L	Cd ²⁺ , µg/L	Cr ⁶⁺ , µg/L	Cd ²⁺ , µg/L
Sample				
Sea Water	35.0 ± 2.1	2.2 ± 0.1	196 ± 9	622 ± 8
Bottled Water	ND	ND	367 ± 2	618 ± 11
Tap Water	ND	ND	231 ± 6	620 ± 11
Soda	ND	3.1 ± 0.2	262 ± 5	634 ± 9

Enrichment factor was Cr^{6+} and Cd^{2+} was determined as 200 fold and 560 fold, respectively. The method is found to be successful on real samples. The method is rapid as compared with previously reported procedures for the enrichment of heavy metal ions. The method is successfully used in the assessment of the ingredient materials.

Table 7. Works reported in the literature used for the removal of heavy metal ions

Materials	Element	Amount of adsorbent	Time	pH	Apparatus	Ref.
ZnO nanoparticles	Cr^{3+} , Co^{2+} , and Ni^{2+}	0.5 g	1.5 mins - 180 mins	2	UV-Vis	[28]
ZnO nanoflowers	Cd and Pb	0.8 g/L	100 mins	6.0	AAS	[29]
MgO nanoparticles	Cd and Pb	2294 mg/g for Cd(II) and 2614 mg/g for Pb(II)	30 min and 15 min for the adsorption of Cd(II) and Pb(II), respectively	2.0 and 3.0	Voltammetry	[30]
Nano-HAP composites	Cr (VI)	20 mg	10 mins	5.0	FAAS	[31]
Mf (magnetite that the modified with triethylenetetramine)-graphene oxide	Cr(VI) and Cr(III)	50 mg	10 mins and 30 mins of Cr(VI) and Cr(III), respectively	2.0 and 8.0 of Cr(VI) and Cr(III), respectively	FAAS	[32]

4. Conclusions

Today, heavy metal ions threatening the natural water sources. Therefore, reliable, and affordable methods are important to fight against this problem. Nanoparticles may have high adsorption rates due to their structural properties and they can be mass produced using conventional methods. Hence, flower-like Co_3O_4 nanostructures were produced using hydrothermal synthesis method and heavy metal removal rates were checked in this work. Structural characteristics of the nanoflowers were assessed using different microscopic and elemental methods. Methods confirmed that nanoflowers consisted of well-ordered Co_3O_4 crystals which are consisting of Co and O molecules. There was not any contamination related signal in EDS spectra. Co_3O_4 nanoflowers were then used for the recovery of Cr^{6+} and Cd^{2+} heavy metal ions. Numerous factors affecting the recovery of heavy metal ions such as pH, eluent type, eluent concentration, adsorbent amount, solution volume and adsorption duration were studied. The optimum conditions to obtain max recovery rate were determined. It was seen that our nanoparticles managed to remove almost 99.0% of Cr^{6+} and Cd^{2+} heavy metal ions. The case was also tasted in real samples where sea water, bottled water, tap water and soda were used. It was seen that our nanoflowers perform similar characteristics where 99.2% of Cd^{2+} and 98.3% Cr^{6+} heavy metal ions were removed from real samples. Our result indicates that Co_3O_4 nanoflowers exhibit outstanding heavy metal removal performance for Cr^{6+} and Cd^{2+} metal ions. It illustrates that Co_3O_4 nanoflowers have potential to be used as a nanomaterial for the removal of heavy metal ions especially in aqueous media.

Peer-review: Externally peer - reviewed.

Author contributions: Cemile ÖZCAN: Concepting the work, defining experimental procedures, preparation of the manuscript; Nurdan KURNAZ YETİM: Concepting the work, collecting experimental data, data processing, preparation of manuscript; Mumin Mehmet KOÇ: Conceptualization, preparation of manuscript; Elif Aybike BERBEROĞLU: Collecting experimental data, preparation of manuscript.

Conflict of Interest: No conflict of interest was declared by the authors. (Part of the data presented in the manuscript has been presented in an oral presentation at the NEM 2022 (2nd International Conference on Engineering Technologies).

Financial Disclosure: The authors declared that this study has received no financial support.

References

1. Barrak, H., Kriaa, A., Triki, M., M'nif, A., Hamzaoui, A.H.: Study of the Adsorption and Desorption of Zn (II) and Pb (II) on CaF₂ Nanoparticles. *Iran J. Chem. Chem. Eng.* 39, 191–201 (2020)
2. Khan, I., Saeed, K., Khan, I.: *Nanoparticles: Properties, applications and toxicities*, (2019)
3. Luan, L., Tang, B., Liu, Y., Wang, A., Zhang, B., Xu, W., Niu, Y.: Selective capture of Hg(II) and Ag(I) from water by sulfur-functionalized polyamidoamine dendrimer/magnetic Fe₃O₄ hybrid materials. *Sep. Purif. Technol.* 257, 117902 (2021). <https://doi.org/10.1016/j.seppur.2020.117902>
4. Mokarram, M., Saber, A., Obeidi, R.: Effects of heavy metal contamination released by petrochemical plants on marine life and water quality of coastal areas. *Environ. Sci. Pollut. Res.* 28, 51369–51383 (2021). <https://doi.org/10.1007/S11356-021-13763-3/FIGURES/9>
5. Kurnaz Yetim, N., Berberoğlu, E.A., Aslan, N., Koç, M.M., Özcan, C.: Sonochemical removal of Pb (II) ions from the water medium using Bi₂S₃ nanostructures. (2022). <https://doi.org/10.1080/03067319.2022.2088288>
<https://doi.org/10.1080/03067319.2022.2088288>
6. Üner, O., Körükçü, B.C., Özcan, C.: Adsorption application of activated carbon from ripe black locust seed pods for wastewater taken from Ergene River, Turkey. *Int. J. Environ. Anal. Chem.* 1–16 (2021). <https://doi.org/10.1080/03067319.2021.1889533>
7. Ozcan, C., Akozcan, S.: Determination of ni, pb and cd in drinking fountain water in kirkclareli/turkey by faas after preconcentration on quercetin modified using granular activated carbon. *Desalin. Water Treat.* 175, 219–228 (2020). <https://doi.org/10.5004/DWT.2020.24900>
8. Klatt, V., Kunze, J., Timur, I., Filiz Senkal, B., Kaplan, O., Kaya, G., Ozcan, C., Karaaslan, N.M., Yaman, M., Jia, W.-P., Han, D.-M., Gao, T., Li, F., Keshav Krishna, A., Rama Mohan, K., Murthy, N., Sudarshan, V., Zhu, L., Chen, S., Lu, D., Cheng, X.: Synthesis of new polymeric resin and its application in solid phase extraction of copper in water samples using STAT-FAAS. *Atom. Spectrosc.* 30, 191–200 (2009)
9. Hemmati, M., Rajabi, M., Asghari, A.: Magnetic nanoparticle based solid-phase extraction of heavy metal ions: A review on recent advances. *Microchim. Acta* 2018 1853. 185, 1–32 (2018). <https://doi.org/10.1007/S00604-018-2670-4>
10. Roduner, E.: Size matters: Why nanomaterials are different. *Chem. Soc. Rev.* 35, 583–592 (2006). <https://doi.org/10.1039/b502142c>
11. L. Johnston, R.: *Atomic and Molecular Clusters*. Taylor & Francis, London, New York (2002)
12. Aslan, N., Ceylan, B., Koç, M.M., Findik, F.: Metallic nanoparticles as X-Ray computed tomography (CT) contrast agents: A review. *J. Mol. Struct.* 1219, 128599 (2020). <https://doi.org/10.1016/j.molstruc.2020.128599>
13. Singh, M., Manikandan, S., Kumaraguru, A.K.: Nanoparticles: A New Technology with Wide Applications. *Res. J. Nanosci. Nanotechnol.* 1, 1–11 (2011).

<https://doi.org/10.3923/rjnn.2011.1.11>

14. Koç, M.M., Aslan, N., Kao, A.P., Barber, A.H.: Evaluation of X-ray tomography contrast agents: A review of production, protocols, and biological applications. *Microsc. Res. Tech.* 82, (2019). <https://doi.org/10.1002/jemt.23225>
15. Kurnaz Yetim, N., Kurşun Baysak, F., Koç, M.M., Nartop, D.: Characterization of magnetic Fe₃O₄@SiO₂ nanoparticles with fluorescent properties for potential multipurpose imaging and theranostic applications. *J. Mater. Sci. Mater. Electron.* 31, 18278–18288 (2020). <https://doi.org/10.1007/s10854-020-04375-7>
16. Tao, Y., Zhang, C., Lü, T., Zhao, H.: Removal of Pb(II) Ions from Wastewater by Using Polyethyleneimine-Functionalized Fe₃O₄ Magnetic Nanoparticles. *Appl. Sci.* 2020, Vol. 10, Page 948. 10, 948 (2020). <https://doi.org/10.3390/APP10030948>
17. Sivalingam, D., Gopalakrishnan, J.B., Rayappan, J.B.B.: Nanostructured mixed ZnO and CdO thin film for selective ethanol sensing. *Mater. Lett.* 77, 117–120 (2012). <https://doi.org/10.1016/J.MATLET.2012.03.009>
18. Fareed, S., Medwal, R., Vas, J.V., Khan, I.A., Rawat, R.S., Rafiq, M.A.: Tailoring oxygen sensing characteristics of Co₃O₄ nanostructures through Gd doping. *Ceram. Int.* 46, 9498–9506 (2020). <https://doi.org/10.1016/J.CERAMINT.2019.12.211>
19. Karaçam, R., Yetim, N.K., Koç, M.M.: Structural and Magnetic Investigation of Bi₂S₃@Fe₃O₄ Nanocomposites for Medical Applications. *J. Supercond. Nov. Magn.* 33, 2715–2725 (2020)
20. Kurnaz Yetim, N., Aslan, N., Sarioğlu, A., Sarı, N., Koç, M.M., Yetim, N.K., Aslan, N., Sarioğlu, A., Sarı, N., Koç, M.M.: Structural, electrochemical and optical properties of hydrothermally synthesized transition metal oxide (Co₃O₄, NiO, CuO) nanoflowers. *J. Mater. Sci. Mater. Electron.* 31, 12238–12248 (2020). <https://doi.org/10.1007/s10854-020-03769-x>
21. Liu, S., Zhang, R., Lv, W., Kong, F., Wang, W.: Controlled Synthesis of Co₃O₄ Electrocatalysts with Different Morphologies and Their Application for Oxygen Evolution Reaction. *Int. J. Electrochem. Sci.* 13, 3843–3854 (2018). <https://doi.org/10.20964/2018.04.54>
22. Ince, M., Kaplan, O., Yaman, M.: Solid-Phase Extraction and Preconcentration of Copper in Mineral Waters with 4-(2-Pyridyl-Azo) Resorcinol-Loaded Amberlite XAD-7 and Flame Atomic Absorption Spectrometry. *Water Environ. Res.* 80, 2104–2110 (2008). <https://doi.org/10.2175/106143008X266805>
23. Soylak, M.: Solid Phase Extraction of Cu(II), Pb(II), Fe(III), Co(II), and Cr(III) on Chelex-100 Column Prior to Their Flame Atomic Absorption Spectrometric Determinations. <http://dx.doi.org/10.1081/AL-120034064>. 37, 1203–1217 (2011). <https://doi.org/10.1081/AL-120034064>
24. Tuzen, M., Soylak, M.: Multi-element coprecipitation for separation and enrichment of heavy metal ions for their flame atomic absorption spectrometric determinations. *J. Hazard. Mater.* 162, 724–729 (2009). <https://doi.org/10.1016/J.JHAZMAT.2008.05.087>
25. Soylak, M., Elçi, M.: Solid phase extraction of trace metal ions in drinking water samples from Kayseri-Turkey. *J. TRACE MICROPROBE Tech.* 18, 343–354 (2000). <https://doi.org/10.2/JQUERY.MIN.JS>
26. Ge, M.Y., Han, L.Y., Wiedwald, U., Xu, X.B., Wang, C., Kuepper, K., Ziemann, P., Jiang, J.Z.: Monodispersed NiO nanoflowers with anomalous magnetic behavior Related content Monodispersed NiO nanoflowers with anomalous magnetic behavior. *Nanotechnology.* 21, 5 (2010). <https://doi.org/10.1088/0957-4484/21/42/425702>

27. Bai, G., Dai, H., Deng, J., Liu, Y., Ji, K.: Porous NiO nanoflowers and nanourchins: Highly active catalysts for toluene combustion. *Catal. Commun.* 27, 148–153 (2012). <https://doi.org/10.1016/j.catcom.2012.07.008>
28. Salem, I.A., Salem, M.A., El-Ghobashy, M.A.: The dual role of ZnO nanoparticles for efficient capture of heavy metals and Acid blue 92 from water. *J. Mol. Liq.* 248, 527–538 (2017). <https://doi.org/10.1016/J.MOLLIQ.2017.10.060>
29. Kataria, N., Garg, V.K.: Optimization of Pb (II) and Cd (II) adsorption onto ZnO nanoflowers using central composite design: isotherms and kinetics modelling. *J. Mol. Liq.* 271, 228–239 (2018). <https://doi.org/10.1016/J.MOLLIQ.2018.08.135>
30. Xiong, C., Wang, W., Tan, F., Luo, F., Chen, J., Qiao, X.: Investigation on the efficiency and mechanism of Cd(II) and Pb(II) removal from aqueous solutions using MgO nanoparticles. *J. Hazard. Mater.* 299, 664–674 (2015). <https://doi.org/10.1016/J.JHAZMAT.2015.08.008>
31. Zhan, M., Gao, W., Nguyen, W., Yu, H., Amador, E., Chen, W.: The investigation of triadic silica-supported polyhexamethylene guanidine@nano-hydroxyapatite nanocomposites for Cr (VI) detection. *Mater. Today Adv.* 15, 100268 (2022). <https://doi.org/10.1016/J.MTADV.2022.100268>
32. Islam, A., Ahmad, H., Zaidi, N., Kumar, S.: A graphene oxide decorated with triethylenetetramine-modified magnetite for separation of chromium species prior to their sequential speciation and determination via FAAS. *Microchim. Acta.* 183, 289–296 (2016). <https://doi.org/10.1007/S00604-015-1641-2/TABLES/3>

The study on determination interactions between liquid crystals and nanoparticle: Fluorescence spectra of nanoparticle-doped liquid crystals

*¹ Yunus Emre KARA , ¹ Yadigar GÜLSEVEN SIDIR , ² Sabit HOROZ 

¹ Faculty of Science and Arts, Department of Physics, Bitlis Eren University, Bitlis, Türkiye.

² Faculty of Natural Sciences and Engineering, Engineering Basic Sciences, Sivas Science and Technology University, Sivas, Türkiye

* Corresponding author, e-mail: yemrekara1313@gmail.com

Submission Date: 29.12.2022

Acceptation Date: 28.03.2023

Abstract - Liquid crystals are compounds interesting molecular structures between the solid state and the liquid state. Nanoparticles are materials whose physical and more different properties change depending on the nano-particle size. In this study, interactions between ZnS, CdSe and CdS nanoparticles with 4-Pentylphenyl 4-Methoxybenzoate (4PP4MetoxB), 4-Pentylphenyl 4-Pentylbenzoate (4PP4PentB) and 4-Pentylphenyl 4-(Octyloxy)Benzoate (4PP4OctoxB) were have been investigated determined by using fluorescence spectra in different solvent medium. The motivation of the study can determine the possible interactions of liquid crystals and nanoparticles. We have been observed to difference fluorescence spectra in different medium of new compose nanomaterials. So, it can be said that there are interactions between nanoparticle with liquid crystals. It can be said that possible interactions between 4PP4OctoxB liquid crystal and nanoparticles have been done more interactions than other LCs molecules. Solvents used in this study are DMSO (Polar aprotic), Methanol (polar protic) and Toluene (non-polar). Except for toluene, it can be said that nanoparticle-doped liquid crystals interact in two solvent environments.

Keywords: Liquid crystals, nanoparticles, fluorescence spectra, solvent effect, nanomaterial

1. Introduction

Liquids with a specific positional and orientational order are defined as liquid crystals [1]. Molecular structures of liquid crystals (L.C.) have fluidity with a long-range order that can act together. In addition, these self-organizing molecules are interesting materials with unique optical, electrical, and magnetic properties [2]. The discovery of liquid crystals was made by studying cholesteryl benzoate, which has two melting points and birefringence. Liquid crystals are called liquid crystals because they are between a solid state and a liquid state and show both crystal and liquid properties [3]. The molecular structures of liquid crystals are anisotropic and can interact with external fields and surfaces [4]. Liquid crystals are basically divided into two main groups thermotropic and lyotropic. The main parameter of thermotropic liquid crystals is temperature and they are composed of individual molecules and do not need another molecule for the formation of the liquid crystal phase [5]. Lyotropic liquid crystals form their molecular structures in the liquid crystal phase under the influence of solvents and consist of multiple molecules [6]. Weak external effects can significantly change the molecular structure of liquid crystals. Due to this sensitivity to external effects, they are used in application areas such as biomedical detectors from display technology [7].

The size of nanomaterials ranges from 100 nm (nanometer) to 1 nm and varies according to their size and shape. It is possible to synthesize nanomaterials of various shapes and sizes from different materials. Many nanomaterials show luminescence depending on their size. The production of small-sized electronic materials has caused semiconductor nanoparticles in nanomaterials to attract more attention from researchers [8]. Nano-sized particles are interesting materials due to their unique properties and ability to be synthesized in different sizes. It has also been reported that the physical

¹ Corresponding author: E-mail: yemrekara1313@gmail.com

and chemical properties of materials change when the size of the materials is reduced to the nm scale [9], [10]. Nano-sized materials have significant differences compared to bulk materials. Control over these nanomaterials will also enable them to be used in important technological applications [11].

There are studies on doping nanomaterials with different properties and molecular structures into liquid crystals. In these studies, optical-electronic changes, photoluminescence depending on size, and improved diffraction efficiency results were obtained from doping nanoparticles into liquid crystals [12]. It can be said that advanced photoluminescence and electronic-optical properties develop with nanoparticles in applications where liquid crystal materials are used. The doping of liquid crystals with nanoparticles may have caused the development of dielectric permeability and spontaneous polarization of material [13], [14].

The molecular structure of nanoparticles added to liquid crystals tries to form an aligned and regular structure and allows electron transfer to occur more easily in photovoltaic cells, which is one of the application areas of liquid crystal nanoparticles [15]. There are studies for the use of liquid crystal nanoparticles in display technology, which is another application area. These studies varied according to the size of the nanoparticles and the method of doping. There are studies where it is reported that the threshold voltage decreases with liquid crystal nanoparticle materials [16]. Both liquid crystals and nanoparticles are materials that have been studied with interest by researchers. The important reason for the interest in these materials is due to their molecular structures. In this study, the fluorescence spectra of new materials formed by combining liquid crystals and nanoparticles dissolved in three different organic solvents were investigated. While making this study, a comparison was made with the fluorescence spectra of liquid crystalline solutions. Energy band gaps (E_g) of the synthesized nanoparticles were found by the Tauc method [17], [18]. Here, electronic emission transitions are investigated in detail in order to determine the possible interactions of liquid crystals and nanoparticles. Thus, it is aimed to have information about the electronic behavior of nanomaterials.

2. Materials and Methods

2.1. Materials

The 4-Pentylphenyl 4-Methoxybenzoate (4PP4MetoxB), 4-Pentylphenyl 4-Pentylbenzoate (4PP4PentB) and 4-Pentylphenyl 4-(Octyloxy)Benzoate (4PP4OctoxB) liquid crystals purchased from Sigma-Aldrich were used in this study. It can be seen from Figure 1 to molecular structures of 4PP4MetoxB, 4PP4PentB and 4PP4OctoxB liquid crystals. The liquid crystals in figure 1 were drawn using ChemOffice programs. The nanoparticles used in the study are CdS, CdSe and ZnS. The synthesis and characterization of these nanoparticles are as given in the references [19]–[21].

2.2. Experimental Methods

Liquid crystals were prepared in 10^{-5} M solution of methanol, toluene and DMSO in solvents with different properties such as polarity and polarizability. CdS, CdSe and ZnS nanoparticles have been prepared as about 2×10^{-4} M in DMSO, 1.3×10^{-4} M in Toluene, and 1.6×10^{-4} M in Methanol solvent. The electronic absorbance spectra of the prepared nanoparticle solutions were measured in Perkin Elmer Lambda-35 UV-vis spectrophotometer. In the last step, liquid crystal and nanoparticle solution was prepared by taking 1 ml of nanoparticle solution from 9 ml of liquid crystal solution. Then they were mixed in a magnetic stirrer, and after the samples were ready, fluorescence spectrums were taken at room temperature. The fluorescence spectra have measured using the Perkin Elmer LS-55 fluorescence spectrophotometer. Electronic band analysis of absorbance and fluorescence spectra was performed with Spectragraphy v1.2.16 and Origin lab 2019b versions [22], [23].

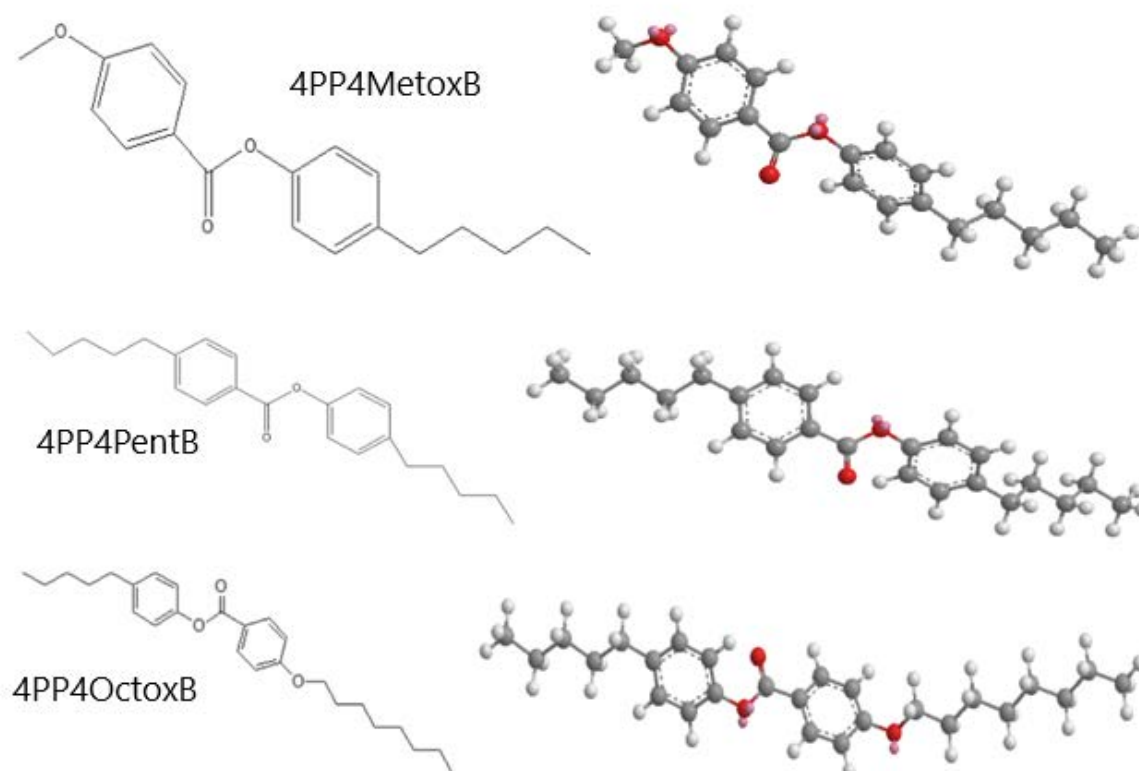


Figure 1. Molecular structures of 4PP4MetoxB, 4PP4PentB and 4PP4OctoxB liquid crystals.

3. Results and Discussions

The absorbance-wavelength and $\alpha h\nu$ -energy graphs of CdS, CdSe, and ZnS nanoparticles are shown in Figure 2-4, respectively. The band gaps of synthesized semiconductor nanoparticles using the Tauc equation given in Equation 1 were calculated as 3.34 eV for CdS, 2.73 eV for CdSe, and 4.30 eV for ZnS, respectively.

$$\alpha h\nu = B*(h\nu - E_g)^p \quad (1)$$

Here, $h\nu$ is the energy of the incident light, E_g is the band gap value, B is a unitless constant expressing the transition probability between energy levels, and p is a unitless constant whose value is 0.5 for direct transitions and 2 for indirect transitions [24], [25].

The most important observation obtained as a result of absorbance measurements is that the forbidden energy gaps calculated for the synthesized CdS, CdSe, and ZnS nanoparticles are larger than the bulk forbidden energy gaps of these materials. The bulk forbidden energy range for CdS is 2.42 eV, the bulk forbidden energy range for CdSe is 1.74 eV, and the bulk forbidden energy range for ZnS is 3.56 to 3.76 eV. As the band gap of the synthesized semiconductor quantum dots increases due to the quantum confinement effect, it can be said that the crystallite sizes of these materials are very small.

In some studies on nanoparticles, absorbance spectrum of CdSe nanoparticle with particle size smaller than 5.4 nm has been reported [8]. Based on this, it can be said that the particle size of the CdSe nanoparticle used in this study is around 5 nm.

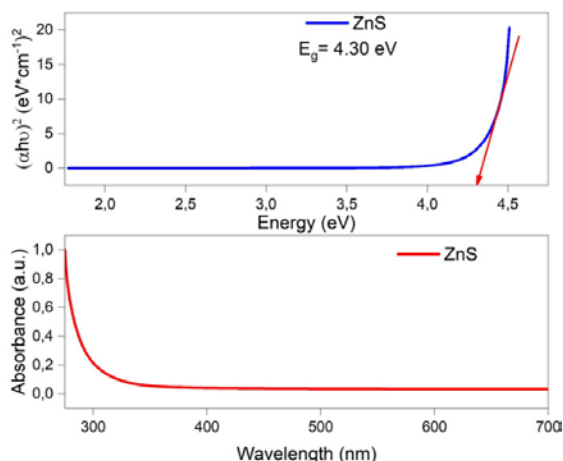


Figure 2. The absorbance spectra and graph of $\alpha h\nu$ vs. energy for ZnS nanoparticle.

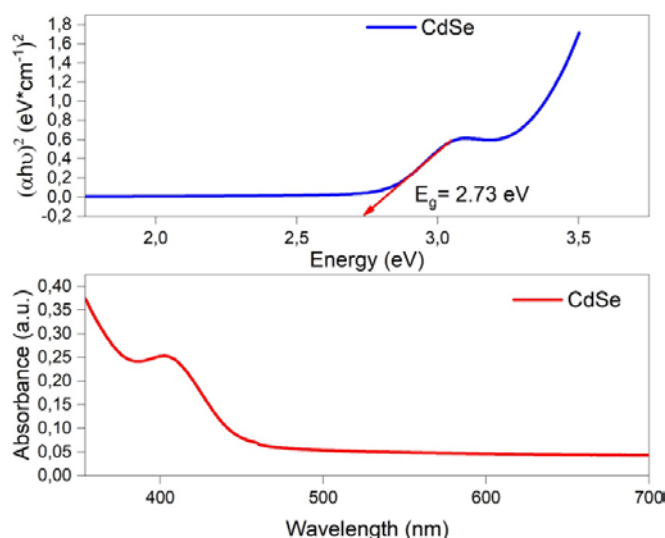


Figure 3. The absorbance spectra and graph of $\alpha h\nu$ vs. energy for CdSe nanoparticle.

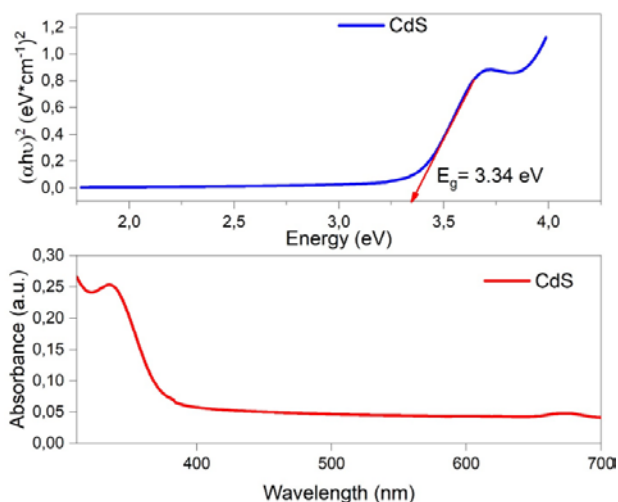


Figure 4. The absorbance spectra and graph of $\alpha h\nu$ vs. energy for CdS nanoparticle.

Fluorescence spectra of nanomaterials are given in figure 5-13. Fluorescence spectra of nanomaterials with the liquid crystal solutions can be examined and compared. Changes in the maximum wavelengths of fluorescence spectra of nanoparticle doped liquid crystal solutions and liquid crystal solutions only were also evaluated. Some excitation peaks seen in fluorescence spectra

are not given in the tables. The reason for this is not to confuse the wavelengths seen in the spectra with the excitation peaks and to perform better spectrum analysis.

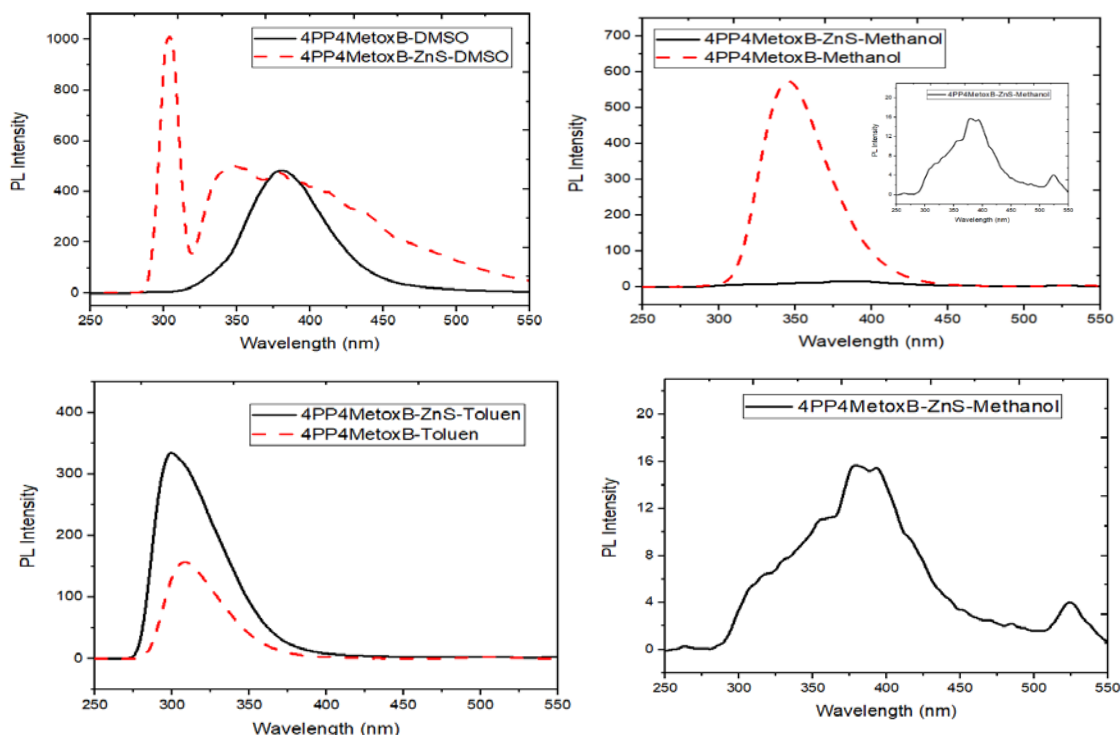


Figure 5. Fluorescence spectra of ZnS nanoparticle doped 4PP4MetoxB and 4PP4MetoxB liquid crystal.

Table 1. Data of fluorescence spectra of ZnS nanoparticle doped 4PP4METOXB and 4PP4METOXB liquid crystal.

	DMSO	Methanol	Toluene
4PP4MetoxB (nm)	381	345	308
4PP4MetoxB-ZnS (nm)	348-378-435	318-358-377-393	300

Fluorescence spectra of new nanomaterials formed with 4PP4MetoxB liquid crystal and ZnS nanoparticles in 3 different solvents are given in figure 5. The change in the maximum wavelengths of the fluorescence spectra of 4PP4MetoxB-DMSO liquid crystal solution and 4PP4MetoxB-ZnS-DMSO nanomaterial is seen as approximately 33 nms. In addition to this change, more peaks are observed in the 4PP4MetoxB-DMSO solution, while a single and wide peak is observed in the 4PP4MetoxB-ZnS-DMSO solution. The data of the fluorescence spectra of the 4PP4MetoxB-Methanol solution and the 4PP4MetoxB-ZnS-Methanol solution, which has a weak peak, are given in Table 1. By examining this table 1 and fluorescence spectra we obtained, it can be said that charge transfers occur between liquid crystals and nanoparticles in methanol solvent. It is seen that the fluorescence spectra of the 4PP4MetoxB-Toluene solution and the 4PP4MetoxB-ZnS-Toluene solution are similar to each other and the difference between the maximum wavelengths is 8 nms.

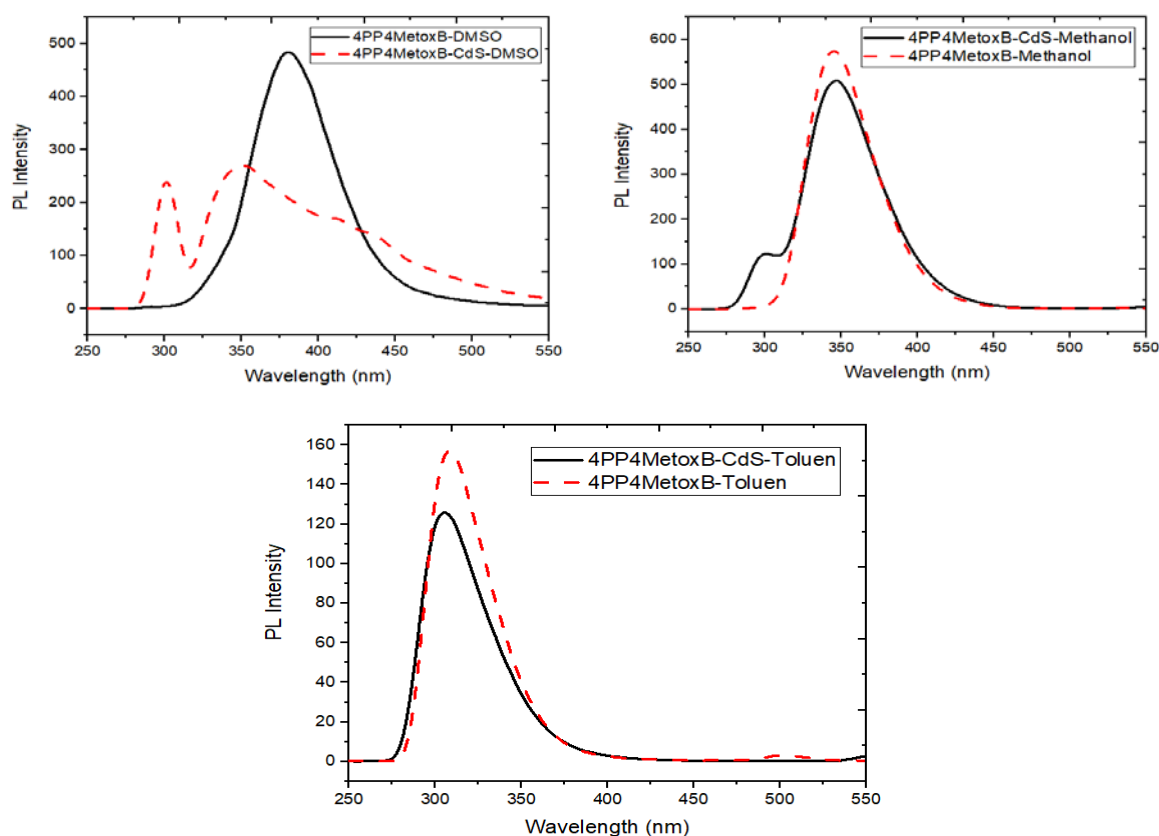


Figure 6. Fluorescence spectra of CdS nanoparticle doped 4PP4MetoxB and 4PP4MetoxB liquid crystal.

Table 2. Data of fluorescence spectra of CdS nanoparticle doped 4PP4MetoxB and 4PP4MetoxB liquid crystal.

	DMSO	Methanol	Toluene
4PP4MetoxB (nm)	381	345	308
4PP4MetoxB-CdS (nm)	350-407	300-346	305

Fluorescence spectra of new nanomaterials formed with 4PP4MetoxB liquid crystal and CdS nanoparticles in 3 different solvents are given in Figure 6. It is seen that there is a difference of approximately 31 nms in the maximum wavelengths on the fluorescence spectra between 4PP4MetoxB-DMSO and 4PP4MetoxB-CdS-DMSO solutions. There are an interaction between the 4PP4MetoxB liquid crystal and the CdS nanoparticle in the DMSO solvent and charge transfer occurred. The fluorescence spectra of the 4PP4MetoxB-Methanol solution and the 4PP4MetoxB-CdS-Methanol solution overlap each other. It can be said that charge transfer between the 4PP4MetoxB liquid crystal and the CdS nanoparticle in the methanol solvent does not occur and there is no interaction between them. Another nanomaterial in which liquid crystals and nanoparticles do not interact was the 4PP4MetoxB-CdS-Toluene solution. Here, it is seen that the fluorescence spectra of 4PP4MetoxB and 4PP4MetoxB-CdS solutions in toluene solvent are similar and there is only a difference of about 3 nm at their maximum wavelengths.

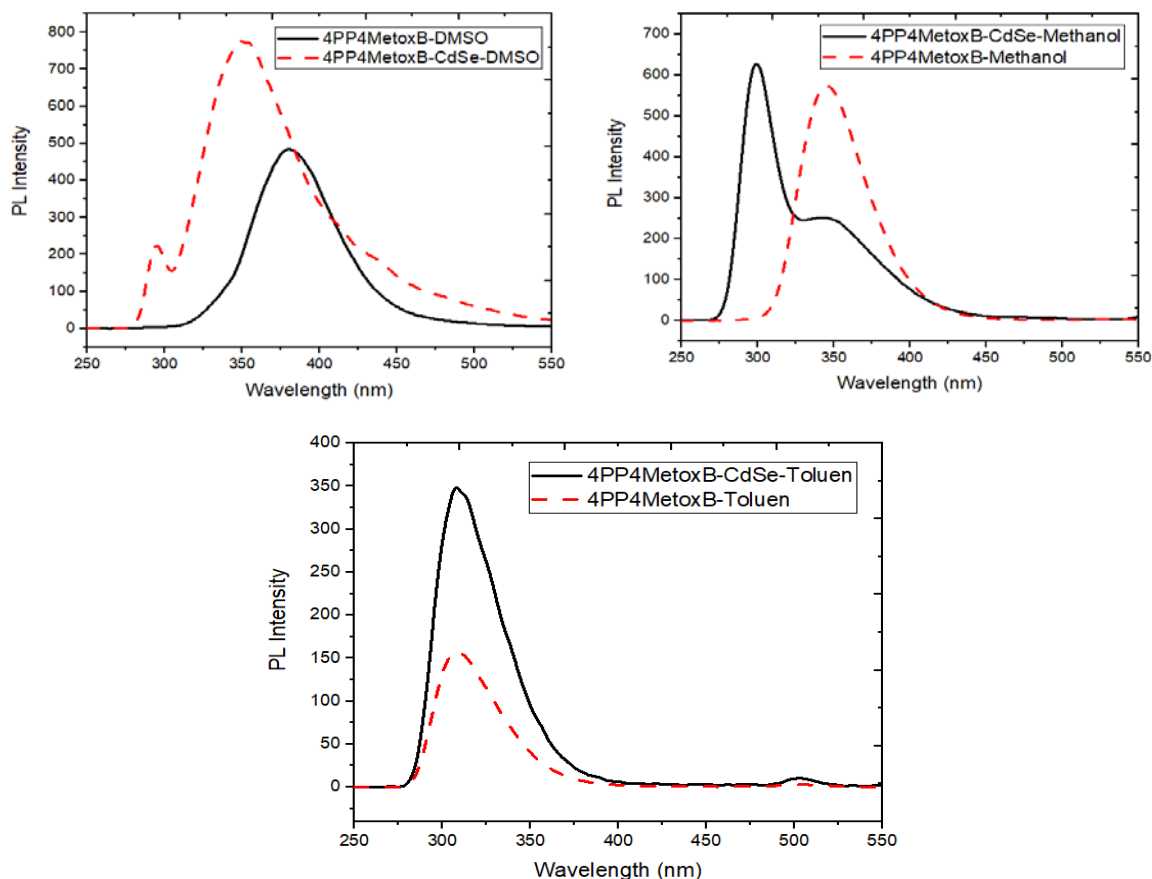


Figure 7. Fluorescence spectra of CdSe nanoparticle doped 4PP4MetoxB and 4PP4MetoxB liquid crystal.

Table 3. Data of fluorescence spectra of CdSe nanoparticle doped 4PP4MetoxB and 4PP4MetoxB liquid crystal.

	DMSO	Methanol	Toluene
4PP4MetoxB (nm)	381	345	308
4PP4MetoxB-CdSe (nm)	350	298-343	308

It is seen that there is a 31 nm difference in the maximum wavelengths of the fluorescence spectra of the 4PP4MetoxB-DMSO solution and the 4PP4MetoxB-CdSe-DMSO solution. It is seen that the fluorescence spectra of 4PP4MetoxB-DMSO solution and 4PP4MetoxB-CdSe-Methanol solution have a difference of 47 nms at their maximum wavelengths. It is seen that the fluorescence spectra of the 4PP4MetoxB-Toluene solution and the fluorescence spectra of the 4PP4MetoxB-CdSe-Toluene solution are quite similar to each other. When these fluorescence spectra are investigated, it can be said that 4PP4MetoxB liquid crystal and CdSe nanoparticle do not interact in Toluene solution.

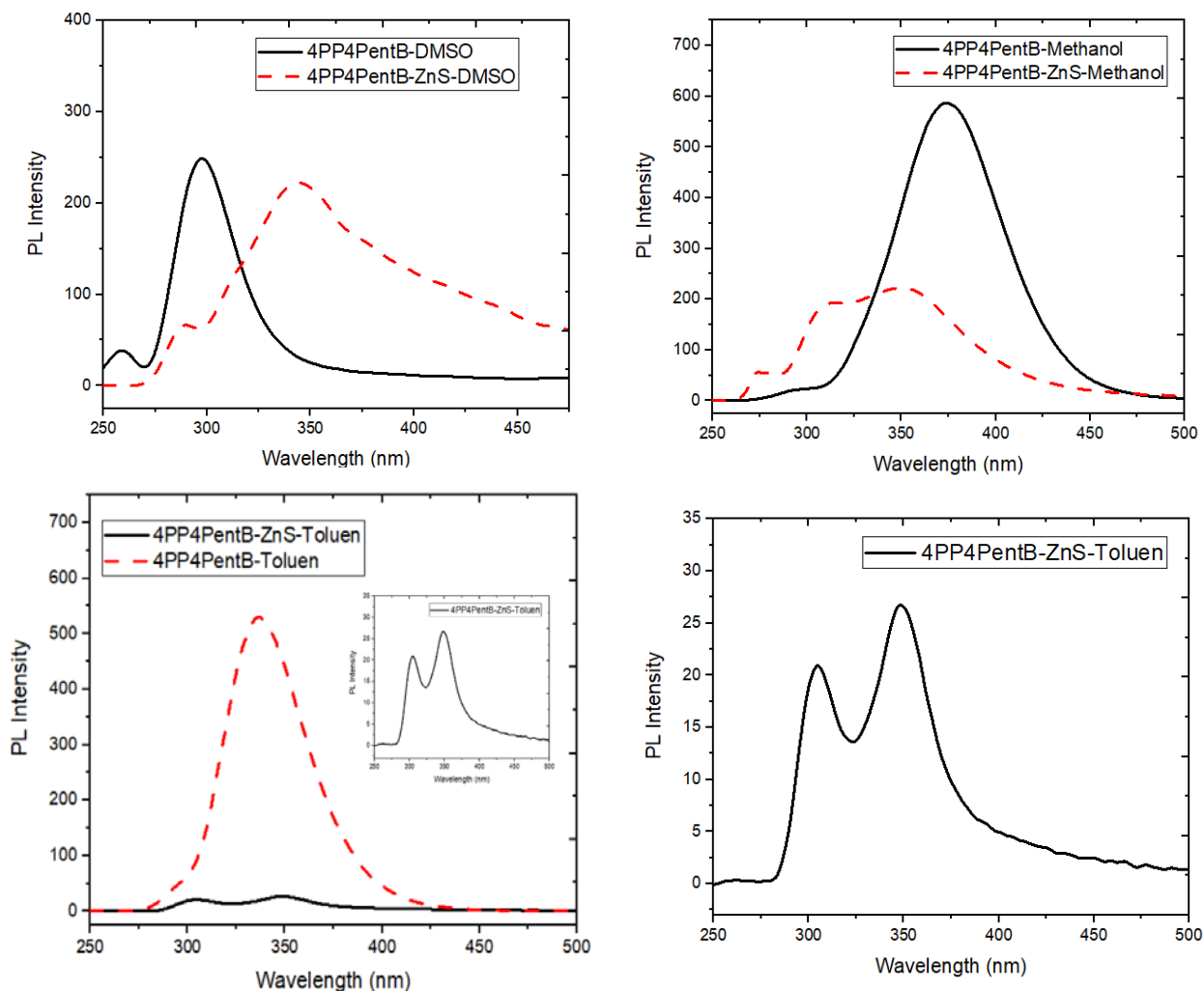


Figure 8. Fluorescence spectra of ZnS nanoparticle doped 4PP4PentB and 4PP4PentB liquid crystal.

Table 4. Data of fluorescence spectra of ZnS nanoparticle doped 4PP4PentB and 4PP4PentB liquid crystal.

	DMSO	Methanol	Toluene
4PP4PentB (nm)	297	294-373	336
4PP4PentB-ZnS (nm)	345	312-350	304-347

The fluorescence spectra of the solutions obtained by combining 4PP4PentB liquid crystal and ZnS, CdS and CdSe nanoparticles in a solvent medium and the fluorescence spectra of the liquid crystalline solutions are given in Figure 8-10. Between the 4PP4PentB-DMSO solution and the 4PP4PentB-ZnS-DMSO solution, a 48 nm red shift occurred at the fluorescence maximum wavelength. The ZnS nanoparticle added to the 4PP4PentB-DMSO solution was the element of change in the new 4PP4PentB-ZnS-DMSO solution. This change shows that 4PP4PentB liquid crystal and ZnS nanoparticle interact in DMSO solvent. In the fluorescence spectra of 4PP4PentB-Toluene solution and 4PP4PentB-ZnS-Toluene solution, a difference of 11 nm occurred at the maximum wavelength. In addition to this difference, it can be said that the fluorescence intensity of the 4PP4PentB-ZnS-Toluene solution is very low and the fluorescence spectra change compared to the 4PP4PentB-Toluene solution.

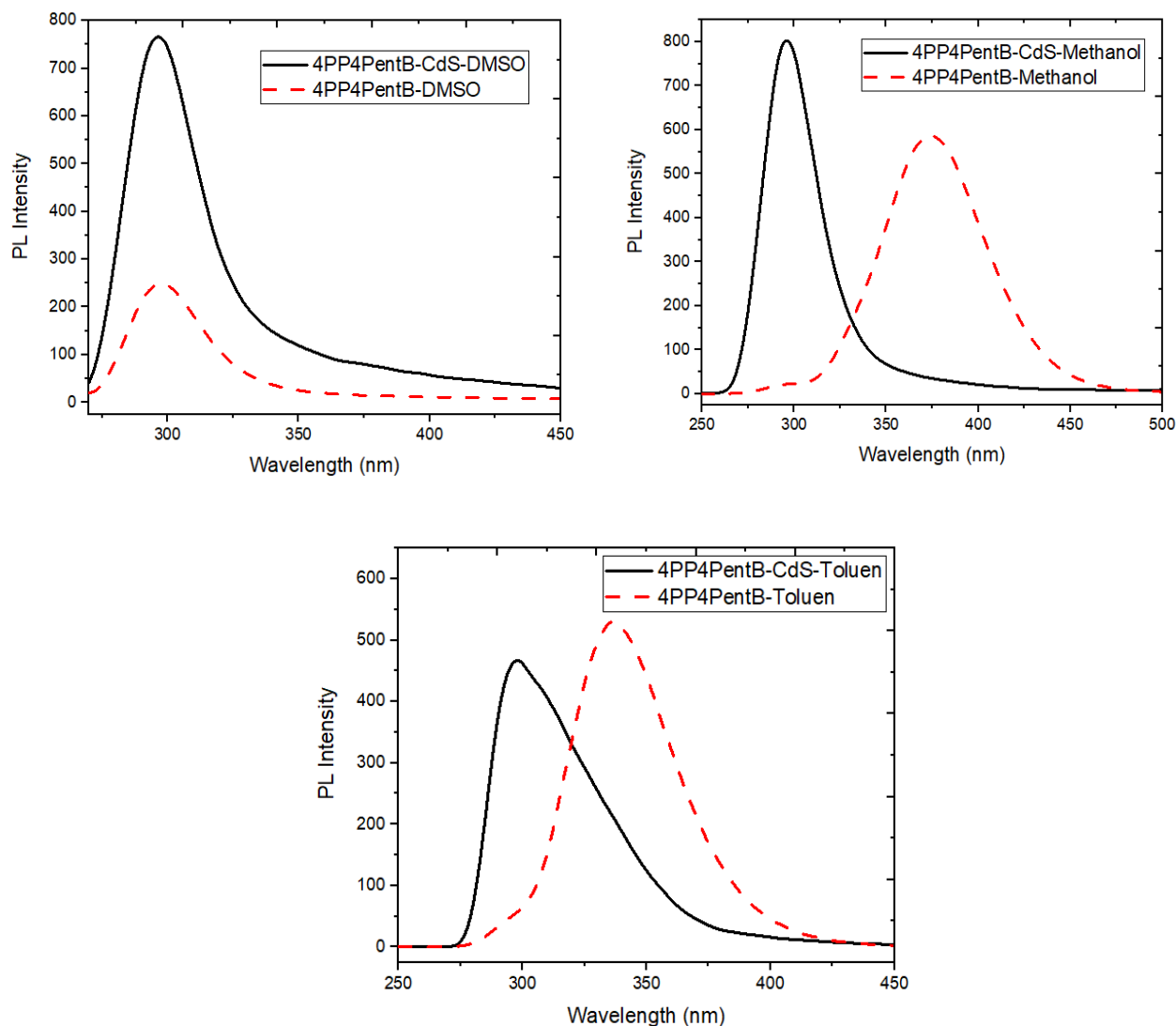


Figure 9. Fluorescence spectra of CdS nanoparticle doped 4PP4PentB and 4PP4PentB liquid crystal.

Table 5. Data of fluorescence spectra of CdS nanoparticle doped 4PP4PentB and 4PP4PentB liquid crystal.

	DMSO	Methanol	Toluene
4PP4PentB (nm)	297	294-373	336
4PP4PentB-CdS (nm)	295	296	297

It is seen that the fluorescence spectra of the 4PP4PentB-DMSO solution and the 4PP4PentB-CdS-DMSO solutions are similar except for the fluorescence intensities. No charge transfers or interaction was probably took place in the 4PP4PentB liquid crystal and the CdS nanoparticle DMSO solution. The fluorescence spectra of the 4PP4PentB-Methanol solution and the 4PP4PentB-CdS-Methanol solution are different, with a difference of 77 nm at the maximum wavelengths. It is observed that the maximum wavelength of the 4PP4PentB-CdS-Methanol solution is shifted towards the blue region compared to the maximum wavelength of the 4PP4PentB-Methanol solution. It was measured that there is a difference of 39 nm between the maximum wavelength of the fluorescence spectra of the 4PP4PentB-Toluene solution and the maximum wavelength of the fluorescence spectra of the 4PP4PentB-CdS-Toluene solution. It is seen that charge transfers take place by interacting with 4PP4PentB liquid crystal and CdS nanoparticle in Toluene solvent.

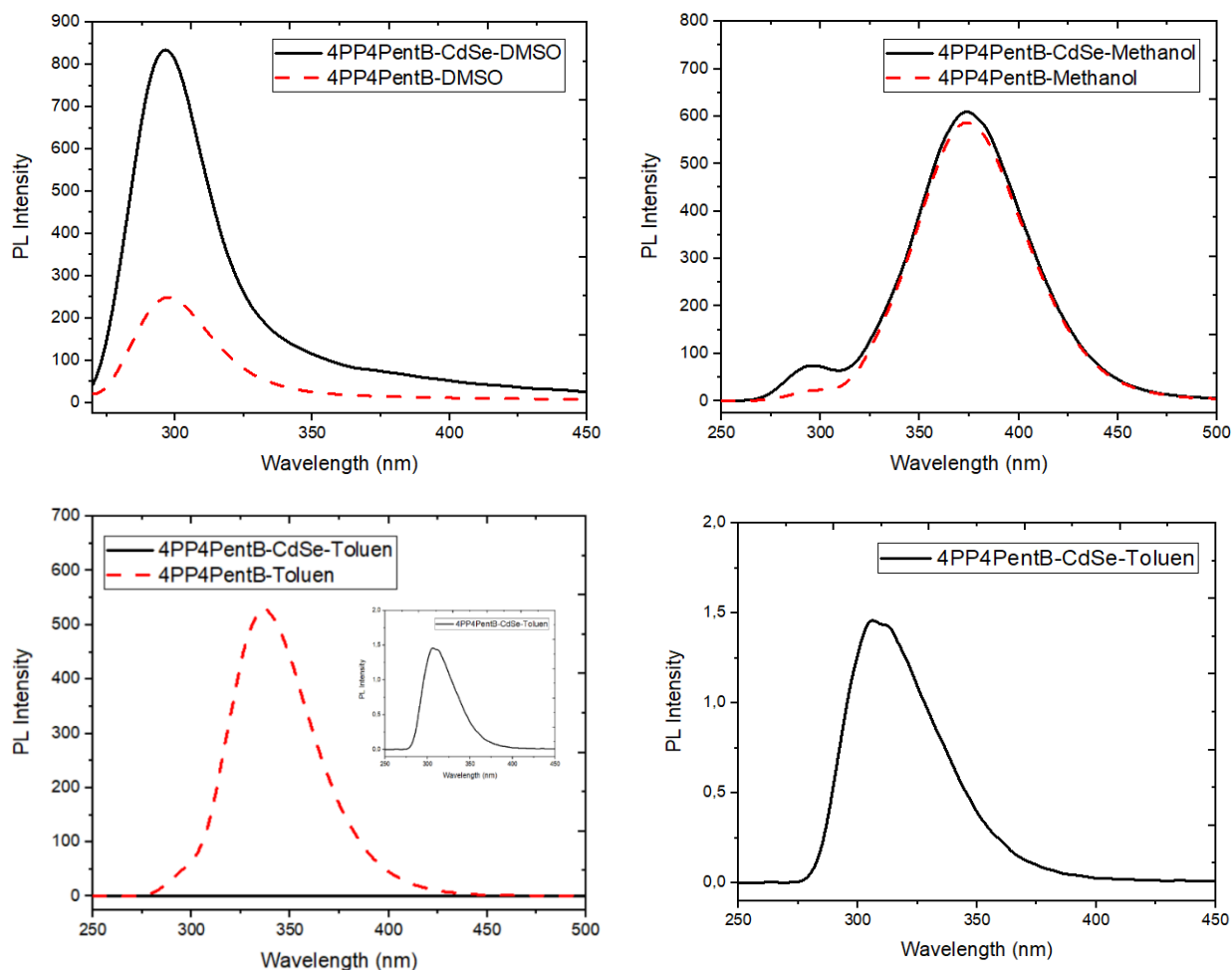


Figure 10. Fluorescence spectra of CdSe nanoparticle doped 4PP4PentB and 4PP4PentB liquid crystal.

Table 6. Data of fluorescence spectra of CdSe nanoparticle doped 4PP4PentB and 4PP4PentB liquid crystal.

	DMSO	Methanol	Toluene
4PP4PentB (nm)	297	294-373	336
4PP4PentB-CdSe (nm)	297	293-375	307

It is seen in Figure 10 that the fluorescence spectra of the 4PP4PentB-DMSO solution and the 4PP4PentB-CdSe-DMSO solution is similar. Likewise, the fluorescence spectra of the 4PP4PentB-Methanol solution and the 4PP4PentB-CdSe-Methanol solution is similar. It is understood that the CdSe nanoparticle of the 4PP4PentB liquid crystal does not interact in DMSO and Methanol solvents. It is observed that the fluorescence spectra of the 4PP4PentB-Toluene solution and the 4PP4PentB-CdSe-Toluene solution are different and there is a 29 nm difference in the maximum wavelengths. The intensity of the fluorescence spectra of the 4PP4PentB-CdSe-Toluene solution was also lower than the other solutions.

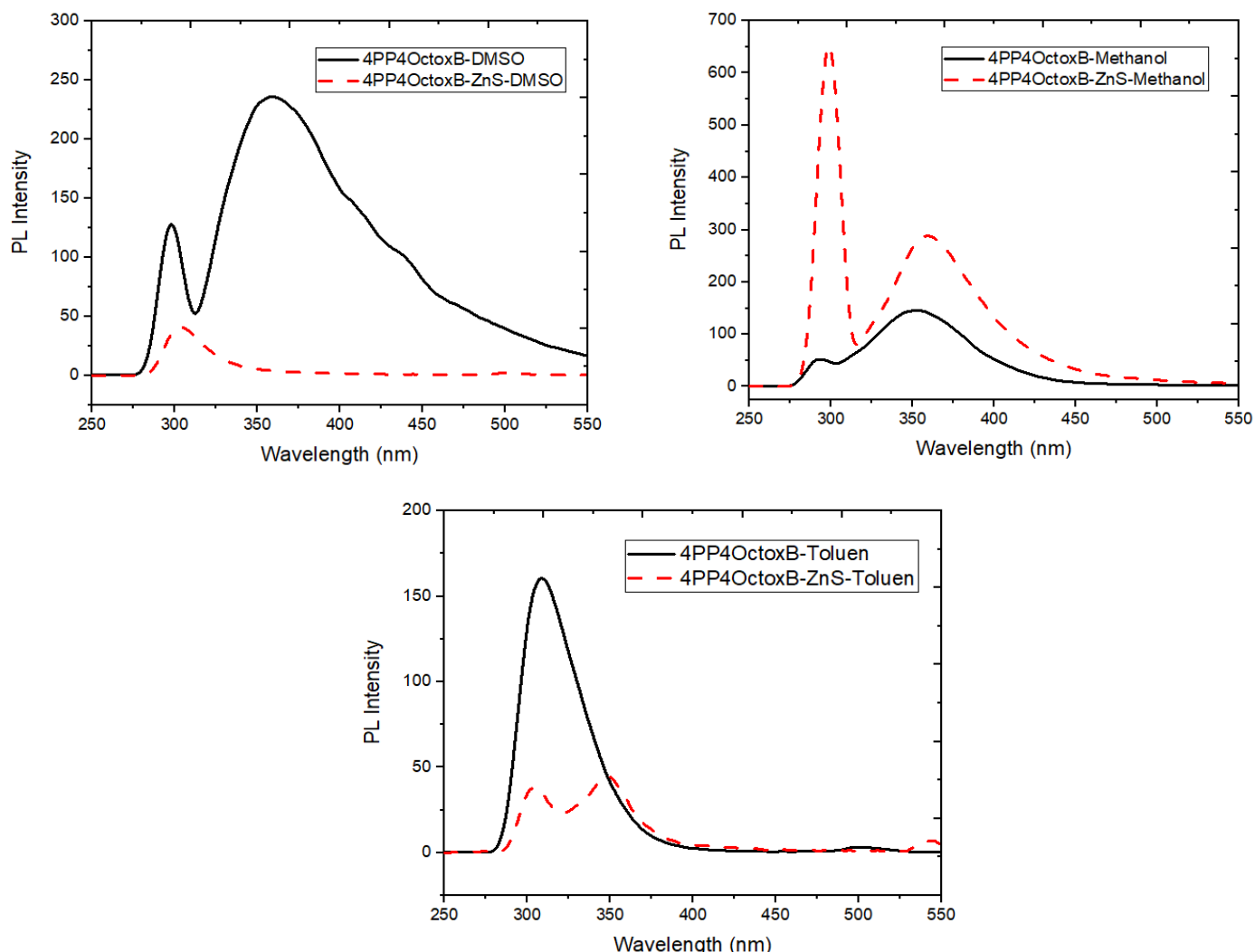


Figure 11. Fluorescence spectra of ZnS nanoparticle doped 4PP4OctoxB and 4PP4OctoxB liquid crystal.

Table 7. Data of fluorescence spectra of ZnS nanoparticle doped 4PP4OctoxB and 4PP4OctoxB liquid crystal.

	DMSO	Methanol	Toluene
4PP4OctoxB (nm)	359-407-439	351	308
4PP4OctoxB-ZnS (nm)	303	358	304-347

The fluorescence graphs of the 4PP4OctoxB liquid crystal solutions and the new solutions formed by the combination of 4PP4OctoxB liquid crystal and ZnS, CdSe, and CdS nanoparticles in the solvent are given in Figure 11-13. It was determined that the fluorescence spectra of the 4PP4OctoxB-DMSO solution and the 4PP4OctoxB-ZnS-DMSO solution were different and there was a 56 nm difference between the maximum wavelengths. A 56 nm blue shift occurred at the maximum wavelength of the 4PP4OctoxB-ZnS-DMSO solution compared to the 4PP4OctoxB-DMSO solution. It can be said that the fluorescence spectra of the 4PP4OctoxB-Methanol solution and the 4PP4OctoxB-ZnS-Methanol solution show close spectroscopy. It can be said that the fluorescence spectra of the 4PP4OctoxB-Toluene solution and the 4PP4OctoxB-ZnS-Toluene solution are different from each other. It can be understood that 4PP4OctoxB liquid crystal and ZnS nanoparticle interact in Toluene solvent.

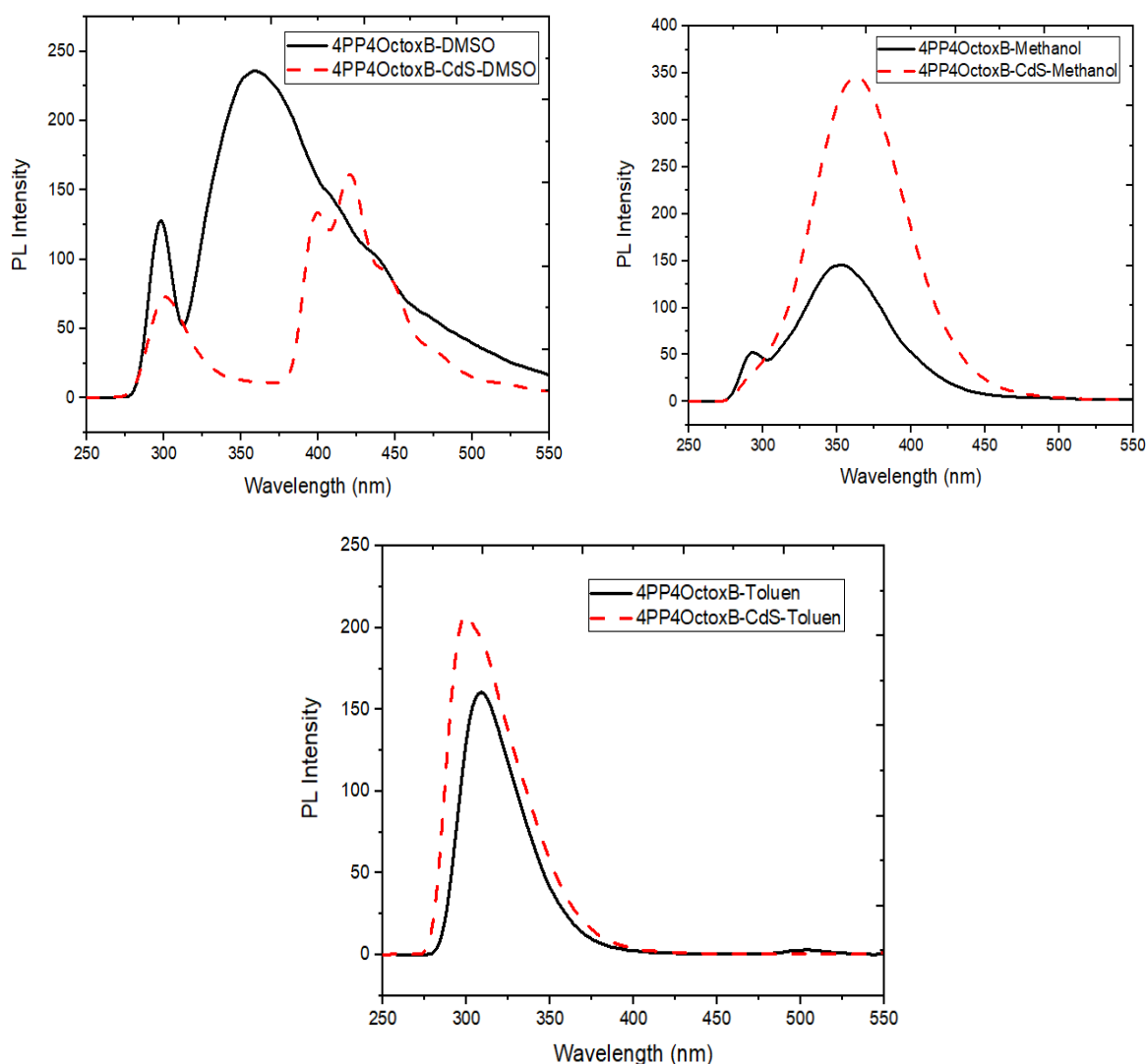


Figure 12. Fluorescence spectra of CdS nanoparticle doped 4PP4OctoxB and 4PP4OctoxB liquid crystal.

Table 8. Data of fluorescence spectra of CdS nanoparticle doped 4PP4OctoxB and 4PP4OctoxB liquid crystal.

	DMSO	Methanol	Toluene
4PP4OctoxB (nm)	359-407-439	351	308
4PP4OctoxB-CdS (nm)	300-399-420-445-479	363	300

There are remarkable differences in the fluorescence spectra of 4PP4OctoxB-DMSO solution and 4PP4OctoxB-CdS-DMSO solution. It can be said that fluorescence spectra of 4PP4OctoxB liquid crystal and CdS nanoparticle interact in DMSO solvent and differentiate as a result of charge transfers. It is seen that the fluorescence spectra of the 4PP4OctoxB-Methanol solution and the 4PP4OctoxB-CdS-Methanol solution are similar to each other. Likewise, it can be seen from figure 12 that the fluorescence spectra of the 4PP4OctoxB-Toluene solution and the 4PP4OctoxB-CdS-Toluene solution are similar to each other.

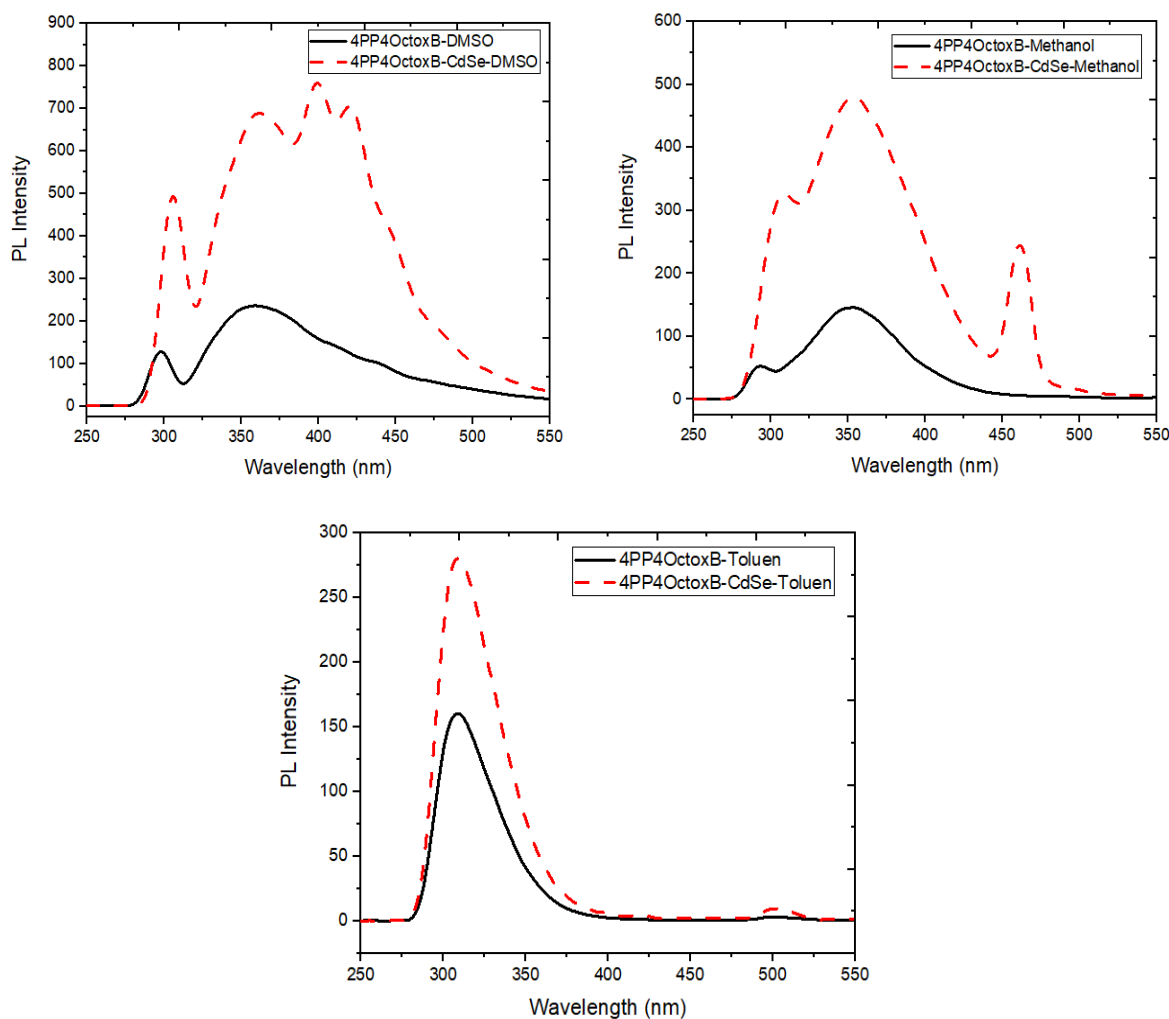


Figure 13. Fluorescence spectra of CdSe nanoparticle doped 4PP4OctoxB and 4PP4OctoxB liquid crystal.

Table 9. Data of fluorescence spectra of CdSe nanoparticle doped 4PP4OctoxB and 4PP4OctoxB liquid crystal.

	DMSO	Methanol	Toluene
4PP4OctoxB (nm)	359-407-439	351	308
4PP4OctoxB-CdSe (nm)	360-399-419	308-353	308

It is understood that there are significant differences between the fluorescence spectra of the 4PP4OctoxB-DMSO solution and the 4PP4OctoxB-CdSe-DMSO solution. It can be said that 4PP4OctoxB liquid crystal interacts with CdSe nanoparticle in DMSO solvent. It can be said that the fluorescence spectra of the 4PP4OctoxB-Methanol solution and the 4PP4OctoxB-CdSe-Methanol solution are similar. It is seen that the fluorescence spectra of the 4PP4OctoxB-Toluene solution and the 4PP4OctoxB-CdSe-Toluene solution are similar to each other. These similarities tell us that liquid crystals and nanoparticles do not interact and there is no charge transfer between them.

4. Conclusions

The changes in fluorescence spectra and maximum wavelengths of liquid crystals and nanoparticle doped liquid crystals were investigated. The CdS nanoparticle added to the 4PP4MetoxB liquid crystal interacted only in the DMSO environment and was blue-shifted at the maximum wavelength of the fluorescence spectrum. In the CdSe nanoparticle added to the 4PP4MetoxB liquid crystal, a blue shift occurred at the maximum wavelength of the fluorescence spectrum of this liquid crystal in the DMSO and Methanol solvent medium. The ZnS nanoparticle added to the 4PP4MetoxB liquid

crystal showed a blue shift in DMSO and a red shift in Methanol. Since charge transfer did not occur between the 4PP4MetoxB liquid crystal in the toluene environment and the nanoparticles, the electronic structure of these molecules did not change. CdS nanoparticle doped into 4PP4PentB liquid crystal did not interact in DMSO while blue shifting occurred in Methanol and Toluene compared to the liquid crystal. While the CdSe nanoparticle added to the 4PP4PentB liquid crystal did not interact in DMSO and Methanol, electronic transitions occurred in Toluene and a blue shift occurred. In the ZnS nanoparticle added to the 4PP4PentB liquid crystal, charge transfers occurred in the entire solvent medium used and shifts occurred at the maximum wavelengths. CdS nanoparticle added to 4PP4OctoxB liquid crystal has been transferred in all solvents used, and the electronic structure of the liquid crystal has changed. Charge transfers took place in DMSO and Toluene solvents of ZnS and CdSe nanoparticles added to this liquid crystal in the same way. As a result, both blue-shift and red-shift occurred in the fluorescence spectrum compared to the liquid crystal.

Peer-review: Externally peer - reviewed.

Author contributions: Concept – Y. G. S., S. H.; Data Collection &/or Processing - Y. E. K.; Literature Search - Y. E. K.; Writing - Y.E.K., Y. G. S., S. H.

Conflict of Interest: No conflict of interest was declared by the authors.

Financial Disclosure: The author thanks for support given via Bitlis Eren University Research Foundation (BEBAP-2013.04).

References

- [1] J. Beeckman, "Liquid-crystal photonic applications," *Optical Engineering*, vol. 50, no. 8, p. 081202, 2011, doi: 10.1117/1.3565046.
- [2] T. Ikeda, "Photomodulation of liquid crystal orientations for photonic applications," *Journal of Materials Chemistry*, vol. 13, no. 9, pp. 2037–2057, 2003, doi: 10.1039/b306216n.
- [3] H. Kawamoto, "The History of Liquid-Crystal Displays," vol. 90, no. 4, 2006.
- [4] S. J. Woltman, G. D. Jay, and G. P. Crawford, "Liquid-crystal materials find a new order in biomedical applications," *Nature Materials*, vol. 6, no. 12, pp. 929–938, 2007, doi: 10.1038/nmat2010.
- [5] J. P. F. Lagerwall and G. Scalia, "A new era for liquid crystal research: Applications of liquid crystals in soft matter nano-, bio- and microtechnology," *Current Applied Physics*, vol. 12, no. 6, pp. 1387–1412, 2012, doi: 10.1016/j.cap.2012.03.019.
- [6] C. Noël and P. Navard, "Liquid crystal polymers," *Progress in Polymer Science*, vol. 16, no. 1, pp. 55–110, Jan. 1991, doi: 10.1016/0079-6700(91)90007-8.
- [7] I. I. Smalyukh, "Liquid Crystal Colloids," *Annual Review of Condensed Matter Physics*, vol. 9, no. November 2017, pp. 207–226, 2018, doi: 10.1146/annurev-conmatphys-033117-054102.
- [8] M. Bangal *et al.*, "Semiconductor nanoparticles," *Hyperfine Interactions*, vol. 160, no. 1–4, pp. 81–94, 2005, doi: 10.1007/s10751-005-9151-y.
- [9] K. J. Si, Y. Chen, Q. Shi, and W. Cheng, "Nanoparticle Superlattices: The Roles of Soft Ligands," *Advanced Science*, vol. 5, no. 1, 2018, doi: 10.1002/advs.201700179.
- [10] J. R. Lakowicz, I. Gryczynski, Z. Gryczynski, and C. J. Murphy, "Luminescence spectral properties of CdS nanoparticles," *Journal of Physical Chemistry B*, vol. 103, no. 36, pp. 7613–7620, 1999, doi: 10.1021/jp991469n.

- [11] T. Hegmann, H. Qi, and V. M. Marx, “Nanoparticles in liquid crystals: Synthesis, self-assembly, defect formation and potential applications,” *Journal of Inorganic and Organometallic Polymers and Materials*, vol. 17, no. 3, pp. 483–508, 2007, doi: 10.1007/s10904-007-9140-5.
- [12] R. K. Shukla, Y. G. Galyametdinov, R. R. Shamilov, and W. Haase, “Effect of CdSe quantum dots doping on the switching time, localised electric field and dielectric parameters of ferroelectric liquid crystal,” *Liquid Crystals*, vol. 41, no. 12, pp. 1889–1896, 2014, doi: 10.1080/02678292.2014.959571.
- [13] V. Kumar, A. Kumar, A. M. Biradar, G. B. Reddy, D. Sachdev, and R. Pasricha, “Enhancement of electro-optical response of ferroelectric liquid crystal: the role of graphene quantum dots,” *Liquid Crystals*, vol. 41, no. 12, pp. 1719–1725, 2014, doi: 10.1080/02678292.2014.949888.
- [14] A. Anczykowska, S. Bartkiewicz, M. Nyk, and J. Myśliwiec, “Enhanced photorefractive effect in liquid crystal structures co-doped with semiconductor quantum dots and metallic nanoparticles,” *Applied Physics Letters*, vol. 99, no. 19, pp. 1–4, 2011, doi: 10.1063/1.3659485.
- [15] L. J. Martínez-Miranda, K. M. Traister, I. Meléndez-Rodríguez, and L. Salamanca-Riba, “Liquid crystal-ZnO nanoparticle photovoltaics: Role of nanoparticles in ordering the liquid crystal,” *Applied Physics Letters*, vol. 97, no. 22, 2010, doi: 10.1063/1.3511736.
- [16] T. Zhang, C. Zhong, and J. Xu, “CdS-Nanoparticle-doped liquid crystal displays showing low threshold voltage,” *Japanese Journal of Applied Physics*, vol. 48, no. 5, pp. 0550021–0550026, 2009, doi: 10.1143/JJAP.48.055002.
- [17] J. Tauc and A. Menth, “States in the gap,” *Journal of Non-Crystalline Solids*, vol. 8–10, no. C, pp. 569–585, 1972, doi: 10.1016/0022-3093(72)90194-9.
- [18] J. C. Tauc, “Semiconductor Amorphous and Liquid,” p. 195, 1974.
- [19] O. Baytar, O. Sahin, H. Kilicvuran, and S. Horoz, “Synthesis, structural, optical and photocatalytic properties of Fe-alloyed CdZnS nanoparticles,” *Journal of Materials Science: Materials in Electronics*, vol. 29, no. 6, pp. 4564–4568, 2018, doi: 10.1007/s10854-017-8406-0.
- [20] S. Horoz *et al.*, “CdSe quantum dots synthesized by laser ablation in water and their photovoltaic applications,” *Applied Physics Letters*, vol. 101, no. 22, pp. 1–5, 2012, doi: 10.1063/1.4768706.
- [21] O. Sahin and S. Horoz, “Synthesis of Ni:ZnS quantum dots and investigation of their properties,” *Journal of Materials Science: Materials in Electronics*, vol. 29, no. 19, pp. 16775–16781, 2018, doi: 10.1007/s10854-018-9771-z.
- [22] OriginPro19b (Version 9.5), OriginLab Corporation, Northampton, MA (USA), 2022.
- [23] SpectraGryph 1.2, Spectroscopy Software, <https://www.effemm2.de/spectragryph/down.html>.
- [24] Y. Li, L. Ma, X. Zhang, A. G. Joly, Z. Liu, and W. Chen, “Synthesis and optical properties of sulfide nanoparticles prepared in dimethylsulfoxide,” *Journal of Nanoscience and Nanotechnology*, vol. 8, no. 11, pp. 5646–5651, Nov. 2008, doi: 10.1166/JNN.2008.474.
- [25] F. Rodríguez-mas, J. C. Ferrer, J. L. Alonso, S. F. de Ávila, and D. Valiente, “Reduced Graphene Oxide Inserted into PEDOT:PSS Layer to Enhance the Electrical Behaviour of Light-Emitting Diodes,” *Nanomaterials 2021, Vol. 11, Page 645*, vol. 11, no. 3, p. 645, Mar. 2021, doi: 10.3390/NANO11030645.